UNIVERSITY OF CALIFORNIA,
IRVINE

Characterizing dynamics of DNA binding proteins; p53 and DinB homolog polymerase (Dbh)

DISSERTATION

submitted in partial satisfaction of the requirements
for the degree of

DOCTOR OF PHILOSOPHY

in Pharmaceutical Sciences

by

Jenaro Soto

Dissertation Committee:
Associate Professor Melanie Cocco, Chair
Professor John Chaput
Professor Andrej Lupták

2023

DEDICATION

To my parents in recognition of their hard work and sacrifice. And to all my family for always supporting me and showering me with love.

And to my beautiful girlfriend, Jennifer, for all your support and love!

I am a better man because all of you are part of my life.

TABLE OF CONTENTS

LIST OF FIGURES

LIST OF TABLES

LIST OF TABLES

ACKNOWLEDGEMENTS

I would like to express my deepest appreciation to my committee chair and advisor, Dr. Melanie Cocco, for being a great advisor. Your support, patients, and guidance has been key to my success in graduate school. Without her guidance and support, this dissertation would not have been possible.

I would like to thank my committee members, Professor Andrej Lupták and Professor John Chaput. Thank you Dr. Lupták, your positive attitude showed me that working on world-changing science can be fun. Dr. Chaput, thanks for the work you do in your lab. It has been a source of inspiration ever since I first heard your presentation during my undergraduate studies.

And thank you UCI, Rose Hill Foundation, and the UC Drug Discover Consortium for the financial support.

A special thanks to Dr. Marlene De La Cruz and the MSP program, for providing financial support and guidance during my undergraduate studies and into my graduate work.

Thanks, University of California, Irvine, for providing a community where I have felt safe and welcomed to live and learn all these years.

VITA

Jenaro Soto

Education

University of California, Irvine, Irvine CA 2017- 2023
PhD Pharmaceutical Sciences

University of California, Irvine, Irvine, CA 2014-2017
B. S., Neurobiology

Cerritos Community College, Norwalk, CA 2010-2014
A.A., Natural Sciences

Completed Pharmaceutical Courses

- Bio Macromolecules
- Topics in Pharmaceutical sciences
- Medicinal Chemistry
- Proteomics
- High-Resolution Structures: NMR and X-ray
- Frontiers of Chemistry/ Synthetic biology
- Drug discovery computing techniques

Research Experience

Cocco laboratory **June 2017-Present**

University of California, Irvine

Project: p53 protein dynamics, Dbh protein dynamics

- Used solution state NMR to investigate dynamics of DNA binding proteins; p53 and Dbh polymerase.
- Used CcpNmr to analyze HSQC, T1, T2, and NOE data.
- Conducted literature search to aid data analysis.
- Have created figures and writing 2 manuscripts for publication.
- Presented at 3rd Annual Drug Discovery Symposium and the 64-66th Annual Biophysical Society meeting.
- Analyzed microscope images of neuronal axon growth via neuron J.

Reeve Irvine Research Center (RIRC) **June 2015-September 2016**

University of California, Irvine

Project: Neuronal activity

- Assessed the effect of conditional deleting PTEN from motor cortex neurons.
- Performed immunohistochemistry on coronal brain sections.
- Imaged and analysis brain tissue using Images J.

Work experience

UCDDC Grant Administrator **Jan. 2021-Present**

- Aided in organizing grant application RFAs and submissions.
- Research pharmaceutical companies and reach-out for potential collaboration with UCDDC.
- Organized University of California (10 campus) webinar to promote funding opportunities.
- Help plan, organize, and execute UCDDC annual symposium/conference.
- Facilitate biweekly and weekly meetings for executive committee members by gathering discussion topics, taking meeting minutes, and organizing Box drive for file sharing.
- Web master for UCDDC Wix webpage. Maintained news feed for DDC webpage, created webpage for event promotion, and event registration.

Teacher Assistant at UCI **Sep. 2017-June 2021**

- Help teach **biochemistry** lab and **advance molecular biology** lecture. Conducted weekly meeting to discuss assignment and biochemistry concept. (Spring 2021)
- Assisted in teaching **Medicinal Chemistry** lab techniques to students. (Winter 2021)
- Help organize and teach **advance biochemistry** lecture and laboratory. (Fall 2020)
- Conducted three discussion section per week. Taught **molecular biology** in an active learning environment. (Spring 2019)
- Taught **Anatomy and physiological** function. Managed 3 discussion section/week. (Fall 2017)

Activities and Leadership Experience

Summer Journal Club Administrator **June 2021- August 2021**

Organized and managed weekly journal club meetings for college biology and chemistry students. Trained students to interpret primary scientific literature and taught them how to effectively communicate their own scientific research through PowerPoint presentations.

Founder & president of Through Inclusive Eyes (TIE) **Jan. 2018- Feb 2020**

I established Through Inclusive Eyes (TIE); a student organization geared toward improving disability inclusion throughout UCI campus. Advocate for accessibility on campus. Help UCI attain a wheelchair friendly golfcart.

INSITE accessibility lead **Oct. 2018-Jan 2020**

The INSĪT lab is interested in designing and building universally usable technologies. Serve as the accessibility expert. Duties included community networking, organizing accessible conference, and accessibility research.

Publications

- **Soto, J**., **Cocco M.J.. (2023)** Dynamics of the Bypass Polymerase, dinB homolog (DBH). In progress
- **Soto, J.**, Moody, C., AlHoshani, A., Sanchez-Bonilla, M., Cocco M.J.. (2021) NMR hydrogen exchange and relaxation rates reveal positions stabilized by p53 rescue mutants N239Y and N235K. *bioRxiv* DOI:10.1101/2021.02.26.433080
- Barros, E.P., Özlem, D., **Soto, J.,** et al. Publish article. Markov State Models and NMR Uncover an Overlooked Allosteric Loop in p53. Chemical Science, 2021.
- Moody CL, **Soto, J**, Tretyachenko-Ladokhina V, Senear DF, Cocco MJ. Dynamic Consequences of Specificity within the Cytidine Repressor DNA-Binding Domain. *bioRxiv* DOI:10.1101/2021.02.28.433298
- 2016-2023 Six poster presentations at international conferences.

Awards

- UC Presidential Dissertation Fellowship.
- Rose Hills Foundation Science Fellowship
- UC Drug Discovery Consortium Fellowship.
- Irvine Faculty Mentor Program Fellowship
- NIH-IMSD Fellowship
- NIH-IMSD Graduate Summer Program

ABSTRACT OF THE DISSERTATION

Characterizing dynamics of DNA binding proteins; p53 and DinB homolog polymerase (Dbh)

by

Jenaro

Doctor of Philosophy in Pharmaceutical Sciences

University of California, Irvine, 2023

Associate Professor Melanie Cocco, Chair

Solution state NMR was used to study two DNA-binding proteins. Chapter one covers the different NMR techniques used, including hydrogen exchange, relaxation, chemical shift analysis, and temperature coefficients. In addition, I also implement circular dichroism and protein sequence analysis to supplement the NMR studies. Chapter two covers the p53 project, in which we compare protein dynamics between WT and rescue mutants to understand the mechanism of stabilization. We measured and compared dynamics from NMR hydrogen exchange rates of backbone amides and find that both rescue mutants impose a global stabilizing effect that dampens their motions in the beta-sandwich compared to WT DBD. We also compared NMR relaxation results to obtain flexibility information in the ps to ns timescale regime. Chapter three covers the dynamics of the DinB homolog polymerase (Dbh). This polymerase belongs to the Y-family of translesion DNA polymerases that can synthesize using a damaged DNA template. Since Dbh comes from the thermophilic archaeon *Sulfolobus acidocaldarius,* it is capable of functioning in a wide range of temperatures. Here we use NMR and circular dichroism to understand how the structure and dynamics of Dbh are affected by temperature (2-65°C)

magnesium and manganese. HX reveals that both the thumb and finger domains are very dynamic relative to the palm and LF domains. These trends remain true at high temperatures with dynamics increasing as temperatures increase from 35 °C to 50 °C. Notably, NMR and CD spectra show that Dbh tertiary structure cold denatures beginning at 25 °C and increasing in denaturation as the temperature is lowered to 5 °C with little change observed by CD. Chemical shift perturbation analysis in the presence and absence of magnesium and manganese reveals three ion binding sites, even in the absence of DNA.

INTRODUCTION

We used different nuclear magnetic resonance (NMR) methods to understand the dynamics of DNA-binding proteins. Protein dynamics play a critical role in protein stability and functionality. While X-ray crystallography can generate an image of the protein in a static state it doesn't provide a complete explanation of how proteins execute their biological functions. In contrast, several Nuclear Magnetic Resonance (NMR) techniques allow us to visualize protein motions which can give us further insight into the function and stability of proteins. NMR uses the magnetic properties of nuclei. Each element on the protein has a unique procession frequency that is dependent on its chemical environment. This includes the immediate bonding between neighbors and their spatial neighbors. The procession property can be measured when exposed to a strong magnetic field and exited with resonance frequency radio waves. Specific probing allows us to excite nuclei of interest, so they emit measurable signals. All my experiments follow the NMR signals of amine groups (^{15}N and ^{1}H).

I analyzed the ^{1}H-^{15}N- Heteronuclear Single-Quantum Coherence (^{1}H-^{15}N- HSQC) spectra. These spectra have cross peaks for every covalently bonded ^{1}H-^{15}N (amine group). We can measure the amine groups in the backbone of proteins formed between each amino acid, except for prolines. Given that amine groups are formed at each peptide bond, we get atomic resolution information from all areas of the protein. So, whether we are analyzing fast, slow dynamics, or ligand binding the ^{1}H-^{15}N HSQC NMR spectra allow us to get a high-resolution analysis of the entire protein.

NMR can provide dynamics from a wide range of time scales. Proteins do not exist as singular structures but rather they are dynamic and capable of moving to perform their functions. All proteins have fast dynamics, while some use much slower motions for catalysis. Fast (ns-ps) dynamics can be accessed with relaxation NMR. This type of motion informs on internal motion and local flexibility. While slower (ms-s) motion can be accessed via hydrogen exchange experiments (HX). This type of monitions informs us on large domain motions and protein unfolding/folding.

Chapter 1 Techniques Used to Understand DNA Binding Proteins.

Chapter 1A: Hydrogen exchange (HX).

We implemented HX experiments to obtain slower dynamics that correspond to the folding and unfolding of proteins. HX takes advantage that amine hydrogens (amides) exchange with hydrogen in solution. We can distinguish between protein hydrogens and solution hydrogens by using different isotopic hydrogens; hydrogen (^1H) and deuterium (^2H). Proteins containing amides with ^1H are exposed to a solution containing D_2O. are not static, they are in a dynamic state, sampling different confirmations. While sampling confirmations proteins undergo a breathing motion that allows amides to exchange (**Figure 1.1**). Hydrogen exchange occurs at different rates depending on the local structure of the protein. For amides in unstructured regions, i.e., loop regions, and surface-exposed areas exchange occurs at fast rates, while amides in secondary structures have a slower exchange rate. I used the hydrogen exchange rate (k_{ex}) to calculate the protection factor (PF), which is a stability measurement for the local protein structures. PF is a simple ratio between k_{rc}/k_{ex}. Where k_{rc} is the theoretical exchange rate of a backbone amide in random coil[1] and k_{ex} is the experimental exchange rate calculated from fitting peak intensity for each residue at a different time point to a single exponential. By analyzing PF across the entire protein, we can reveal the parts of the proteins that are stable and dynamic. I used HX NMR to understand the dynamics of WT p53 and to see how it compares with the dynamics of the more stable cancer rescue mutants N235K and N239Y. I also used the same

technique to understand the dynamics of DinB homolog polymerase(Dbh) at 35 °C and 50 °C.

Chapter 1B: NMR Relaxation.

The second NMR technique I used was nuclear spin relaxation which monitors the reorientation of ^{15}N-H bond vectors to obtain backbone data in the ps-ms timescale [2]. Relaxation parameters R1, R2, and NOE are used to obtain order parameters (S^2) by using Lipari-

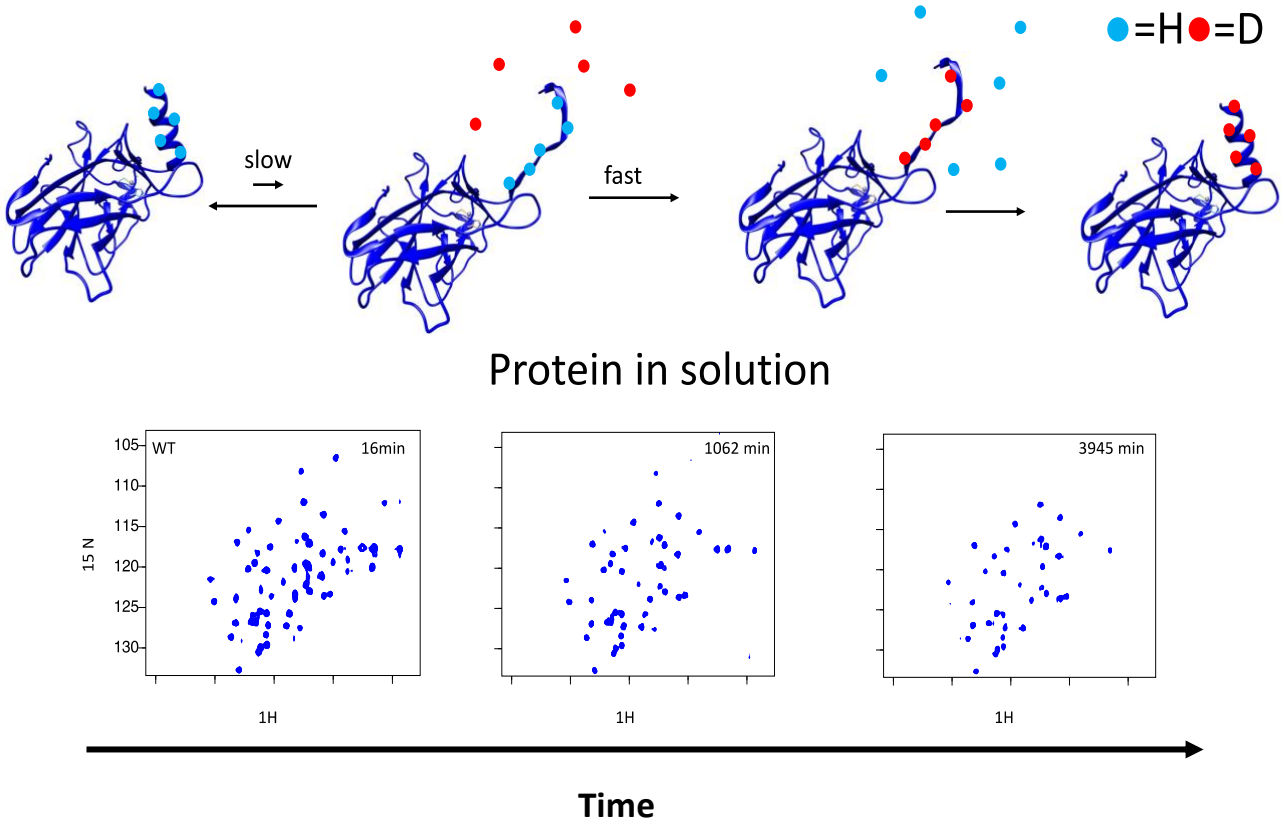

Figure 1.1 : Hydrogen exchange experiment concept. Protein with ^{1}H is added to D_2O solution . ^{1}H is exchanges for ^{2}D (^{2}H) in solution (top schematic). At the start of the experiment amides that are localized in unstructured region exchange immediately. As time progresses exchange occurs for all amides throughout the protein because proteins sample many conformations while in solution. At multiple timepoint ^{1}H-^{15}N- HSQC spectra are collected. We monitor exchange by measuring peak intensity overtime (bottom spectra). We fit the data to exponential to obtain exchange rate (**see figure X**) deduced dynamics of proteinsl

Szabo calculation [3] via ModelFree [4] [5]. Furthermore, I used FastModelFree[6] to iterate on the ModelFree calculations. I analyzed the relaxation data and obtained order parameters to understand the fast dynamics of WT p53 and rescue mutants N235K and N239Y. We also analyzed the relaxation parameters of CytR (**Appendix A**).

Chapter 1C: Chemical shift mapping

Aside from dynamics we also used ^{1}H-^{15}N HSQC spectra to understand ligand binding and confirm protein mutations. This was done by monitoring peak displacement with chemical shift analysis. Peak perturbation reflects most changes that occur to proteins, whether its ligand binding, mutations, or structures change. By comparing WT vs experiment spectra, we can pinpoint what location in the protein experienced a chemical change. I performed chemical shift analysis to confirm the successful missense mutation in rescue mutants p53 N235K and N239Y. Furthermore, I used chemical shift analysis to confirm the binding of magnesium (Mg2+), and Manganese Mn2+ to specific regions in DBH. As you will see this technique yields precise locations on the protein thereby demonstrating the powerful resolutions obtained with NMR.

Chapter 1D: Temperature coefficient.

^{1}H-^{15}N HSQC spectra were also used to calculate the temperature coefficient (TC) of DBH. TC analysis is useful at highlighting the effects of temperature on local and global structural. TC values are the slope calculated from the linear fit of 1H peak position vs temperature (K). They are great at distinguishing between amides involved in structural hydrogen bonding or amides exposed to the solution. It has been shown that amides not involved in intramolecular hydrogen bonding and amides sensitive to temperature

fluctuation have TC values below -4.6 ppb/K [7-10]. Furthermore, group averaging across secondary structures and domains can give insight into temperature-dependent structural changes across the protein [11]. We used TC analysis to understand how temperature affects the individual domain of DBH polymerase. Furthermore, we show how PF and the average TC can be used together to highlight the dynamic regions of a protein.

In addition to ^{1}H-^{15}N HSQC spectra, I conducted other miscellaneous analyses to supplement my work on p53 and DBH. For p53 I conducted a protein sequence analysis across several species I analyzed circular dichroism (CD) for DBH to complement the ^{1}H-^{15}N HSQC spectra experiments.

Refefrences

1. Molday, R.S., S.W. Englander, and R.G. Kallen, *Primary structure effects on peptide group hydrogen exchange.* Biochemistry, 1972. **11**(2): p. 150-8.
2. Kay, L.E., *Protein dynamics from NMR.* Biochem Cell Biol, 1998. **76**(2-3): p. 145-52.
3. Lipari, G. and A. Szabo, *Model-Free Approach to the Interpretation of Nuclear Magnetic-Resonance Relaxation in Macromolecules .2. Analysis of Experimental Results.* Journal of the American Chemical Society, 1982. **104**(17): p. 4559-4570.
4. Mandel, A.M., M. Akke, and A.G. Palmer, 3rd, *Backbone dynamics of Escherichia coli ribonuclease HI: correlations with structure and function in an active enzyme.* J Mol Biol, 1995. **246**(1): p. 144-63.
5. Palmer, A.G., M. Rance, and P.E. Wright, *Intramolecular Motions of a Zinc Finger DNA-Binding Domain from Xfin Characterized by Proton-Detected Natural Abundance C-12 Heteronuclear Nmr-Spectroscopy.* Journal of the American Chemical Society, 1991. **113**(12): p. 4371-4380.
6. Cole, R. and J.P. Loria, *FAST-Modelfree: a program for rapid automated analysis of solution NMR spin-relaxation data.* J Biomol NMR, 2003. **26**(3): p. 203-13.
7. Ohnishi, M. and D.W. Urry, *Temperature dependence of amide proton chemical shifts: the secondary structures of gramicidin S and valinomycin.* Biochem Biophys Res Commun, 1969. **36**(2): p. 194-202.
8. Baxter, N.J. and M.P. Williamson, *Temperature dependence of 1H chemical shifts in proteins.* J Biomol NMR, 1997. **9**(4): p. 359-69.
9. Cierpicki, T. and J. Otlewski, *Amide proton temperature coefficients as hydrogen bond indicators in proteins.* Journal of Biomolecular Nmr, 2001. **21**(3): p. 249-261.
10. Cierpicki, T., et al., *Hydrogen bonds in human ubiquitin reflected in temperature coefficients of amide protons.* Journal of Magnetic Resonance, 2002. **157**(2): p. 178-180.
11. Doyle, C.M., et al., *Concurrent Increases and Decreases in Local Stability and Conformational Heterogeneity in Cu, Zn Superoxide Dismutase Variants Revealed by Temperature-Dependence of Amide Chemical Shifts.* Biochemistry, 2016. **55**(9): p. 1346-61.

Chapter 2 Dynamics of p53 wild type and N235K and N239Y.

p53 is a transcription factor involved in apoptosis, senescence, and DNA repair. When inactivated, cells proliferate unchecked and lead to cancerous tumor growth. Mutations in the *TP53* gene can cause inactivation of the p53 protein through a variety of mechanisms. Many of these missense mutations are disruptive due to the propensity of p53 to unfold (reviewed in [1]). The prevalence of mutated p53 in cancer has motivated researchers to find drugs that could restore function to these destabilized mutants [2, 3].

Some cancer-causing mutations in p53 can be counteracted by the introduction of additional point mutations known as rescue mutations [4]. N235K and N239Y are rescue mutations capable of restoring function to multiple prevalent p53 cancer mutants [5, 6]. This restorative ability of N235K and N239Y has motivated efforts aimed at understanding the mechanism of rescue [4, 6-10].

Both rescue mutations maintain or slightly increase the stability compared to that of wild-type p53. The stability of N235K is virtually the same as WT with a small increase in $\Delta\Delta G$ reported as 0.3 kcal mol^{-1} or less [9, 10]. The stability of N239Y has been reported to increase more substantially compared to WT with DDG of ranging from 0.9 - 1.49 kcal mol^{-1} [6, 8, 10]. The crystal structures for both rescue mutations show that the structures are virtually identical compared to the WT structure [10]. Since the crystal structures do not reveal a structural mechanism for stabilization, we hypothesize that the mode of rescue may be dynamic in nature. The DBD is comprised of 190 residues (102-292) (**Figure 2.1**). The secondary structure within p53 includes a β-sandwich with Greek key topology, two helices, and a zinc-binding region. The β-sandwich consists of two anti-parallel β-sheets

with four (S1, S3, S8, and S5) and seven (S2, S2', S4, S6, S7, S9, and S10) strands that pack against each other to form a hydrophobic core [1]. Understanding the mechanisms that stabilize the DBD structure could guide future therapeutic interventions for cancers related to p53 instability.

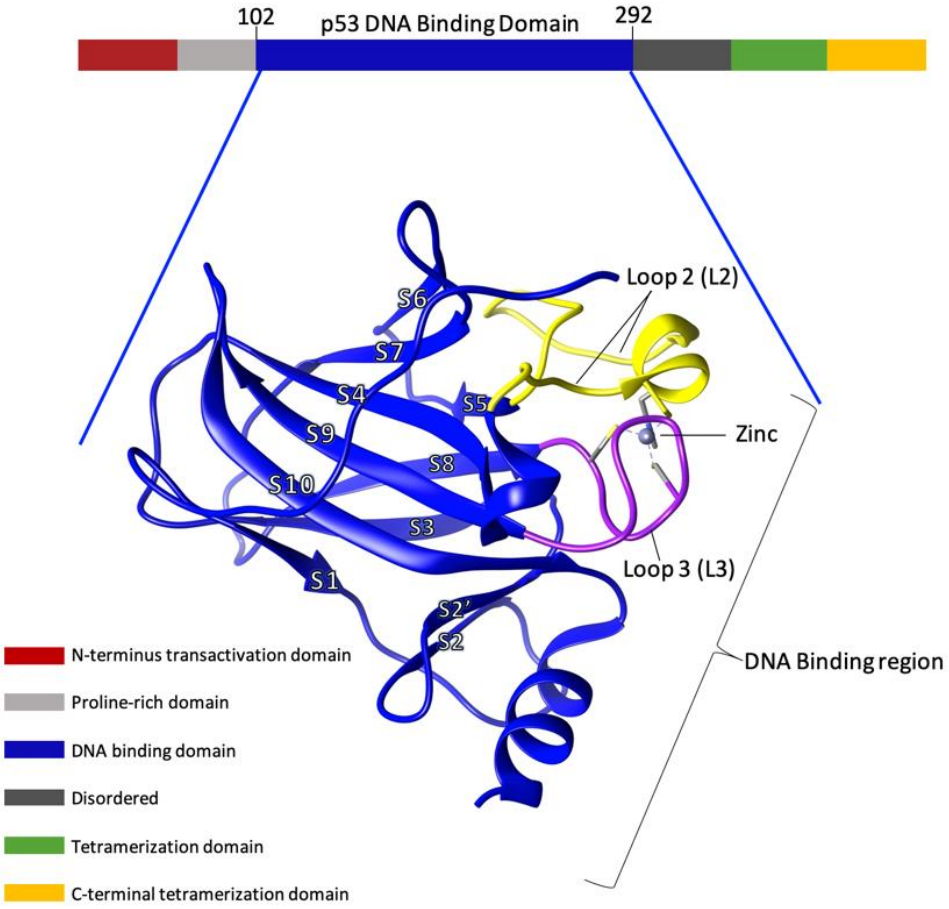

Figure 2.1: Ribbon diagram of p53 DBD. domains and, highlighted in blue, the structure of the p53 DNA-binding domain (DBD) (PDB: **2XWR)** is shown. Most cancer mutations occur in the DBD. Loop 2 (L2) and loop 3 (L3) are highlighted in yellow and purple respectively [adapted from (11)].

Molecular dynamics (MD) simulations [12] and graphical theoretical analysis of DBD crystal structures [13] show p53 cancer mutants to be more flexible than WT. Simulations have also shown that rigidity is restored by rescue mutants [12]. Most recently, an MD simulation performed by Pradhan and coworkers shows that cancer mutant

conformations undergo opening more readily compared to WT and rescue mutants [14]. This 'open' conformation is thought to expose a region of the protein that is prone to aggregation thereby promoting deleterious accumulation of p53 aggregates. It has also been suggested that p53 has evolved to be less stable than the more ancient p63 and p73 proteins as a mechanism of protein level control. Rapid degradation of p53 is believed to be enabled by enhanced rates of folding/unfolding in the cell with buried unsatisfied hydrogen bonds of polar groups playing a role in destabilizing the p53 DBD compared to p63 and p73 [1, 15]. Together these studies predict that dynamics may play a dominant role in p53 stability and consequently, ability to function.

We used solution state NMR spectroscopy to compare protein dynamics between the WT, N235K, and N239Y DBDs. We compared reversible unfolding dynamics by calculating protection factors from backbone amide hydrogen-deuterium exchange rates. In addition, we determined relaxation parameters (R1, R2, NOE) to obtain flexibility information in the ps to ns time scale. Protection factors show that both N235K and N239Y restore function by imposing a global stabilizing effect throughout the DBD. Interestingly, the distribution of amino acids stabilized by each rescue mutation are distinct: N235K strongly stabilizes the smaller sheet of the β-sandwich while N239Y results in extensive stabilization of both sheets. Relaxation data showed both rescue mutants effect dynamics of loop region across the DBD, imposing new flexibility compared to WT. We find that the effects of these suppressor mutations are far-reaching as we see changes that correlate with either more rigid or flexible local structures throughout the DBD.

Chapter 2A: p53 rescue mutations do not change the overall structure of p53.

Although the crystal structures of WT and rescue mutants are very similar (RMSD = 0.48 Å for N235K/WT and 0.39 Å for N239Y/WT, overlay in, NMR chemical shifts may reveal changes to the local environments when the protein is free in solution. To investigate if these rescue mutations change the average solution structure, we performed a chemical shift analysis of ^{1}H-^{15}N HSQC spectra. The spectra for the two p53 variants were well dispersed and our WT spectra were in excellent agreement with the published data WT p53 spectra [16] (**Figures 2.2 and 2.3).** Peak positions were compared between the published WT assignments and rescue mutant DBDs. We used 3D ^{1}H-^{15}N TOCSY and NOESY and spectra to confirm assignments in N235K and N239Y and we were able to catalog chemical shifts for 84 % and 82 % of residues, respectively. Several peaks in the mutant spectra experience a significant chemical shift because of the residue substitution **(Figure 2.3, Appendix B and C)**. We calculated the change in chemical shift ($\Delta\delta_{amide}$) of each peak on the ^{1}H-^{15}N HSQC spectra using equation (8) from Williamson 2013 [17] **(Figure 2.4)**. Overall, we found that most peaks remained relatively unchanged in both rescue mutants. N235K

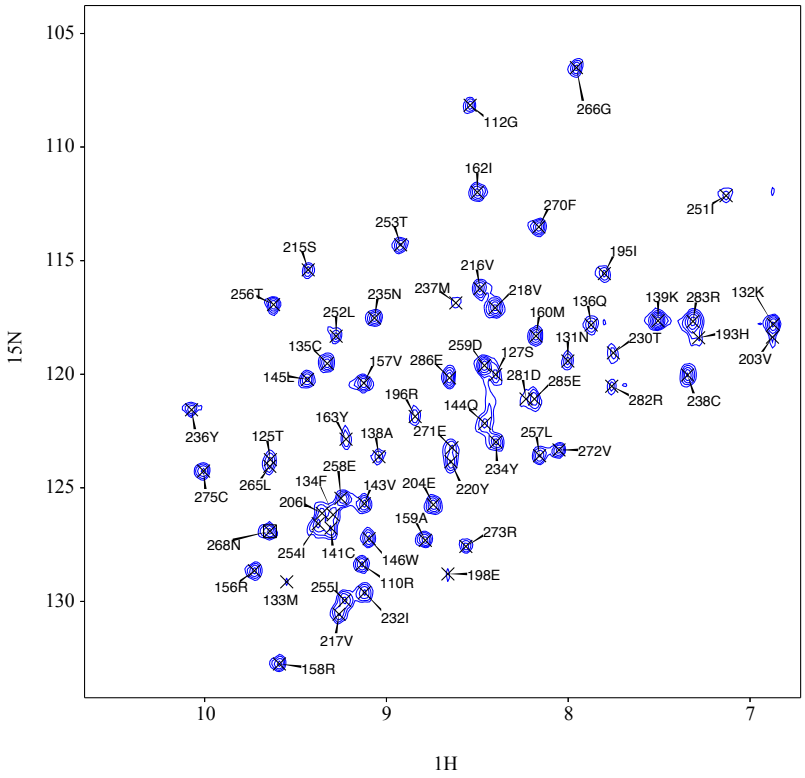

Figure 2.2. ^{1}H-^{15}N HSQC spectra of wild-type p53 16 minutes after D_2O exposure. Peak assign to the corresponding amide. WT spectra is in excellent agreement with published p53 data.

had an average $\Delta\delta_{amide}$ ± SD of 0.04 ± 0.09 ppm, and that of N239Y was 0.03 ± 0.05 ppm. The peaks with the largest chemical shift changes are located near the site of mutations, including residue 139, 141, 143, 196, 234-238 for N235K, and 139, 273, 275, 279, 235-241 for N239Y. This is expected due to the change in the local chemical environment caused by the introduction of the rescue mutation side chain. The lack of chemical shift changes further away from the mutation site suggests that N239Y retains the WT structure like what was seen in the crystal structure. In contrast, N235K has two peaks with modest chemical shift changes that are far from the site of mutation. These peaks correspond to residue 117 ($\Delta\delta_{amide}$ =0.14, 19.9 Å) and 125 ($\Delta\delta_{amide}$ = 0.16, 11.5 Å), which are near to each other in the three-dimensional structure of p53 in the vicinity of L1 and S2.

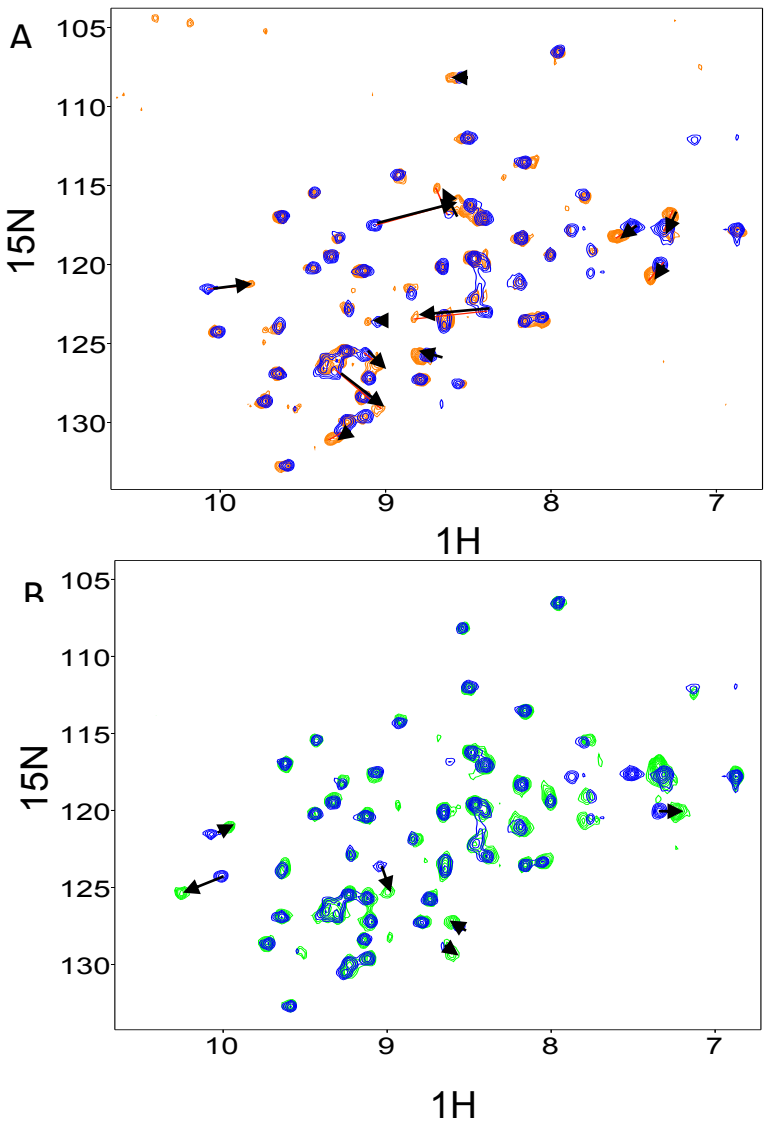

Figure 2.3: ^{1}H-^{15}N HSQC spectra of wild-type p53 (blue) overlayed with rescue mutant **A.)** N235K (orange) and B) N239Y(green). Peaks that experience significant shift are linked with arrows. All shifted peaks localized around mutation location, as expected. List of shifted peaks can be found on **Appendix C**.

Thus, N235K may impose some local structural perturbation in the proximity of this region near the DNA binding interface. In conclusion, both rescue mutants remain structurally similar in solution to p53 WT.

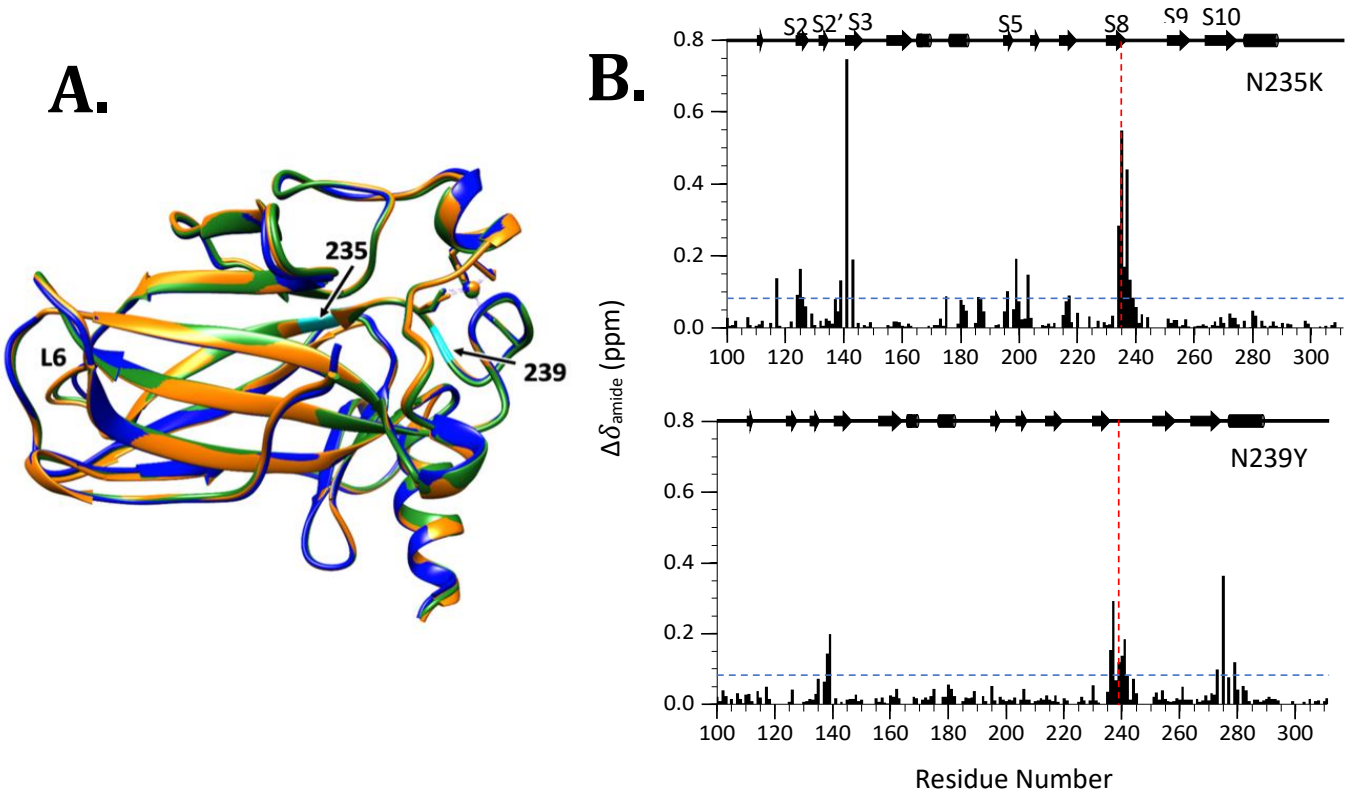

Figure 2.4 Confirming that rescue mutants do not change three-dimensional structure of p53. **A)** Overlay of p53 structures: WT (blue, PDB: **2XWR**); N235K (orange, PDB: **4LO9**); N239Y (green, PDB: **4LOE**). Crystal structure of WT and rescue mutants are superimposable suggestion that mechanism of recue is not do to structural differences. Mutation positions 235 and 239 are highlighted in cyan. Only minor changes are seen in side-chain positions near the site of mutation and in L6 in the static structures. **B)** Change in chemical shift $\Delta\delta_{amide}$ for residues in N235K (top), and N239Y (bottom) compared to WT. The diagram above illustrates secondary structure elements. Red dashed lines indicate site of mutation. Blue lines indicate changes in chemical shifts that were significant in the

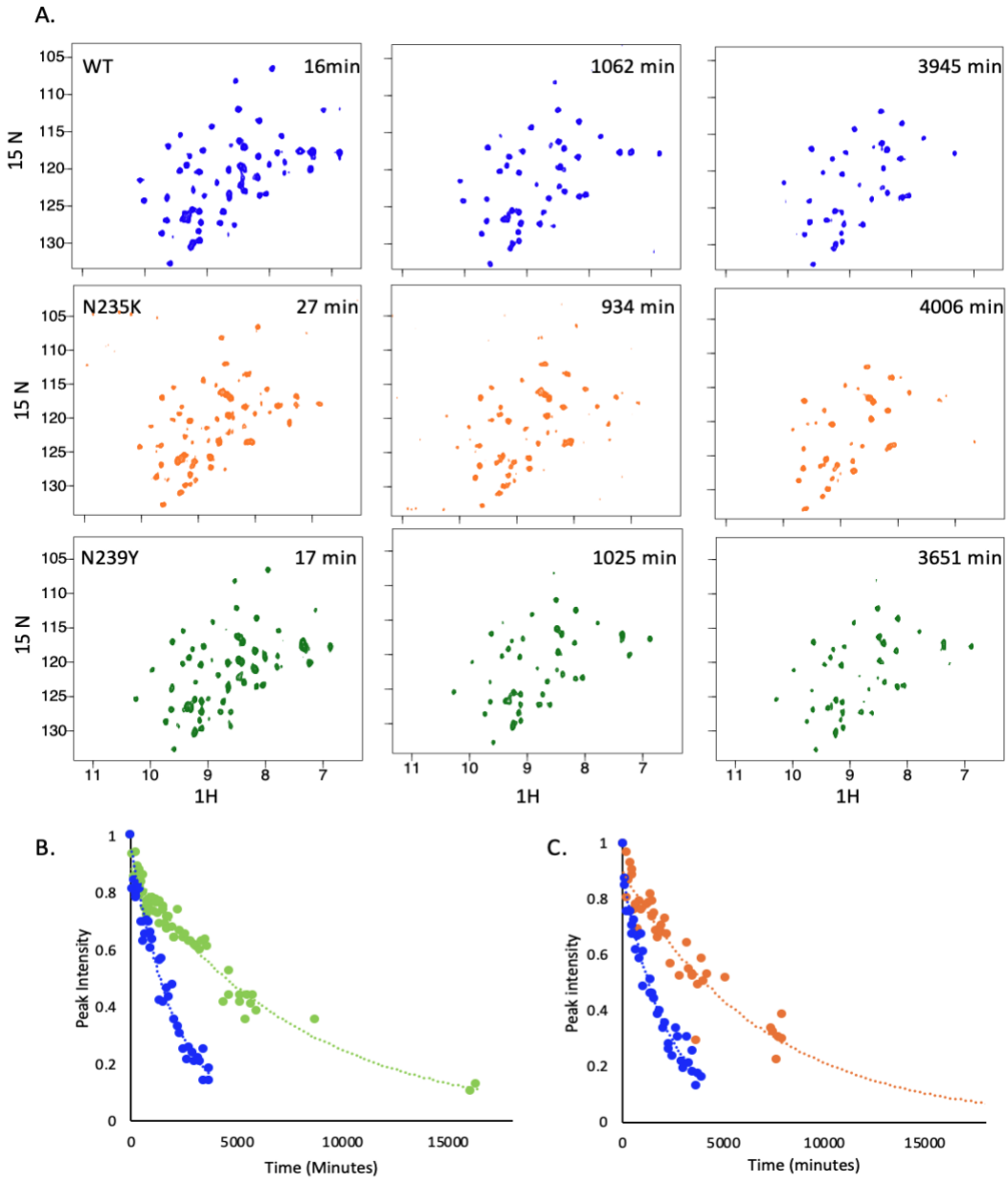

Figure 2.5 Hydrogen exchange rate for p53 (A) ^{15}N-HSQC spectra of p53 wild-type (blue), N235K (orange), and N239Y (green) at different time points after transferred into D_2O. Peaks were integrated at each time point over a period of two weeks and plotted as a function of time. Hydrogen exchange rates (k_{ex}) were calculated from a fit to a single exponential. Representative data: (**B)** 135Cys hydrogen signal intensities in N239Y (green) and WT (blue) p53 DBD. **(C)** 204Glu hydrogen signal intensities in N235K (orange) and WT (blue) p53 DBD.

Chapter 2B: Backbone dynamics of p53 via Hydrogen Exchange.

We assessed protection factors (PFs) by measuring the exchange rates of backbone amides. Since we know that WT, N235K and N239Y crystal structures are virtually superimposable and most chemical shifts are unaffected by these mutations, solvent accessibilities should be very similar. Consequently, differences in the rate of exchange should reflect the influence of the mutation on the local unfolding of that particular amide.

We determined k_{ex} by measuring peak volumes as a function of time after transfer into D_2O and fit the results to calculate the exchange rate **(Figure 2.5).** PFs were calculated by k_{rc}/k_{ex}, where k_{rc} is the exchange rate of a backbone amide in a random coil and k_{ex} is the experimental exchange rate calculated from our data. k_{rc} was calculated based on equation 2b in Bai, et. al. [18] **(Appendix D, E and F)**

Obtaining PFs for residue across the entire protein gave us a thorough understanding of the protein dynamics. Our DBD construct is composed of 218 residues (94-312), 18 of which are prolines that do not have corresponding amide hydrogen. Out of the 200 amide signals possible, ~140 backbone hydrogens exchange with the solvent (D_2O) within the dead time for this experiment (~16 minutes). We were able to obtain hydrogen-deuterium exchange rates for 54 residues of the WT, 48 residues of N235K, and 52 residues of N239Y **.** Protected residues are found throughout the secondary structures of the entire DBD in all variants (mapped onto the structure in(**Appendix G**). We calculated the average PF for the top 10 protected residues for each protein ($<PF>_{top\ 10}$). N235K had the highest $<PF>_{top\ 10}$ of 15.9×10^6, followed by N239Y with a $<PF>_{top\ 10}$ of 9.2×10^6, and lastly the WT with the lowest $<PF>_{top\ 10}$ of 5.6×10^6. Thirty-five amides were more protected in N235K than in the WT, and 45 amides had larger protection in N239Y compared to WT. Both rescue mutants protect

amides that are far from the site of mutations, including residue 156, 259, 268, and 270 for both rescue mutants, plus 206 and 259 for N235K. The magnitude of increased PF varied between the two rescue mutants **(Appendix H)**. Each rescue mutant had 18 residues with considerably higher (>2-fold) PF compared to WT. These highly protected amides are found throughout the β-sheet sandwich **(Figure 2.6)**. N235K has the most protected amide which belongs to 237, with a protection factor of 45.9 x10^6. Residue 268 was the highest protected amide for both WT and N239Y, with a protection factor of 17.0 x 10^6, and 23.6 x 10^6, respectively. In general, we found that the amides in the rescue mutations show a higher PF than the amides in WT, but the distribution is distinct for each rescue mutant.

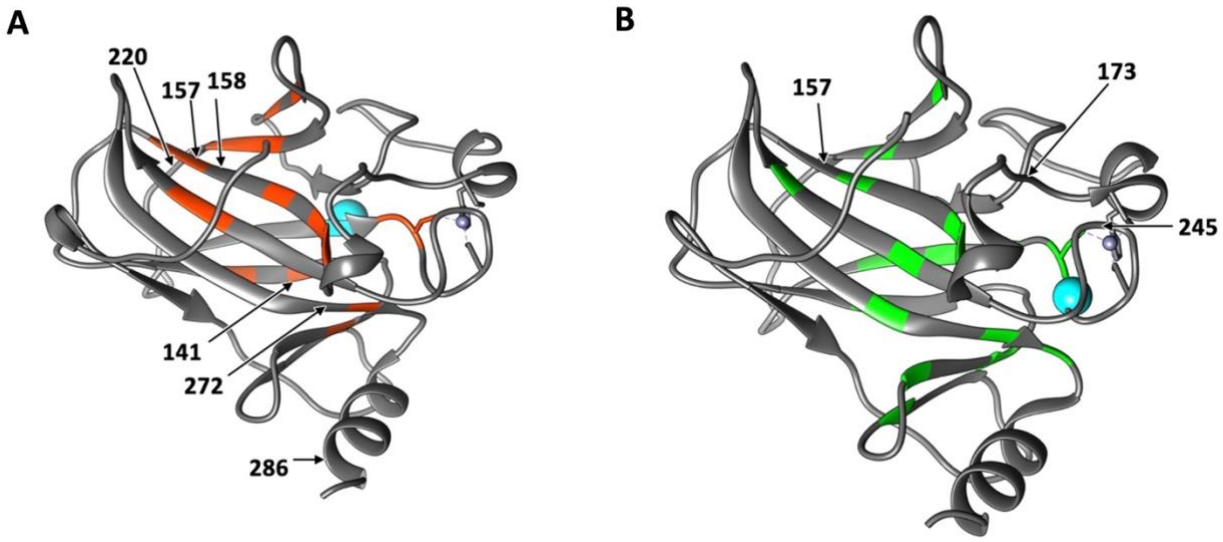

Figure 2.6 Highly protected amides in rescue mutants. Positions where PF's increase two-fold in N235K and N239Y compared to wild-type p53. **A)** 18 backbone hydrogens of N235K more resistant to exchange correspond to residues 134, 141,143, 156, 157, 160, 162, 163, 204, 206, 216, 217, 218, 237, 238, 255, 256, and 273. These residues are highlighted in orange on the structure of the N235K rescue mutation (PDB: **4LQ9**). **B)** 18-back-bone hydrogens of N239Y more resistant to exchange correspond to residues 127, 132, 135, 143, 158, 162, 163, 206, 217, 232, 234, 236, 238, 253, 257, 270, 273, and 275. The residues are highlighted in green on the structure of the N239Y rescue mutation (PDB: **4LQE**). Positions of rescue mutations are denoted by cyan spheres. Arrows point out cancer mutation positions known to be rescue by N235K and N239Y, respectively. The pattern of positions with increased protection are different between the two rescue mutants. Notably these mutants rescue different cancer mutations.

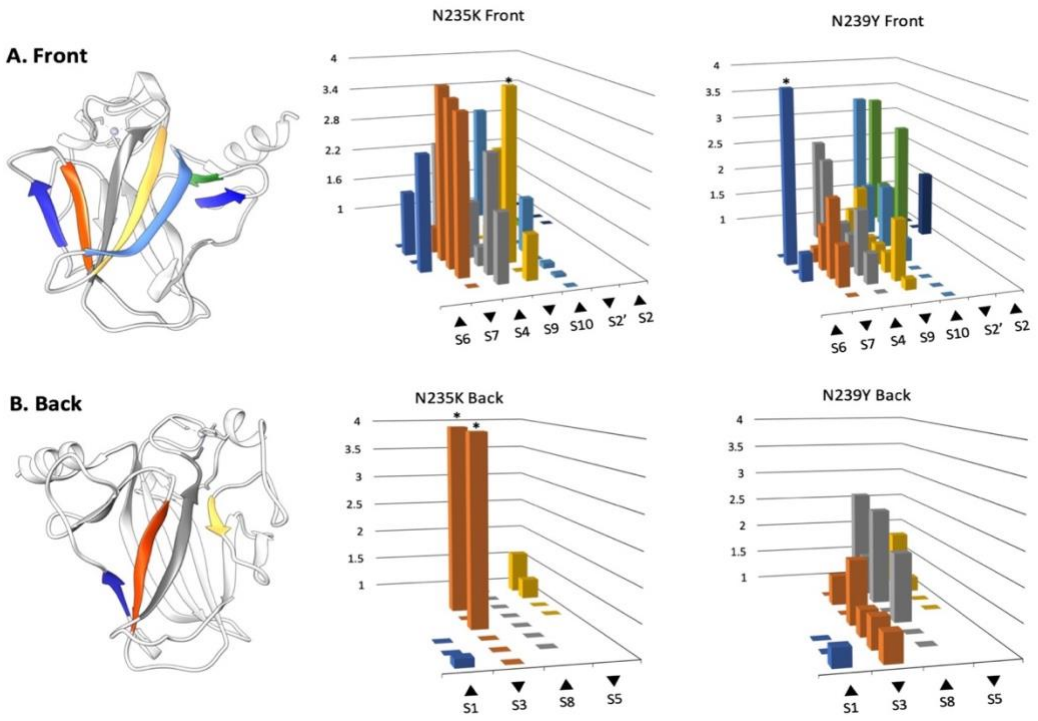

Figure 2.7: Exchange Rate Ratios, mutant/WT. Left panels show the structure of the p53 DBD with β-strands colored to correspond with PF ratios shown in right two panels. Middle and right panels show relative changes in exchange rates as a 3D bar graph representing β-stands organized by their respective position within the p53 protein. Graphs include the β-sandwich 'front' side on top **A)** (S6, S7, S4, S9, S10, S2', S2), and 'back' side on bottom **B)** (S1, S3, S8, S5). Bars with asterisks (*) have a mutant/WT ratio above 4. For N235K this includes residue 141(S3), 143(S3), 256 (S9) with ratios of 6.5, 5.4, and 4.6, respectively. For N239Y this includes residue 206 (S6) with a ratio of 30. Larger ratios correlate with a larger increase of PF (slower rate of exchange) in rescue mutants – these positions are stabilized in the mutant compared to WT.

PF ratios reveal regions of increased stability in both rescue mutants compared to WT. Although PFs are usually plotted as a function of sequence number, we found it useful to plot the ratio of PFs (mutant/WT) by secondary structure unit. **Figure 2.7** shows a 3D bar graph organized by β-strand for each β-sheet of the sandwich. We observe that N235K stability is increased on the side of the β-sandwich opposite to the mutation but only two positions on the side containing the mutation. This includes increase protection in strands S4, S6, S7 and parts of S9(254-256) and S10(265-268). We note that N235K also showed regions of decreased protection compared to WT including S3(144-146) and S8(232-236).

The same analysis was performed on N239Y; in contrast to N235K, we found that stability is increased on both sides of the β-sandwich in N239Y. All strands have residues with increased protection. In general, we observe that the rescue mutations impose long-range stability throughout the DBD; however, the patterns are distinct: N235K shows a clear trend of asymmetric stability while N239Y stability is more widely distributed throughout both sheets of the β-sandwich. Both rescue mutations maintain WT structure and enhanced DNA binding [6, 10] but prevent the unfolding of some cancer mutants compared to WT. Interestingly, the cancer mutations rescued are located throughout the DBD, in some cases far from the site of the rescue mutation (**Figure 2.6**). Here we show that rescue mutations N235K and N239Y dampen motions that lead to hydrogen-deuterium exchange in specific regions within the DBD.

Previous studies on N235K and N239Y indicate that both rescue mutations have far-reaching effects on the DBD. The mechanism by which N235K restores stability and function has been explored through molecular simulations [9] and experimental methods [10]. Both studies attribute the increase in stability to newly formed salt bridges created by the lysine substitution. Wallentine and coworkers speculate that this newly formed salt bridge is sufficient to stabilize the entire β-sandwich [10]. Our data corroborate this speculation of far-reaching stability. We found that 35 amides were more protected in N235K than in the WT; most of which are spread through the β-sandwich including six residues located 15-23 Å from the site of rescue mutation. Interestingly, the most protected amides in N235K are located on one side of the β-sandwich scaffold opposite to the site of mutation **(Figure 2.7)**. In contrast, the regions that are destabilized by the rescue mutation are found on the same

side of the β-sandwich as the mutation. Thus, N235K acts as a fulcrum in increasing rigidity in one sheet but slightly destabilizing the other. The balance of increased protection in one region and decreased in another is consistent with only a very minor increase in thermal stability observed in N235K compared to WT [9, 10]. We found increases in protection factors for N239Y were uniformly distributed on both sides of the β-sandwich **(Figure 2.7)**. This extensive protection indicates that the hydrophobic core is well stabilized and provides a rationale for the increase in thermal stability of ~ 1 kcal mol^{-1} observed in N239Y [6, 8, 10]

N235K and N239Y are both able to rescue cancer mutant V157 even though position 157 is 15 Å away from position 235, and 24 Å away from position 239 (157 is shown in **Figure 2.6**). V157F is characterized as one of the strongest β-sandwich missense mutations since it destabilizes the WT DBD by 3.6 kcal mol^{-1} [7, 9, 26]**.** It has been proposed that the substitutions of a small (valine) to a large (phenylalanine) hydrophobic residue disrupts hydrophobic packing of the DBD [26]. Our data show that both N235K and N239Y stabilize the distant region including position 157. In N235K amide 157 has a three-fold increase in PF compared to WT. In addition, 157 is found in the region of the protein that shows a clear trend of increased stability, including the surrounding strands 4, 7, and 9 **(Figure 2.7)**. A similar trend is observed in rescue mutant N239Y. The increased rigidity in this region of the DBD counteracts the destabilization caused by V157F, allowing for the restoration of function and stability. This stabilizing effect is also likely to be true for other oncogenic mutations found in the same region. Danziger and coworkers found seven cancer mutants that can be rescued by N235K; these include: C141Y, V157F, R158L, Y205C, Y220C, V272M, and E286K [24]. The effect of rescue mutations on cancer mutants at positions 157, 158 were also confirmed in other studies [10, 25]. Five of the seven rescuable cancer mutants are

found on the β-sheet of N235K that we find to have increased protection. Position 141 is also one of the cancer mutants rescued by N235K and we find it to be one of the most protected residues in N235K, significantly higher than in WT. Our hydrogen exchange results show a strong correlation between positions with increased protection from hydrogen exchange that are predictive of distant cancer mutants rescued.

WT p53 DBD is inherently prone to aggregation and amyloid formation compared to other proteins of the same family [27]. These aggregation tendencies have also been shown to be increased in cancer mutations of p53 [28, 29]. Several investigators have attributed this aggregation to transient exposure of sidechains and backbone hydrogen bonds of residues 251-257 in strand 9 (S9) [27, 29, 30]. Our results show that both rescue mutations significantly increase the stability of backbone amide hydrogen bonding in the 251-257 region of S9. N235K had an increase in protection for most residues in S9 compared to WT, except for residues 253 and 257. In N239Y all residues in this region had an increase in protection, with the largest increase in protection observed for residues 253 and 257. Thus, the pattern of protection in S9 is unique to each rescue mutation. In combination, these rescue mutations could increase the protection of the entire S9 strand. N235K and N239Y together would impose an additive protective effect that could explain the synergistic stabilization previously reported in the global rescue motifs involving both rescue mutations [5, 8, 10].

Chapter 2C: Fast dynamics of p53 investigated by Relaxation NMR.

NMR relaxation studies were performed to determine if these rescue mutants alter backbone dynamics in a fast timescale. Measurement of ^{15}N NOE, longitudinal (R1), and transverse (R2) relaxation rates were used to obtain generalized order parameters (S^2) for WT(**Appendix I**), N235K (**Appendix J**), and N239Y (**Appendix K**). Relaxation rates for some residues could not be obtained due to rapid signal decay (not enough points to fit) or significant signal overlap.

R2/R1 allows us to distinguish between fast (ps-ns) and slow (µs-s) dynamics. Residues with R2/R1 greater than the limit of one standard deviation indicate a region of slow (µs-ms) motions and those less than the limit of one standard deviation are fast (ps-ns) dynamics. Regions with slow dynamics are L6, and S10 for all variants. Additionally, both variants show signs of slow dynamics in the loop between S3-S4(147-155)

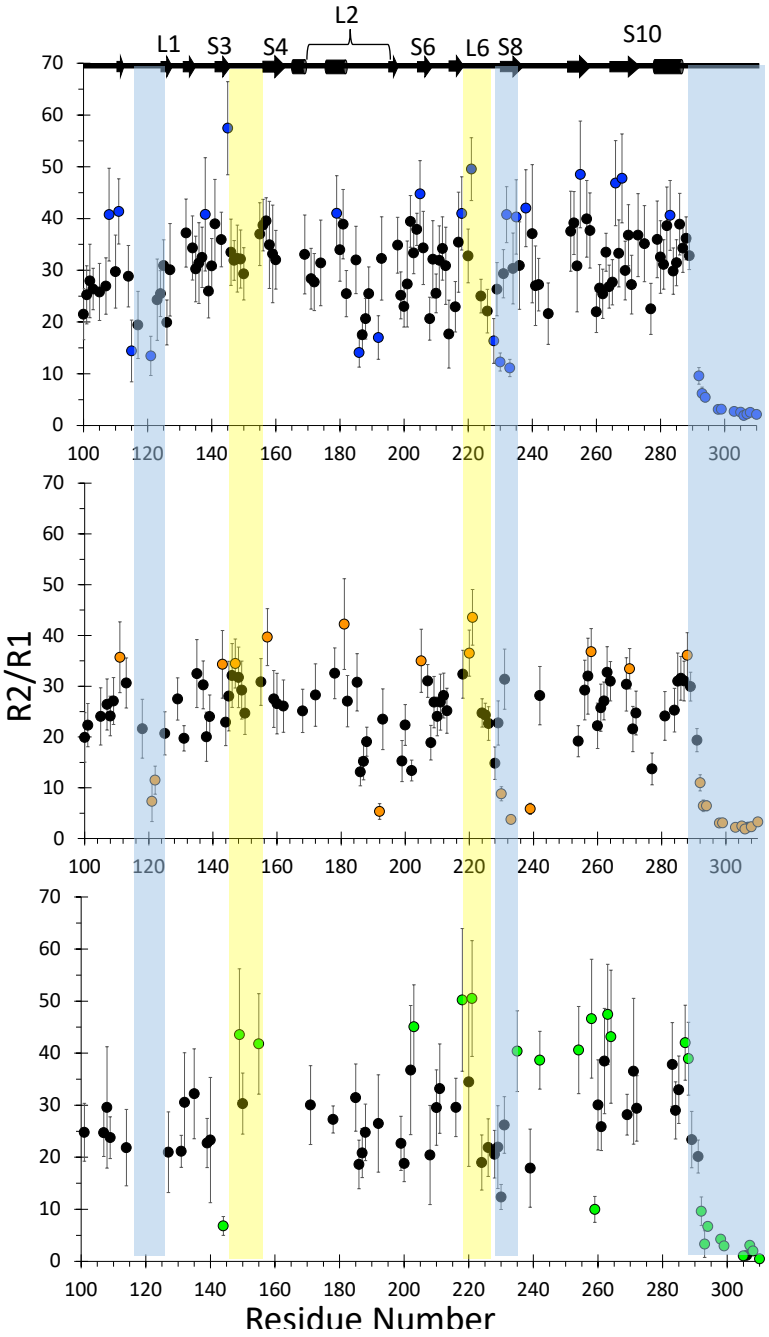

Figure 2.8. R2/R1 plot for qualitative analysis of back bone dynamics. Grey rectangles highlight mean values ± 1 SD of all R2/. Colored data points highlight the residues that are outside the mean ± 1 SD. Yellow vertical shaded rectangle highlights regions of slow dynamics (ms-ms). Similarly, blue shaded rectangle highlights regions of fast dynamics (ps-ns). Most trends are similar across all variants except for the loop between S3 and S4 were rescue mutants appear to have slowe dynamics.

(Figure 2.8). In addition, fast dynamics are observed in loop 1 , loop region immediately presiding S8, and, as expected, in the C-terminus. WT and rescue mutants share fast dynamic timescales in similar locations [19].

Order parameters allow for a more quantitative comparison of flexibility. *Modelfree* uses heteronuclear NOE, R1, R2 measurements and the protein structure to determine the backbone flexibility [20, 21]. Using the *quadric_diffusion* program [22] we found that the best fitted diffusion tensor model for all variants was an axial symmetry model. WT, N235K, and N239Y have an axially symmetric tensor ($D_{\parallel/\perp}$) of 0.29, 0.52, and 0.40 respectively. The average S2 values were 0.88 for WT, 0.85 for N235K, and 0.87 for N239Y with correlation times (τ_m) of 14.7ns for Wt, 14.1 ns for

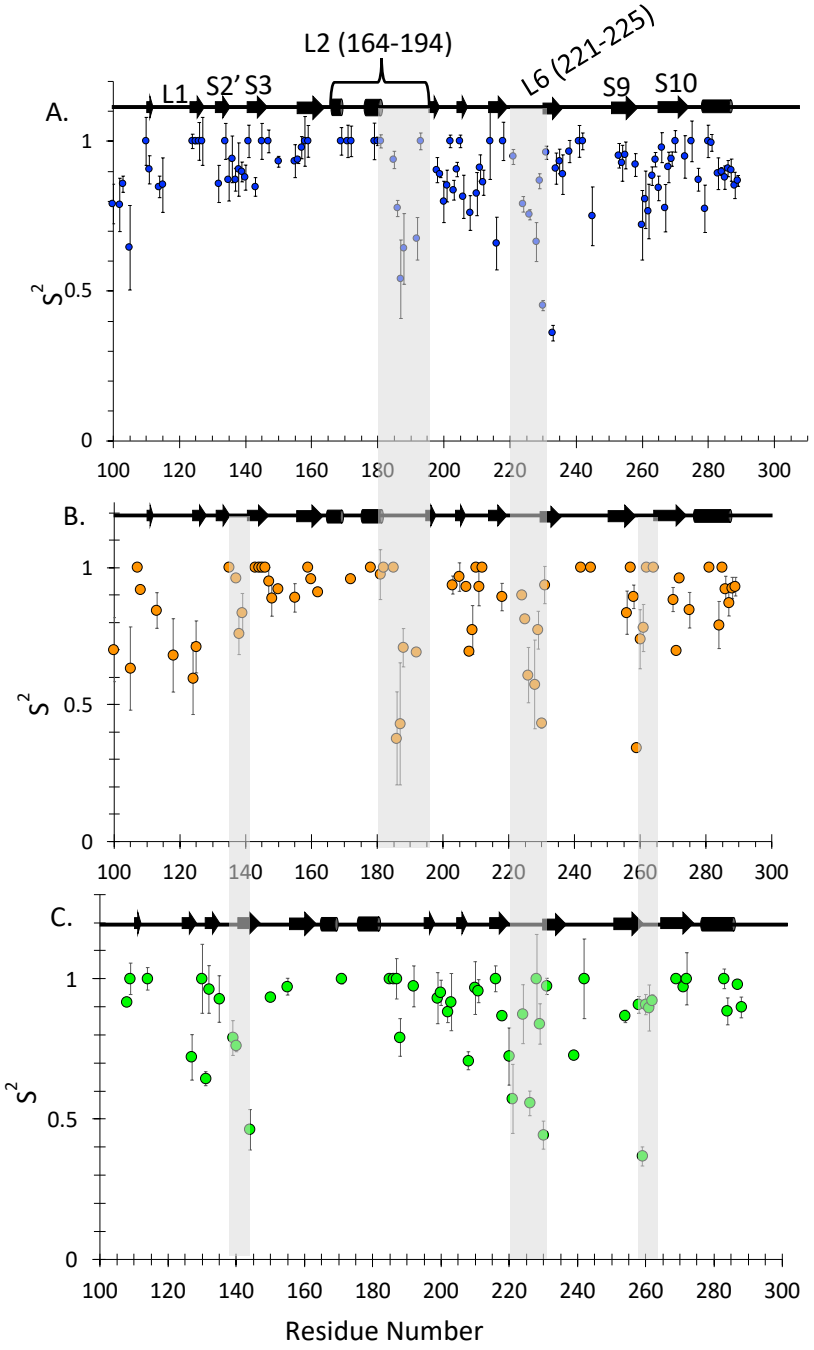

Figure 2.9: Quantitative characterization of fast dynamics. Generalized order parameter (S^2) **A)** WT**, B)**N235K, and **C)** N239Y obtained via *Modelfree* analysis (21-23) of relaxation rates R1, R2, and ^{1}H-^{15}N NOEs at 800 MHz. Grey vertical rectangles highlight regions of flexibility. All variant show dynamics in the L6. N235K, and WT show dynamics in the second part of L2. Bothe rescue mutants are more dynamics S2'-S3 and in the loop region S9-S10.

N235K, and 13.3 ns for N239Y. A plot of calculated S^2 shows that the most flexible parts are in loop regions **(Figure 2.9)**. Flexibility in L6 is conserved between all variants; however, the loop between S2'-S3 and S9-S10 shows distinct flexibility in the rescue mutants.

Both rescue mutants show increased flexibility in regions not observed in WT. S^2 values indicate that both rescue mutants have increased flexibility in S2'-S3 loop (residue 136-140) and in the S9-S10 loop (259-263) (**Figure 2.9**). These rescue mutants are near the S2'-S3 loop in the tertiary structure of the DBD. This is highlighted by the increase in chemical shift changes within the S2'-S3 loop induced by both rescue mutants (**Figure 2.4**). The proximity of this loop to the rescue mutants provides a likely explanation for the change in flexibility. Interestingly, the S^2 plots show that S2'-S3 loop of N239Y is more flexible than in the WT(**Figure 2.9**); however as discussed above, we found slower rates of hydrogen exchange for the same region. From both results, we can conclude that this part of the DNA binding interface is resistant to unfolding but the loop has increased motions in the fast timescale in N239Y. In contrast, the S9-S10 loop is far from the sites of mutation (> 24.6 Å). Chemical shift analysis does not indicate any changes to the local structure within the S9-S10 loop (**Figure 2.4**). The increased flexibility seen in S^2 values in this distant location serves as evidence of the far-reaching effects that both N235K and N239Y impose on the DBD.

Chapter 2D: Understanding the relevance of rescue mutants in nature.

To understand the prevalence of these mutations in nature we performed a comparative sequence analysis of p53 sequences in the UniProtKB/Swiss-Prot database. Using the human p53 DBD sequence to search against, we found 3117 sequences in various

species. By selecting down to 50% identity, 2670 sequences remained. Asparagine present in the human sequence is also the predominant amino acid in positions 235 (95.92%) and 239 (99.96%). Only one variant at position 239 was found: 239H substitution occurs in Chanos chanos (milkfish). In contrast, position 235 can tolerate a range of substitutions including A, K, R, S, and T. Several species of fish have a conserved serine (S) at 235 (**Figure 2.10**). Eleven species contained a K or R in their respective 235 position; most of these were mouse or rat species.

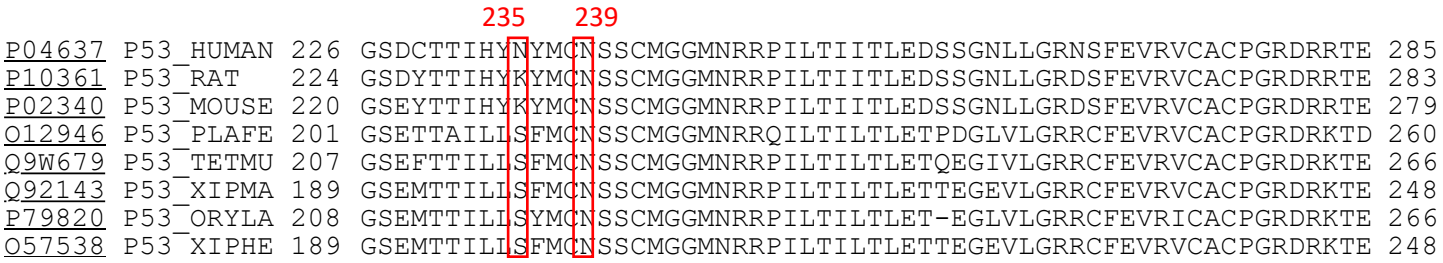

Figure 2.10 . **Comparative sequence analysis of p53 across selected species**. Protein sequence alignment in the region around 235/239 of the human p53 DBD is shown. Both rat and mouse contain a lysine (K) in their respective position 235. Other species also show variations at position 235; Lys, Arg, Ser, Thr, and Ala are found at 235 in various species. All species have a conserved asparagine (N) in position 239.

The p53 sequences of both mouse and humans have been studied and compared. They are very similar in sequence (~ 96.9% similarity) and structures (RSMD < 0.6 $Å^2$). Khoo and coworkers measured and compared the stability of p53 DBD across a wide variety of species and concluded that p53 evolved to be less stable in humans (48, 49). The fact that tyrosine is never found as a substitute at position 239 in any species may be related to the requirement that p53 be degraded easily under certain cellular conditions. N239Y is strongly stabilizing and would limit the ability for cells to regulate p53 function.

The substitution of arginine to lysine at position 235 may have played a critical role in the evolution of p53 from a more stable form in some species to less stable in humans. Our sequence analysis revealed that both mice and rats contain a lysine in the 235 position. Consequently, the stabilizing groups within the p53 fold are distributed differently in these animals compared to human p53. Since 235K is known to be more resistant to cancer mutations, animal studies of cancer using mice or rats should include the humanized p53 sequence.

Ten other positions are found to be conserved between rats and mice but different in humans. These include positions 110, 123, 133, 165, 185, 202, 210, 229 268, and 289. Out of these ten positions, three have been discovered to have stabilizing effects. These include L133, K235, D268. (4, 5, 34, 36). Interestingly, the N268D rescue mutation was discovered through sequence comparisons across species (5, 50). Given that p53s in other species are more stable, sequence comparisons could guide the discovery of future rescue mutations.

In summary, we found that both N235K and N239Y have far reaching effects on the dynamics of the DBD. These rescue mutants increase the overall folding stability of the DBD as measured by hydrogen exchange, while at the same time modifying dynamics at specific loop regions. N235K has an asymmetric stabilizing effect on the b-sandwich with one sheet stabilized while imposing enhanced flexibility in the S2'-S3 and S9-10 loops. N239Y has a stabilizing effect on both sheets of the b-sandwich, reduces flexibility on L2, while imposing the same flexibility in S2'-S3 and S9-10 loops. The change in dynamics imposed by these rescue mutants should play a critical role in their ability to rescue cancer mutants. Therapeutic interventions can be guided by pursuing drugs that can recapitulate the

dynamics of these rescue mutants. Stabilization of residues by slowing the rate of hydrogen exchange may serve as a metric in the development of anticancer drugs to block p53 unfolding and aggregation.

Material and methods:

NMR data collection and sample preparation.

WT and mutant p53 constructs were provided by Rainer Brachman. ^{15}N-labeled p53 DBDs were prepared similarly to published methods [16]. The DBD core domain of human p53 (94-312) and rescue mutants were transformed into BL21 *E. Coli* cells. Bacteria were grown at 30 °C in ^{15}N-enriched Neidharts minimal media to a density of 0.8-1.0 $OD_{(550\ nm)}$. The temperature was lowered to 18 °C and both IPTG and ZnCl2 were added to a final concentration of 1 mM. Cells were allowed to grow for an additional 6-8 hours and then harvested by centrifugation and frozen. The frozen cell pellet was resuspended in 20mM sodium phosphate, pH7.2, 10 mM BME, 0.5 mM PMSF, and lysed using sonication. Cell debris were removed by centrifugation at 4 °C for 30 minutes. The supernatant was applied to a SP-sepharose column and the protein eluted with a gradient of 100 mM - 600mM NaCl. In some cases, additional purification using a Superdex-75 gel filtration column was performed. Samples were dialyzed into 150 mM potassium chloride, 25 mM sodium phosphate, pH 7.1, 10 mM BME and concentrated to a protein concentration of 300-400 μM. 0.5 mM DSS was added as a chemical shift reference.

All NMR experiments were performed on Varian Inova 800 MHz at 20 ^{o}C. NMR data were processed using nmrPipe [36]. Residues assignments and rate measurements (using peak volumes) in all 2D HSQC spectra were accomplished using CcpNmr Analysis [37].

3D ^{15}N-TOCSY-HSQC (t_{mix} = 75 ms) and NOESY-HSQC (t_{mix} = 100 ms) [38] were analyzed for assignment of backbone amide resonances. Published WT assignments [16] were confirmed in our WT sample and these were compared to spectra of N235K and N239Y.

Hydrogen-deuterium exchange experiments were performed with 550 ml samples that were lyophilized and fully suspended into an equivalent volume 99.9% D_2O immediately before data collection (~16 min after initiation of exchange). Since our intent is to compare exchange rates for the most stable positions between WT and two mutants, we chose lyophilization as the technique to transfer protein into D_2O to ensure that all samples would have the same final conditions (*e.g.,* [HDO]). Two-dimensional ^{1}H-^{15}N heteronuclear single quantum coherence (HSQC) NMR spectrum were recorded for each sample every 70 minutes for 24 hours, and then every 180 minutes for 48 hours at 20 ^{o}C. HSQC spectra were collected over a period of one month. ^{1}H spectra were also collected for S/N calibration using the DSS signal. Sealed samples were stored in a water bath at 20 ^{o}C when not in the magnet. Fresh protein samples had an absorbance at 400 nm of 0.05 or less. During the exchange experiment, samples were assessed for aggregation by light scattering and were no longer used if the absorption at 400 nm exceeded 0.1.

Calculation of chemical shift changes,

$\Delta\delta_{amide}$ was calculated using the changes in chemical shift of ^{1}H and ^{15}N according to the following equation from Williamson 2013 [17]:

$$\Delta\delta_{\text{amide}} = \sqrt{\frac{1}{2}[\delta_H^2 + (\alpha \cdot \delta_N^2)]}$$

Where δ_H is the change in chemical shift of ^{1}H and δ_N is the change in chemical shift of ^{15}N between WT and rescue mutant. α is the nitrogen scaling factor of 0.14. Residues were considered to have a significant change in chemical shift if they had a $\Delta\delta_{amide} > 0.075$ (blue dashed line in **Figure 2.4**). Value 0.075 was calculated by using $\delta_H = 0.05$ and $\delta_N = 0.25$, consistent with a previous analysis of p53 mutants [16].

Relaxation analysis.

^{15}N longitudinal T1, transverse T2 relaxation and NOEs were measured using pulse sequences of Farrow, et al [39]. Spectra were recorded with relaxation delays of 10, 50, 100, 200, 400, 750, 1000, 1500 ms for T1 and 10, 30, 50, 70, 90, 110, 130, 150 ms for T2. T1 and T2 times were scrambled during acquisition and 10 ms time spectra were recorded at the beginning and end of both T1 and T2 experiments to confirm S/N had not changed. NOE spectra were recorded with a 5-second irradiation and a 3-second delay. R1 and R2 rates were obtained by measuring peak volume as a function of delay time and fitting them to a single exponential function with CcpNmr software [37]. Errors in relaxation rates were obtained through the covariance method in CcpNmr.

NMR S^2 were calculated by using *Modelfree 4.15* [20, 21] in combination with *FASTModelfree* [40]. Initial estimation of *Modelfree* parameters was obtained through the programs *pdbinertia*, *r2r1_tm*, *quadric_diffusion* provided on the CoMD/NMR website [41]. Residues with NOE and C^2 values less than 0.6 and 10, respectively, were excluded from *quadric_diffusion* calculation. We found no significant difference for S^2 results whether *Modelfree analysis* is performed with crystal or NMR structure files (**Appendix N**). Our final analysis used the Protein Data Bank (PDB) file **2FEJ** for all p53 variants. All *FASTModelfree* analyses used an NH bond length of 1.015 Å and chemical shift entropy (CSA) value of -179

ppm [42] to allow us to compare to published analysis of WT p53 DBD measured at 600 MHz [see figure in 3 [43]]. *FASTModelfree* analysis proceeded until all parameters converged.

Sequence analysis.

The Uniprot database [44] was utilized to select and align p53 sequences from different species. Calculations of sequence identities/similarities were accomplished through the ExPASy alignment program [45].

Protein structure analysis.

UCSF Chimera [46] was used for protein visualization and analysis. Residue distances were calculated by measuring the distance between alpha carbons. Surface area accessibility was calculated with the areaSAS attribute tool from Chimera using amide hydrogens selected from NMR p53 DBD structure **2FEJ**.

Acknowledgements

Funding was provided by the California Cancer Research Coordinating Committee (CRCC9-550862-36240); UCI ACS-IRG award; and NIH-IMSD training grant GM055246.°

References

1. Joerger, A.C. and A.R. Fersht, *Structural biology of the tumor suppressor p53.* Annu Rev Biochem, 2008. **77**: p. 557-82.
2. Joerger, A.C. and A.R. Fersht, *Structure-function-rescue: the diverse nature of common p53 cancer mutants.* Oncogene, 2007. **26**(15): p. 2226-42.
3. Bykov, V.J. and K.G. Wiman, *Mutant p53 reactivation by small molecules makes its way to the clinic.* FEBS Lett, 2014. **588**(16): p. 2622-7.
4. Bullock, A.N. and A.R. Fersht, *Rescuing the function of mutant p53.* Nat Rev Cancer, 2001. **1**(1): p. 68-76.
5. Baroni, T.E., et al., *A global suppressor motif for p53 cancer mutants.* Proc Natl Acad Sci U S A, 2004. **101**(14): p. 4930-5.
6. Nikolova, P.V., et al., *Semirational design of active tumor suppressor p53 DNA binding domain with enhanced stability.* Proc Natl Acad Sci U S A, 1998. **95**(25): p. 14675-80.
7. Bullock, A.N., J. Henckel, and A.R. Fersht, *Quantitative analysis of residual folding and DNA binding in mutant p53 core domain: definition of mutant states for rescue in cancer therapy.* Oncogene, 2000. **19**(10): p. 1245-56.
8. Nikolova, P.V., et al., *Mechanism of rescue of common p53 cancer mutations by second-site suppressor mutations.* EMBO J, 2000. **19**(3): p. 370-8.
9. Tan, Y.H., et al., *Molecular mechanisms of functional rescue mediated by P53 tumor suppressor mutations.* Biophys Chem, 2009. **145**(1): p. 37-44.
10. Wallentine, B.D., et al., *Structures of oncogenic, suppressor and rescued p53 core-domain variants: mechanisms of mutant p53 rescue.* Acta Crystallogr D Biol Crystallogr, 2013. **69**(Pt 10): p. 2146-56.
11. Ang, H.C., et al., *Effects of common cancer mutations on stability and DNA binding of full-length p53 compared with isolated core domains.* J Biol Chem, 2006. **281**(31): p. 21934-41.
12. Demir, O., et al., *Ensemble-based computational approach discriminates functional activity of p53 cancer and rescue mutants.* PLoS Comput Biol, 2011. **7**(10): p. e1002238.
13. Rauf, S.M.A., et al., *A graph theoretical approach to the effect of mutation on the flexibility of the DNA binding domain of p53 protein.* Chemical Papers, 2009. **63**(6): p. 654-661.
14. Pradhan, M.R., et al., *Simulations of mutant p53 DNA binding domains reveal a novel druggable pocket.* Nucleic Acids Res, 2019. **47**(4): p. 1637-1652.
15. Canadillas, J.M., et al., *Solution structure of p53 core domain: structural basis for its instability.* Proc Natl Acad Sci U S A, 2006. **103**(7): p. 2109-14.
16. Wong, K.B., et al., *Hot-spot mutants of p53 core domain evince characteristic local structural changes.* Proc Natl Acad Sci U S A, 1999. **96**(15): p. 8438-42.
17. Williamson, M.P., *Using chemical shift perturbation to characterise ligand binding.* Prog Nucl Magn Reson Spectrosc, 2013. **73**: p. 1-16.
18. Bai, Y., et al., *Primary structure effects on peptide group hydrogen exchange.* Proteins, 1993. **17**(1): p. 75-86.

19. Barros, E.P., et al., *Markov State Models and NMR Uncover an Overlooked Allosteric Loop in p53.* Chemical Science, 2021.
20. Palmer, A.G., M. Rance, and P.E. Wright, *Intramolecular Motions of a Zinc Finger DNA-Binding Domain from Xfin Characterized by Proton-Detected Natural Abundance C-12 Heteronuclear Nmr-Spectroscopy.* Journal of the American Chemical Society, 1991. **113**(12): p. 4371-4380.
21. Mandel, A.M., M. Akke, and A.G. Palmer, *Backbone Dynamics of Escherichia-Coli Ribonuclease Hi - Correlations with Structure and Function in an Active Enzyme.* Journal of Molecular Biology, 1995. **246**(1): p. 144-163.
22. Spectroscopy, C.o.M.D.b.N. *Tutorials at CoMD/NMR and NYSBC*. 2019; Available from: http://comdnmr.nysbc.org/comd-nmr-educ.
23. Brachmann, R.K., et al., *Genetic selection of intragenic suppressor mutations that reverse the effect of common p53 cancer mutations.* EMBO J, 1998. **17**(7): p. 1847-59.
24. Danziger, S.A., et al., *Choosing where to look next in a mutation sequence space: Active Learning of informative p53 cancer rescue mutants.* Bioinformatics, 2007. **23**(13): p. i104-14.
25. Baronio, R., et al., *All-codon scanning identifies p53 cancer rescue mutations.* Nucleic Acids Res, 2010. **38**(20): p. 7079-88.
26. Cho, Y., et al., *Crystal structure of a p53 tumor suppressor-DNA complex: understanding tumorigenic mutations.* Science, 1994. **265**(5170): p. 346-55.
27. Cino, E.A., et al., *Aggregation tendencies in the p53 family are modulated by backbone hydrogen bonds.* Sci Rep, 2016. **6**: p. 32535.
28. Ano Bom, A.P., et al., *Mutant p53 aggregates into prion-like amyloid oligomers and fibrils: implications for cancer.* J Biol Chem, 2012. **287**(33): p. 28152-62.
29. Gaiddon, C., et al., *A subset of tumor-derived mutant forms of p53 down-regulate p63 and p73 through a direct interaction with the p53 core domain.* Mol Cell Biol, 2001. **21**(5): p. 1874-87.
30. Xu, J., et al., *Gain of function of mutant p53 by coaggregation with multiple tumor suppressors.* Nat Chem Biol, 2011. **7**(5): p. 285-95.
31. Butler, J.S. and S.N. Loh, *Structure, function, and aggregation of the zinc-free form of the p53 DNA binding domain.* Biochemistry, 2003. **42**(8): p. 2396-403.
32. Butler, J.S. and S.N. Loh, *Zn(2+)-dependent misfolding of the p53 DNA binding domain.* Biochemistry, 2007. **46**(10): p. 2630-9.
33. Ouaray, Z., et al., *Reactivation of mutant p53: Constraints on mechanism highlighted by principal component analysis of the DNA binding domain.* Proteins, 2016. **84**(10): p. 1443-61.
34. Lukman, S., D.P. Lane, and C.S. Verma, *Mapping the structural and dynamical features of multiple p53 DNA binding domains: insights into loop 1 intrinsic dynamics.* PLoS One, 2013. **8**(11): p. e80221.
35. Lu, Q., Y.H. Tan, and R. Luo, *Molecular dynamics simulations of p53 DNA-binding domain.* Journal of Physical Chemistry B, 2007. **111**(39): p. 11538-11545.
36. Delaglio, F., et al., *NMRPipe: a multidimensional spectral processing system based on UNIX pipes.* J Biomol NMR, 1995. **6**(3): p. 277-93.

37. Vranken, W.F., et al., *The CCPN data model for NMR spectroscopy: development of a software pipeline.* Proteins, 2005. **59**(4): p. 687-96.
38. Muhandiram, D.R. and L.E. Kay, *Gradient-enhanced triple-resonance three-dimensional NMR experiments with improved sensitivity.* . J. Magn. Reson., Ser. B, 1994. **103**: p. 203-216.
39. Farrow, N.A., et al., *Characterization of the backbone dynamics of folded and denatured states of an SH3 domain.* Biochemistry, 1997. **36**(9): p. 2390-402.
40. Cole, R. and J.P. Loria, *FAST-Modelfree: A program for rapid automated analysis of solution NMR spin-relaxation data.* Journal of Biomolecular Nmr, 2003. **26**(3): p. 203-213.
41. Lee, L.K., et al., *Rotational diffusion anisotropy of proteins from simultaneous analysis of 15N and 13Cα nuclear spin relaxation.* Journal of Biomolecular NMR, 1997. **9**: p. 287-298.
42. Yao, L., et al., *Site-specific backbone amide (15)N chemical shift anisotropy tensors in a small protein from liquid crystal and cross-correlated relaxation measurements.* J Am Chem Soc, 2010. **132**(12): p. 4295-309.
43. Rasquinha, J.A., et al., *Intrinsic Differences in Backbone Dynamics between Wild Type and DNA-Contact Mutants of the p53 DNA Binding Domain Revealed by Nuclear Magnetic Resonance Spectroscopy.* Biochemistry, 2017. **56**(37): p. 4962-4971.
44. UniProt, C., *UniProt: a worldwide hub of protein knowledge.* Nucleic Acids Res, 2019. **47**(D1): p. D506-D515.
45. Artimo, P., et al., *ExPASy: SIB bioinformatics resource portal.* Nucleic Acids Res, 2012. **40**(Web Server issue): p. W597-603.
46. Pettersen, E.F., et al., *UCSF Chimera--a visualization system for exploratory research and analysis.* J Comput Chem, 2004. **25**(13): p. 1605-12.

Chapter 3: Dynamics of the Bypass Polymerase, DinB homolog (Dbh).

DinB homolog polymerase (Dbh) is produced by the thermophilic Archaea *Sulfolobus acidocaldarius* (*S. acidocaldarius*), therefore it is important to understand the effects of temperatures on Dbh. *S. acidocaldarius* grows optimally at temperatures close to 75 - 80 °C and pH values between 2-4 [1] [2]. To adapt to extremely acidic environments, extremophiles possess efficient mechanisms to maintain homeostasis, such as proton pumps [3]. However, microorganisms do not have the ability to regulate cell temperature. Consequently, microorganisms require proteins adapted to function in extremely high temperatures. This thermal stability is prevalent in Dbh which has been shown to remain structurally and functionally sound up to 65 °C [4].

The function and efficiency of Dbh are known to be modulated by changes in temperature. This was clearly revealed in a primer extension study that showed that Dbh efficiency increases as temperature increased from 22 °C to 65 °C [4]. Furthermore, *in vivo* studies conducted under physiological temperatures (70-80 °C) for *S. acidocaldarius* Dbh reveal that the enzyme imposes a three base-pair frameshift on triple repeats of Sacp*yrE* and Sso*pyrE* which has never been observed in *in vitro* studies [5] which are not frequently performed at physiological conditions. Since the activity of Dbh is largely dependent on temperature changes we set out to understand how temperature influences Dbh dynamics, tertiary, and secondary structures. In addition, we explored how metal ions bind Dbh in solution and in the absence of DNA.

Dbh is a Y-family polymerase. The Y-family polymerase can synthesize across damaged DNA templates but with high error rates limited by fast off-rates[6]. Compared to

other families of polymerase Y-family polymerase replicates undamaged DNA with an error rate 10 – 100 fold higher [7] [8] [9] [10]. Despite being phylogenetically unrelated to other families of polymerase their structure can be likened to a right-hand conformation found in most polymerase, with the additions of a unique N-terminus refer to as the wrist or other various names (discussed below) (**Figure 3.1**). Polymerases are complex molecular machinery highly dependent on dynamics to perform their functions that include binding substrates, synthesis, and translocation. Although the three-dimensional structure has been studied by several groups, the dynamics of Dbh have not been thoroughly explored.

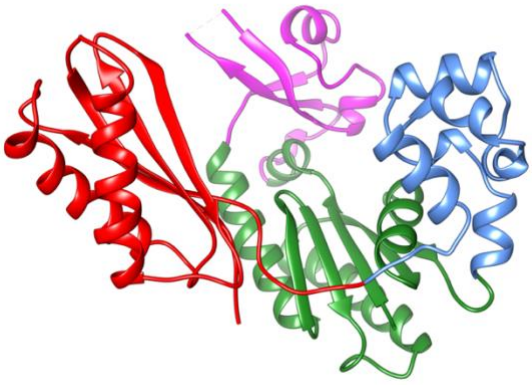

Figure 3.1 The ribbon diagram of Dbh polymerase. Fingers domain (residue 20-35, 39-77: magenta), thumb domain (residue 172-236; cornflower blue), palm domain (1-19, 78-171; green), and wrist (residues 237-344; red).

The fact that Dbh crystallizes readily has facilitated the study of several static structures [11] [12] [13]and biochemical characterizations [14] [13] [15]. The first structures of Dbh were reported by Bo-Lu Zhou et al. [11], and Laura F. Silvian et al.[12]. Initially, these structures were reported to derive from *Sulfolobus solfataricus* (now *Saccharolobus solfataricus* [16]), however, through genomic sequencing it was discovered that they belong to *S. acidocaldarius* [14] [17] [18]. To prevent confusion the Dbh protein sequence studied here is identical to UniProt accessions P96022 and Q4JB80 [19]. With the distinction that this protein sequence contains a cystine to serine mutation on residue 31 to facilitate protein study at high concentrations without the risk of dimerization. The entirety

of this work used the mutated form of Dbh. The crystal structures revealed that Dbh is composed of a catalytic core that includes the finger domain, palm domain, and thumb domain (**Figure 3.1**). In addition, the core structure is connected to the little finger domain (LF) by an unstructured linker. This domain has been referred to by many names. It has been described as the LF in archaeal and bacterial [20] and the wrist domain[12], or Polymerase-associated domain (PDA) in eukaryotic Y-family polymerase [21]. For the remainder of this chapter this domain will be refer to as LF.

At this time, seven crystal structures of Dbh exist with only one study showing Dbh interacting with a metal ion (calcium) bound to the active site [13]. However, multiple related Y-family polymerases have been solved with two magnesium (Mg^{2+}) in the active site [22] [6]. Notably these ions are always present when the structures are solved with DNA. As far as we know it has never been shown that Dbh binds multiple ions in the absence of DNA. Moreover, despite all the detailed structure data available on Dbh we still lack a good understanding of the dynamics of Dbh.

Most of the information on Y-family polymerase dynamics has originated from a related polymerase known as Dpo4, which has been studied to a greater extent. Dpo4 has over 90 crystal structures, and multiple MD simulations [23, 24] [25] [26] compared to Dbh with only seven crystal structures and no simulations. Dpo4 has been studied in multiple states which has allowed researchers to implement MD simulation to understand the dynamics of Dpo4. MD simulations have shown that Dpo4 remains conformational dynamics even after binding DNA [25]. Some of these dynamics may translate to Dbh but considering that Dbh and Dpo4 are only 54 % identical [14] it may be that Dbh has unique

dynamic features consistent with the rate of reaction where Dbh is slower (k_p = 0.64 s^{-1} at 25°C) [27] than Dpo4(k_p = 6.4 s^{-1} at 26 °C) [28], and consistent with fidelity where Dbh has higher fidelity than Dpo4 [14]. Furthermore, these MD simulation studies conducted with Dpo4 in complex with DNA do not address the issue of temperature. Changes in temperature can have a large effect on the dynamics and function of Dbh. For example, it has been shown that changes in temperature affect the rate of opening and closing of other thermally stable polymerases such as *Thermus aquaticus* DNA polymerase [29]. In addition, we know that Dbh function is enhanced by increasing the temperature [4]. To truly understand Dbh dynamics we must first study it alone, in solution, and at a wide range of temperatures (2-65 °C).

To understand how Dbh dynamics are affected by temperature we implement solution-state NMR spectroscopy, circular dichroism (CD), at a range of temperatures (2 °C - 65 °C). In addition, we performed, chemical shift changes of ^{1}H-^{15}N HSQC of DBH in the presence and absence of magnesium (Mg^{2+}) and manganese (Mn^{2+}). To our knowledge, this is the first study to report Dbh directly interacting with Mg^{2+} and Mn^{2+}.

Chapter 3A: Understanding how temperature affects DBH structure.

To determine if Dbh maintains its tertiary structure between 35 and 65 °C we obtained ^{1}H-^{15}N HSQC spectra at 35 °C, 45 °C, 55 °C, and 65 °C. All spectra remained well dispersed and relatively similar across this range of temperatures (**Figure 3.2**). We did observe the normal phenomena of temperature dependent chemical shift changes as temperature increase [30]. We used this temperature dependent chemical shift to calculate TC (discussed later) to determine unfolding sensitivity to temperature changes. The

retention of well dispersed spectra at temperatures ranging between 35-65 °C informs us that Dbh retains a well folded tertiary structure throughout this range of temperatures.

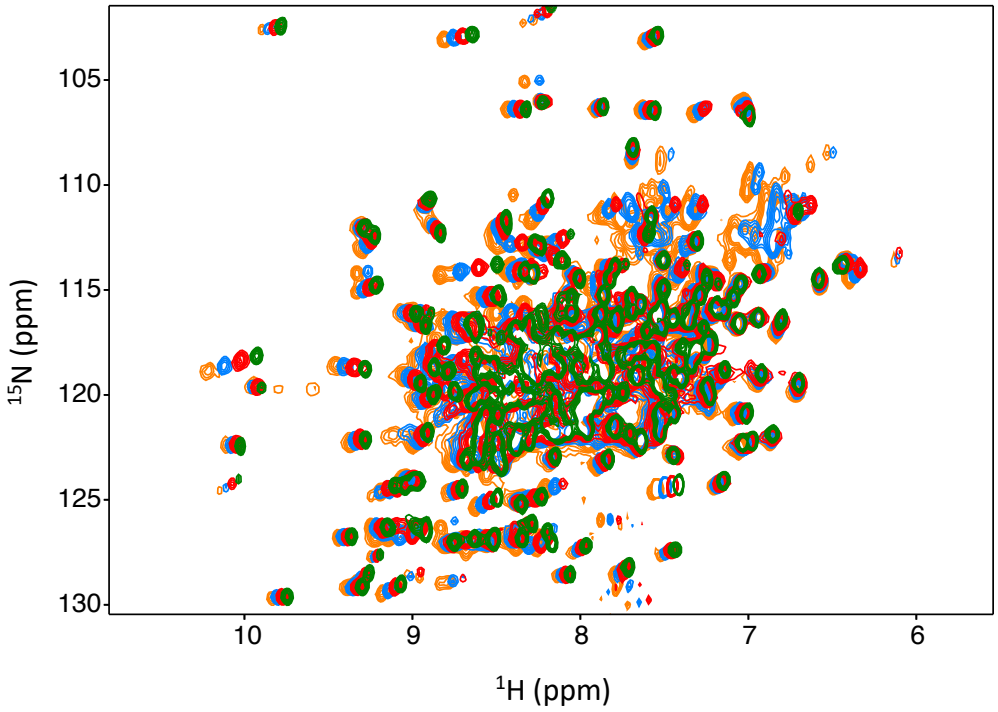

Figure 3.2 Dbh is structurally stable at 35-65 °C. ^{1}N-^{15}N HSQC of Dbh at 35 ° C (orange), 45 °C (blue), 55 °C (red), 65 °C (green). Spectra do not exhibit drastic changes at this range of temperatures. The constant well dispersed spectra tell us that Dbh remains structurally similar across these temperatures. The shifting of ^{1}H peaks (X-axis) are normally shifted with temperature. We analyze the extent of the shift to obtain Temperature Coefficient.

We find that Dbh undergoes cold denaturation of tertiary structure below 25 °C**.** Cold denaturation is a phenomenon that all proteins experience, however, it is extremely rare for it to occur above the freezing point of water (0 °C) [31]. We obtained ^{1}H-^{15}N HSQC at cold temperatures 5 - 25 °C. ^{1}H-^{15}N HSQC spectra show a change of tertiary structures starting at 25 °C and progressing as temperatures get colder (15 °C, 5 °C) (**Figure 3.3).** To determine if this is a complete loss of structure, we assessed CD spectra. CD is sensitive to

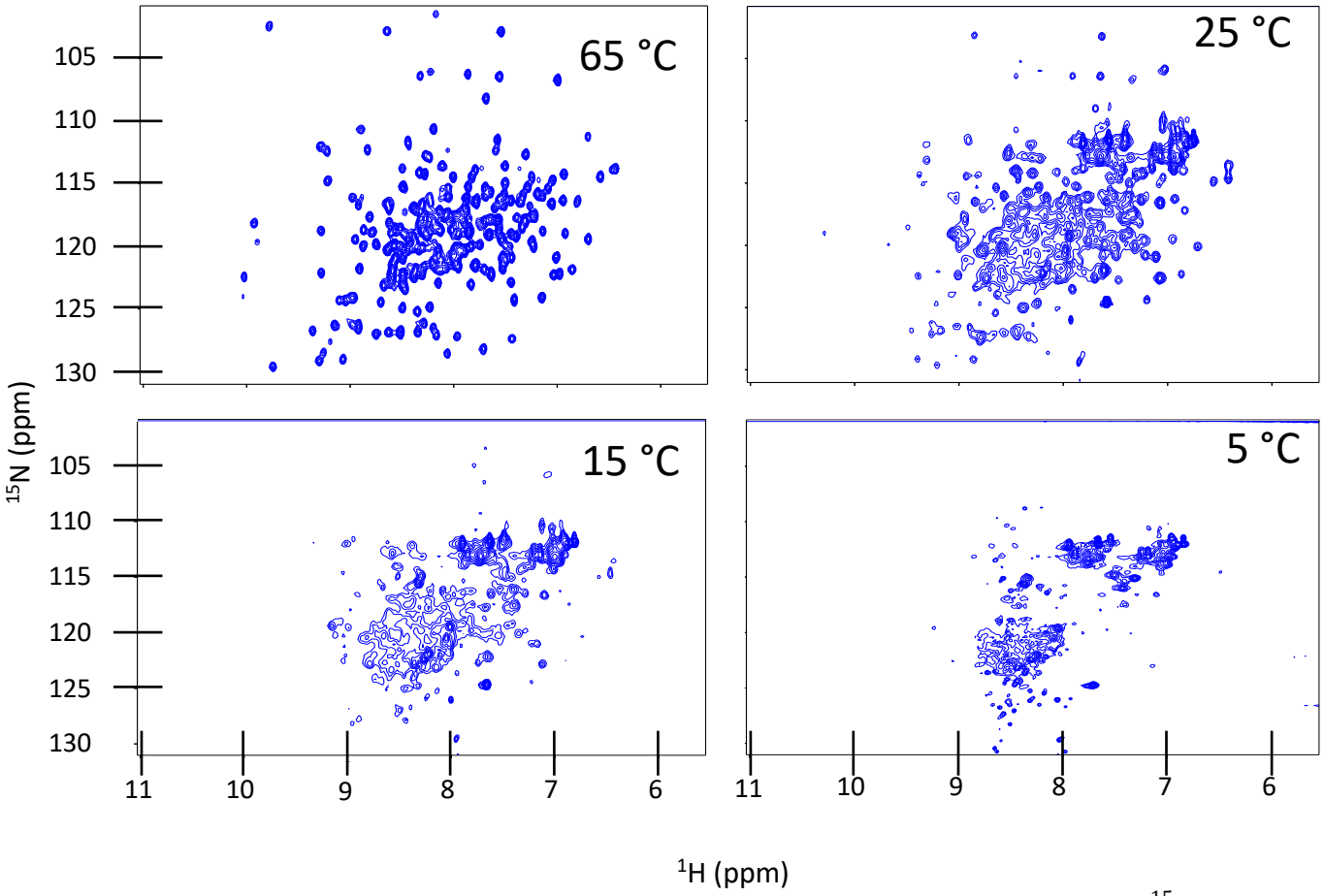

Figure 3.3 Dbh changes tertiary structure at cold temperatures. NMR ^{15}N-HSQC spectra of Dbh at 65 °C, 25 °C , 15 °C and 5 °C . Dispersed peaks of the structured protein shift to the region where random coil signals resonate (8-9 ^{1}H ppm) at cold temperatures indicating a loss of tertiary structure.

changes in the secondary structures of protein, it can discriminate between a-helical, b-sheet, and random coil. Using CD, we examined Dbh at 2 °C, 7 °C, 35 °C, and 65 °C. CD revealed that the secondary structure of Dbh is consistent over this temperature range, similar to what has been reported for Dpo4[32] (**Figure 3.4A**). We deconvoluted the secondary structure content using Beta Structure Selection (BeStSeL) [33] and find a slight decrease in percent helicity and an increase in percent beta strand as temperature decreased (**Figure 3.4B**). Comparison of NMR and CD spectra show contrasting results at

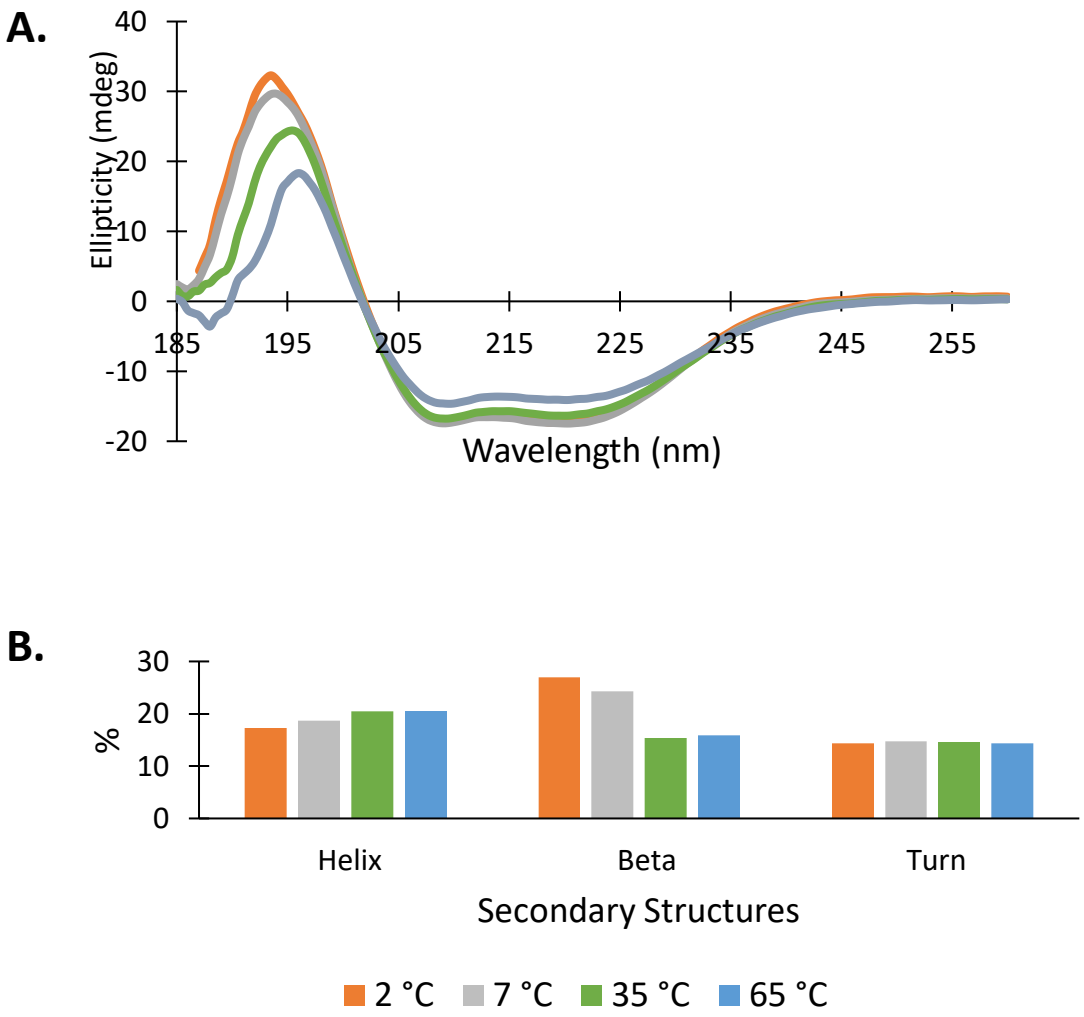

Figure 3.4: Circular Dichroism spectra of Dbh polymerase. DBH retains its secondary structures at temperatures ranging from 2-65 °C**. (A)** CD scans (185-260 nm) of DBH at 2 °C (orange), 7 °C (grey), 35 °C (green), 65 °C (blue). The increase in signal in the region of 190-200 nm could indicate an increase in helical structure with increasing temperature. However, after a **(B)** detailed secondary structure analysis via Beta Structure Selection (BeStSeL)[33] we find that there is a slight decrease in percent helicity and an increase in percent beta strand as temperature decrease.

cold temperatures: Dbh losses its tertiary structure in NMR ^{1}H-^{15}N HSQC spectra below 25 °C, but the protein maintains secondary structures down to 2 °C (**Figure 3.4**). Together these data show that Dbh retains tertiary structure between 35-65 °C, and loses tertiary structures below 25 °C, while retaining secondary structure content down to 2 °C. This corresponds well with the fact the DBH crystals form best at room temperature in contrast to other proteins which crystallize well in the cold [12, 13, 34]. In addition, the loss of

tertiary structure at 25 °C correlates well with the loss of catalytic efficiency observed at 22 °C in a primer extension study [4].

Chapter 3B: Dbh dynamics via HX at 35 and 50 °C

Dbh dynamics were probed at 35 °C and 50 °C by measuring amide hydrogen exchange and calculating protection factors at each temperature (**Figure 3.5)**. As previously mentioned in the p53 section, protection factors allow us to determine what regions/domains of the protein are resistant to exchange, defining regions of rigidity. Amide hydrogens that are readily exposed to solvent will exchange at a higher rate compared to hydrogens that are sequestered away from solvent (i.e., buried in a hydrophobic core) or involved in a secondary structure. There are two mechanisms that could affect rates of amide exchange: changes in local unfolding kinetics or a structural change whereby an amide becomes more or less occluded from solvent. For proteins where the structure does not change significantly, differences in the rates

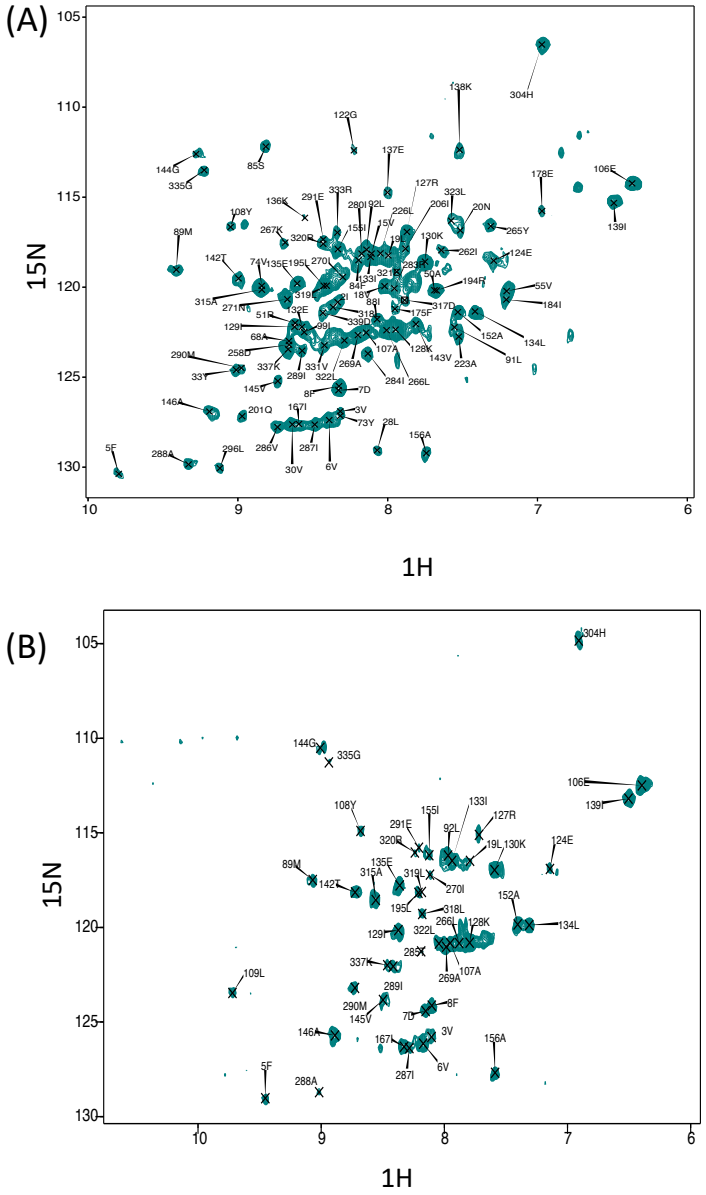

Figure 3.5: First HX spectra of Dbh at 35 and 50 °C for Dbh. Spectra are from the first time point after initiation of exchange with D_2O for DbH at **(A)** 35C (16 minutes) and (B) 50 °C (15 minutes). Extreme fast exchange occurs for a lot amides at 50 °C signifying fast dynamics at this temperature.

of amide hydrogen exchange can reflect the influence of the temperature on the local unfolding of that amide.

Like in the p53 project we determined k_{ex} by measuring peak volumes as a function of time after transfer into D2O and fit the results to calculate the exchange rate (**Figure 2.4, Appendix O**). PFs were calculated by k_{rc}/k_{ex}, where k_{rc} is the exchange rate of a backbone amide in a random coil and k_{ex} is the experimental exchange rate calculated from our data. k_{rc} was calculated based on equation 2b in Bai, et. al. [35]. Obtaining PFs from multiple amides in each domain gives us a thorough understanding of the dynamics throughout the Dbh structure. Our Dbh construct is composed of 353 residues, 15 of which are prolines that do not have corresponding amide hydrogen. At 35 °C we were able to obtain exchange data on 82 residues. 18 residues exchanged too fast to obtain sufficient points to calculate an exchange rate, and 26 remained stable throughout the experiment (**Appendix P**). In contrast, at 50 °C we obtained exchanged information on 43 residues. Seven of these exchanged too fast to obtain sufficient data to reliably fit exchange rates and 21 remained stable throughout the experiment (**Appendix P**).

As previously mentioned Dbh is produced in extremely hot environments (~75°C) therefore the dynamics we observed at temperatures close to Dbh's natural environment should reflect the natural state of the Dbh polymerase. In general, our protection factor data show that Dbh protein is considerably more dynamic at 50 °C than at 35 °C. We mapped PFs at 35 °C and 50 °C on the crystal structure of Dbh (**Figure 3.6**) and a clear pattern of dynamics and stability emerged. PFs show that the palm domain and the little finger domain are the most stable parts of DBH at both temperatures (**Figure 3.6**). In

contrast, the dynamics of the thumb and finger domain are significantly different between this 35 °C and 50 °C. At 35 °C we observe nine residues protected in the finger domain and six residues protected in the thumb domain. All this protection is lost at 50 °C indicating that these domains become significantly more dynamic as the temperature is increased toward the physiological temperature of *S. acidocaldarius*.

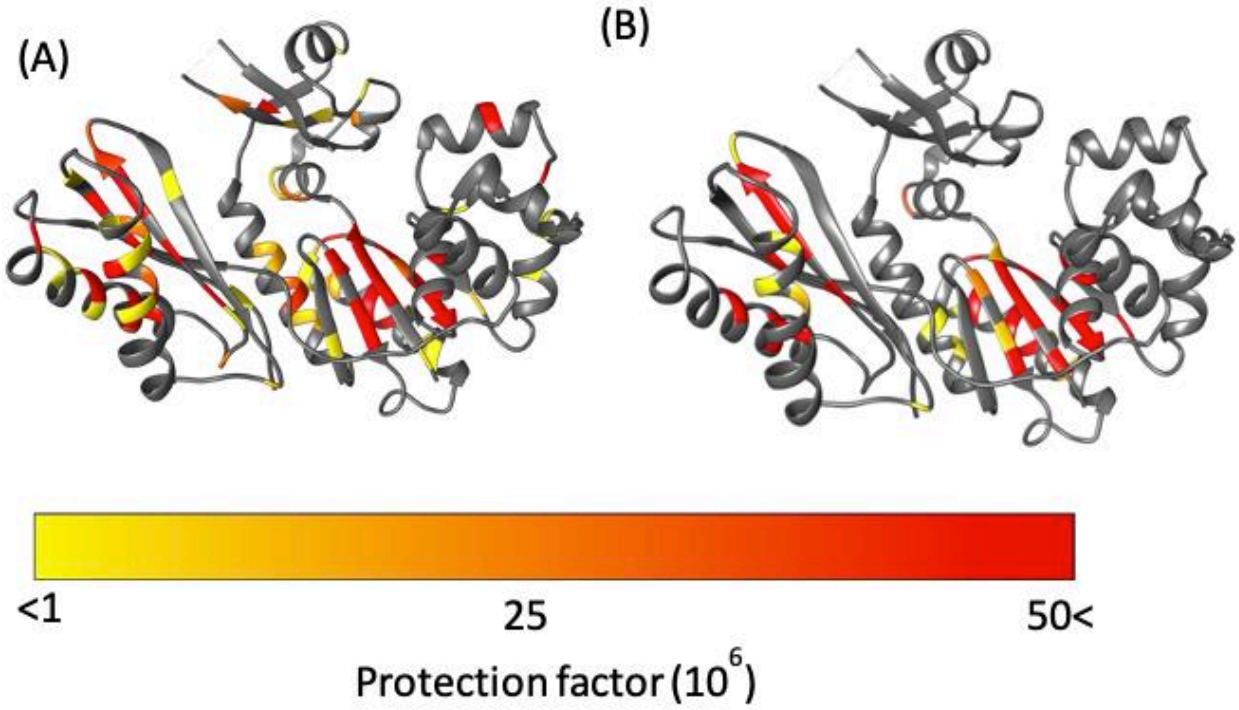

Figure 3.6: Protection factors mapped onto Dbh x-ray structures (PDB 1K1S). **(A)** Dbh PFs at 35 °C**. (B)** Dbh PFs at 50 °C. A few residues were stable throughout the HX experiment. Amides that remained stable through-out the hydrogen exchange experiment where colored in red. In contrast, amides that exchanges too fast to measure exchange rate are colored in yellow.

The fingers domain is one of the most dynamic domains in Dbh, composed of residues 20-77 (**Figure 3.1**). As previously discussed, the protection factor data shows this domain is more dynamic at 50 °C than at 35 °C. At 35 °C this domain contained nine observable residues at the start of the HX experiment. Signals from two residues (20, 68)

are present immediately after transfer to D_2O but exchange too rapidly to determine exchange rates/PF. The remaining seven residues (19, 28, 30, 33 50, 55, 74) are stable enough to obtain an exchange rate and protection factors (**Figure 3.6, Appendix P**). Two residues (50, 74) have relatively high PFs, indicating resistance to local unfolding at 35 °C. Both residues are involved in secondary structure hydrogen binding. Solvent accessibility surface area (SASA) calculations showed these amides are not exposed to the solution. These residues are found 12.88 Å away from each other, indicating the domain's far reaching stability at 35 °C. On the other hand, at 50 °C all residues in the finger domain exchange too fast to measure. These two HX experiments reveal that the finger domain of Dbh is significantly more dynamic at 50°C than at 35 °C.

The thumb domain is the most flexible domain in Dbh. It is composed of residues 172-236 (**Figure 3.1**). Compared to the other domains the thumb domain seems to be most dynamic regardless of temperature. This is deduced from the lack of protected amides (**Figure 3.6**). Nevertheless, like the finger domain the thumb domain shows the same trend with lower PFs at 50 °C than 35 °C. At 35 °C the thumb domain contains 6 observable residues (175, 178, 184, 194, 201, 206) at the start of the HX experiments. Four residues (175, 178, 184, 206) exchanged too fast to calculate exchange rates. The remaining two residues (194, 201) have high protection factors at 35 °C. Residue 194 is involved in a helical section of the protein and residue 201 is in an unstructured part of Dbh between two helices. Both residues 194 and 201 have no exposure to solvent (SASA = 0 Å). At 50 °C there are no protected residues in the Dbh thumb domain. In addition, TC data show that residue 176 is sensitive to temperature increase (TC value = -6.61). Although residue 176 is involved in an intra-molecular hydrogen bond within a helix, its TC value corresponds to an

amide that hydrogen bonds with water (<-4.6 ppb/K, as discussed below). Together the protection factor data and TC calculation show that the thumb domain is a relatively flexible domain in the protein and that this feature increases with temperature.

The palm domain is the most stable domain in DBH (**Figure 3.6**). The palm domain is composed of residues 1-19, 78-171. This is a critical domain because it holds the active site for nucleotide extension. At 35 °C we observe protection for residues in the beta-sheet and two alpha helices that compose the palm domain (**Figure 3.6**). We observe a minor decrease in protection at 50 °C. Much of the decrease in protection is localized near the major helices in the palm domain, which includes helix E and F and strand 6. In this region of the palm domain, we observe seven residues that lose complete protection (84, 85, 88, 91, 136-138) and five residues lose over 70% of their protection (89, 92, 106, 108, 124, 135) In additional, TC data also shows this region in the palm domain is sensitivity to increase temperatures (discussed later).

Like the palm domain, the LF domain is the second most stable part of Dbh. The LF domain is composed of residues 237-344 (**Figure 3.1**). Like the other domains, the LF domain becomes slightly more dynamic at 50 C than at 35 °C. There were seven residues that exchanged too fast to measure the exchange rate at 35 °C. These same signals were nonexistent at the beginning of the 50 °C experiment. Additionally, three amides remained completely stable throughout the experiment at 35 °C but did not have measurable exchange rates at 50 °C. Furthermore, we observed 12 amides that experience a decrease in protection factor when going from 35 °C to 50 °C. Four of them lost all protection (262, 271, 280, 296) and seven lost more than 40% (266, 285, 291, 304, 318, 320, 322). It is worth

noting that we do observe 2 residues that remained stable throughout the experiment at 35 °C (287, 290). The only region that showed a uniform decrease in protection was helix N(258-276) and helix O (307-324) of the LF domain. All other changes in protection factors were evenly distributed throughout the LF domain **(Figure 3.6)**.

HX reveals that Dbh is much more dynamic at 50 than 35° C. Dynamics increase for all domains with the palm domain being the least affected. Considering that Dbh is more efficient at higher temperatures we can conclude that dynamics play a crucial role in the efficiency of Dbh.

Chapter 3C: Confirming Dynamics with Temperature Coefficients

TC values for proteins have been shown to be sensitive to temperature dependent global and local unfolding [30, 36][37]. Historically TC data for protein is analyzed at the individual amide level. Amides not involved in intramolecular hydrogen bonding and amides sensitive to temperature fluctuation have TC values below -4.6 ppb/K [36][38][39]. When we implement this form of analysis, we obtained TC value that agreed with the crystal structure but provided limited dynamic information. Residues with TC values below -4.6 ppb/K belong to amides that aren't involved in hydrogen bonding and TC values more positive than –4.6 ppb/K belonged to hydrogen bonding amides in secondary structure (**Figure 3.7, Appendix P**). Helix E (residue 77-94) of the palm domain with TC values more negative than -4.6 ppb/K. This included residues 82, 86, and 89 all of which are involved in hydrogen bonding and have no solvent exposure base of crystal structure 1K1S. This data indicates that this region of the palm domain is sensitive to increases in temperature. This correlates with our PF data that show that this specific region in the

palm domain becomes slightly more flexible when going from 35 °C to 50 °C (**Figure 3.6**).

Together these two data sets allow us to conclude that although the palm domain is the most protected domain at both temperatures helix E (77-94), and helix F(121-138) of the palm domain adopt flexibility as temperature increases.

Most recently, analysis of TC data has been performed in group averages of secondary structures [40]. It has been shown that this type of analysis is a rich source of information on temperature dependent global stability [40]. We averaged our TC data by secondary structures(**Appendix Q**) and domain (**Table 1**). When averaging by secondary structure (i.e strand and helix)

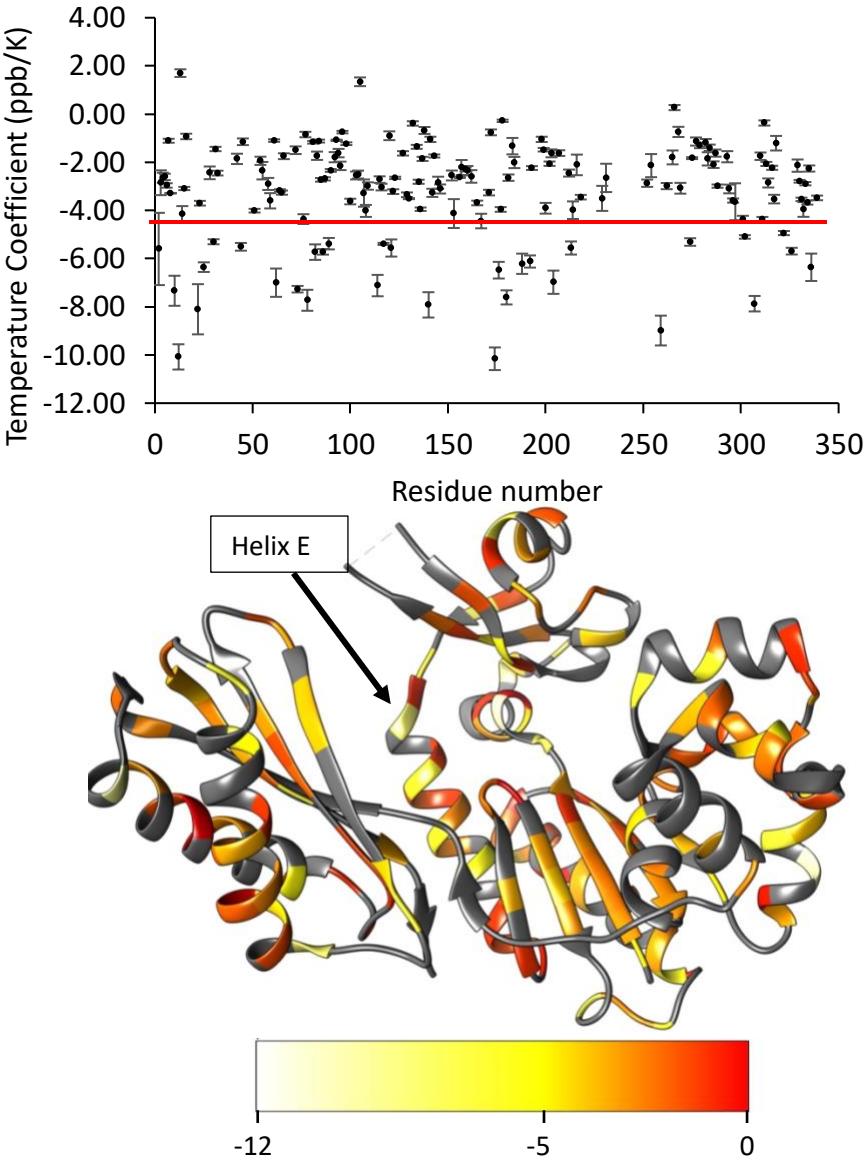

Figure 3.7 TC values for DBH. (A) Bar graphs of temperature coefficient values for amides in Dbh. The red line is a threshold (-4.6 ppb/K) for amides hydrogen bonding with water. Amides involved in intramolecular hydrogen bonding with TC values more negative than the threshold are susceptible temperature increase (B) TC values mapped on to the 3D structure of Dbh (PDB: 1K1S). Most residues with values more negative than -4.6 ppb/K belong to amides that are expose to water. Except for a set of residues found in helix E (77-94) of the palm domain. Helix E has four residues which are involved in intramolecular hydrogen bonding but have TC values more negative than -4.6 ppb/K threshold. This indicates this region is susceptible to unfolded as temperature increase. This dynamics in Helix E is also reflected in the protection factor data.

only limited structural information is obtained. In contrast, averaging the entire domains shows a clear trend that correlates with our hydrogen exchange PF data. We see the most dynamic domain the thumb domain has the most negative TC average of -3.28 ppb/K, followed by the second most dynamic finger domain with a TC domain average of -3.19 ppb/K. For the more stable domain the TC averages do not correlate with our PF data. TC average for the palm domain was -2.77 ppb/K and -2.69 for the LF domain.

Table 3.1: TC averaged across the entire domain. Average excludes amides in loop regions, amides not involved in hydrogen bonds, and amides exposed to solvent. Structural analysis based on the Dbh crystal structure 1K1S. Dynamic regions have a TC average that is more negative compare to rigid regions

TC average by domain	
Domain	**TC average (ppb/K)**
Finger domain (20-77)	-3.19
Palm domain (1-19, 78-171)	-2.77
Thumb domain (172-236)	-3.28
LF domain (246-344)	-2.69

Other groups have correlated TC and HX to obtain structural information on proteins [37][36]. It has been shown that protected amides (slow exchangers) average a less negative TC average compared to lower protected amides (fast exchangers) who have a more negative TC average [37]. Our TC average analysis only included amides in secondary structures (strands and helix). The analysis excluded amides in unstructured regions and amides that did not hydrogen bond and were exposed to water. This was done to avoid artificially decreasing our average TC by including naturally fast-exchanging

amides. Our TC values serve as a confirmation for our protection factor data. Together, these data sets allow us to conclude that the most flexible domains are the thumb and finger domains, in that specific order.

Looking back to 2002 primer extension studies [4] Dbh shows a decrease of primer extension efficiency when decreasing the primer extension temperature from 50 °C to 37 °C, and slightly lower loss of efficiency when comparing 37 °C to 22 °C. Our work suggests the decrease in efficiency when lowering the temperature from 50 °C to 37 °C might be attributed to the loss of flexibility we observed in both the NMR PF and TC results at 35 °C and 50 °C (**Figure 3.6**). Furthermore, we suggest that the decrease in efficiency seen when comparing 37 °C - 22 °C might be attributed to the loss of tertiary structure as observed in our HSQC spectra (**Figure 3.3**). When looking at the two-minute mark of the 2002 primer extension study we see a greater loss (~32%) in efficiency when going from 50 °C – 37 °C, than when comparing 37 °C -22 °C (~22%). This tells us that dynamics plays a critical role in the efficiency of Dbh polymerase.

Chapter 3D: Ion binding Dbh in solution

Our studies show that Mg^{2+} interacts with Dbh in the absence of DNA. We analyzed HSQC spectra of Dbh in the presence and absence of Mg^{2+} (**Figure 3.8**). When ligands, such as Mg^{2+}, bind proteins they change the local chemical environment, which causes chemical shifts for peaks of residues involved in ligand binding and for residues near the binding site. Therefore, residues with shifted peaks in the Dbh-Mg^{2+} spectra inform us of local Mg^{2+} binding. We found shifted peaks clustered in three distinct locations: 1) at the active site in the palm/finger domains, 2) in the thumb domain, and 3) in the little finger domain

(**Figure 3.9**). Notably, reported apo crystal structures of Dbh do not show binding of metal ions (PDB: 1IM4 [11], 1K1Q [12], 1K1S [12]). In contrast, Dbh in complex with DNA has been shown to bind one Ca^{2+} [13]. We find Mg^{2+} binds Dbh in the active site in solution and in the absence of DNA. The active site of Y-family polymerase consists of the palm domain surrounded by the finger domain and to a lesser extent the thumb domain [22] [13] [6]. We found that 10 of the residues that shifted in the presence of Mg^{2+} localized in the active site. Seven of these are found in the palm domain and 3 in the finger domain (**Appendix R**).

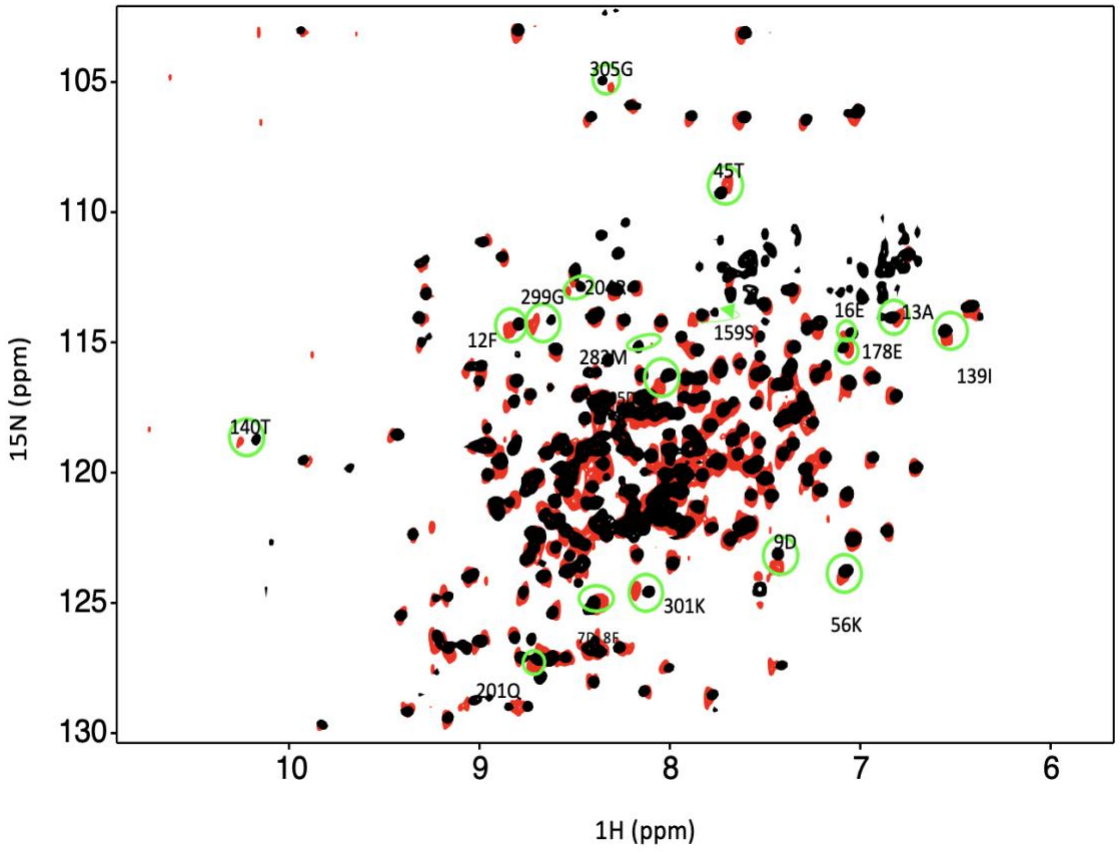

Figure 3.8: Overlay of spectra with apo-Dbh and Dbh with Mg^{2+}. Overlay of an ^{15}N-HSQC of Dbh at 35°C with Mg^{2+} (black) and without Mg^{2+} (red). Shifted peaks are circled in green and the labeled with the residue number and the one letter code of the residue. Shifted peaks in the Dbh-Mg^{2+} spectra inform on local Mg^{2+} binding. Chemical shift changes were localized in three regions of the 3D structures (see Figure 8).

Although they are in different domains, all residues are localized near the active site of Y-family polymerase in the 3D structures (**Figure 3.9**). One Ca^{2+} binds in the active site in Dbh/DNA structures [13]. This Ca^{2+} ion is chelated by Asp7, Phe8, and Asp105. Our solution-state NMR data show that Mg^{2+} interacts with these same residues in Dbh even without DNA bound. Furthermore, these chelating residues are surrounded by residues Asp9, Ile139, Thr140, which also experience chemical shift changes in the presence of Mg^{2+}. In addition, our data also show that Mg^{2+} interacts with three residues that are near the active site but shifted towards the finger domain, this includes Ala13, Glu16, and Thr45. It might be that Mg^{2+} binds more towards the finger domain when Dbh is in solution and not in the presence of DNA. Mg^{2+} also binds the thumb domain in the absence of DNA. HSQC of DBH in the presence of Mg^{2+} shows three peaks shift in the thumb domain (**Appendix R**). As mentioned earlier other Y-family such as Dpo4 polymerase have been shown to crystalize with two Mg^{2+} ions near this active site. This interaction can be attributed to a second $Mg^{2+,}$ which is almost always shown to interact with DNA and the protein. Past work [22] show Dpo4 chelating Mg^{2+} with residues 181-183 (182-184 Dbh). Our work suggests a slightly different binding site near residues 178, 201, and 204 in the absence of DNA. Two residues in this vicinity are positively charged Arg204 and Lys202. Arg204 shifted in the presence of Mg^{2+}, but the peak corresponding to Lys 202 is found in the crowed part of the spectra which could not be accurately measured. Both charged residues have potential salt bridge partners, however, one appears to be too far for the average salt bridge distance of 4 Å (204Arg-205Asp (5.2Å) and 202Lys-180Asp (2.7 Å)). If they are indeed forming salt bridges the introduction of Mg^{2+} in this region could interrupt the salt-bridge partners which leads to significant peak shifts caused by the repulsion forces of two like charges.

We found that Mg^{2+} binds Dbh's LF domain in the absence of DNA. When comparing the spectra with and without Mg^{2+} we observe that four peaks from the LF domain shift in the presence of Mg^{2+}. All four residues are localized within 14 Å from each other in the three-dimensional structure. (**Figure 3.9, Appendix R**). Dpo4 has been shown to bind a Mg^{2+} ion in the LF domain near Asp294 (PDB 2XCA) [22]. However, we found the Dbh

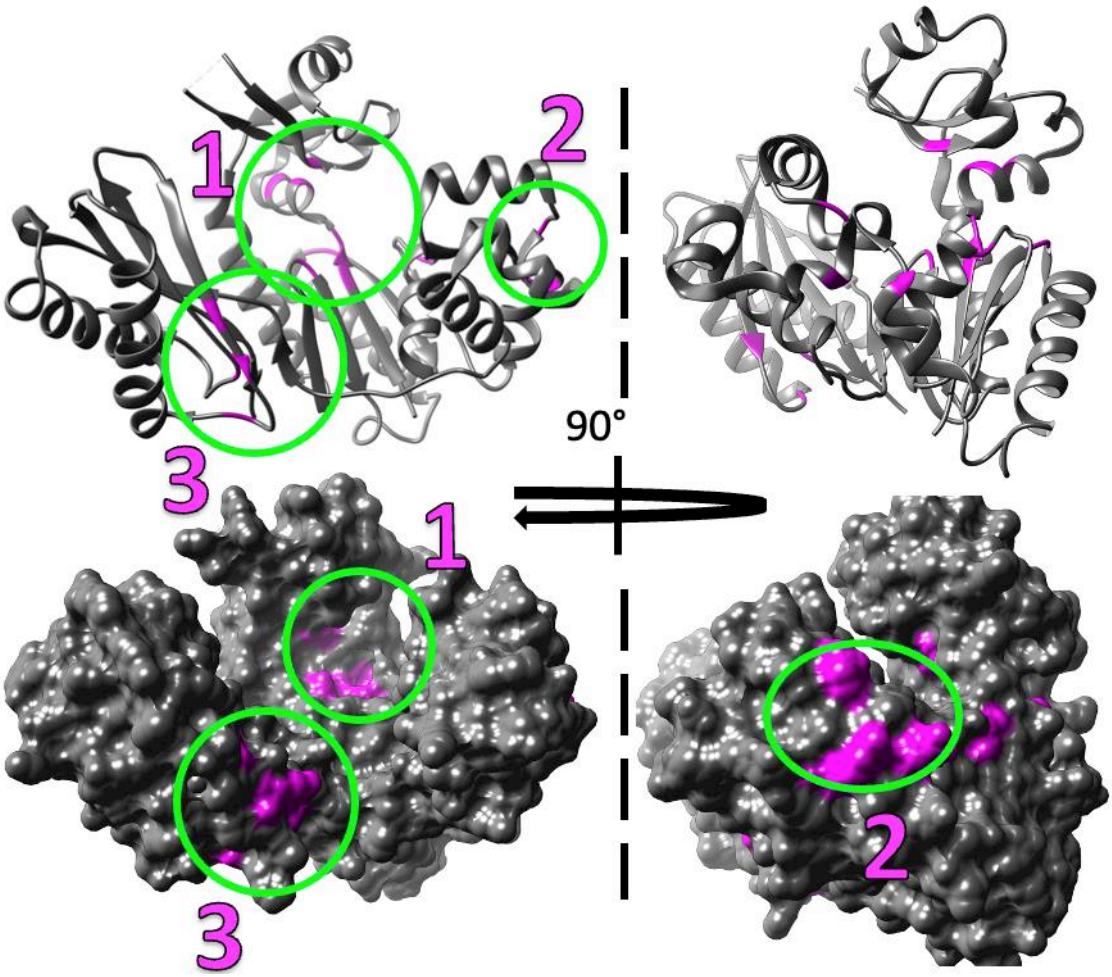

Figure 3.9: Residues affected by Mg^{2+} mapped on to Dbh structure. Mg^{2+} induced chemical shift changes map to three distinct locations when Dbh is in solution alone (without DNA and nucleotides). The shifted peaks from the overlayed ^{15}N-HSQC of Dbh at 35°C with Mg^{2+} and without Mg^{2+} (**Figure 3.7**) were mapped on to the 3D structure of Dbh (PDB: 1K1S) shown as a ribbon diagram (top), and surface filled model (bottom). The shifted peaks were localized in three different locations: 1) at the active site in the palm/finger domain, 2) in the thumb domain, and 3) in the little finger domain.

binding site to be 23.5 Å (a-carbon of 294, 301) away from the reported binding site of Dpo4. This could be attributed to the fact that Dpo4 and Dbh are dissimilarities in the LF domain. Dbh and Dpo4 sequences have the lowest sequence similarity in the LF domain at 42.1% similarity. Furthermore, a sequence alignment across 34 Y-family homologs showed that two of the shifted residues (Gly299, Lys301), are commonly mutated in other Y-family polymerase [41]. We suspect that the unique identity of the LF domain may create a Mg^{2+} binding region only found in Dbh that has never been reported in Dbh or Dpo4. Another explanation for the lack of Mg^{2+} binding in the LF in other crystal structures can be caused by low occupancy Mg^{2+}.

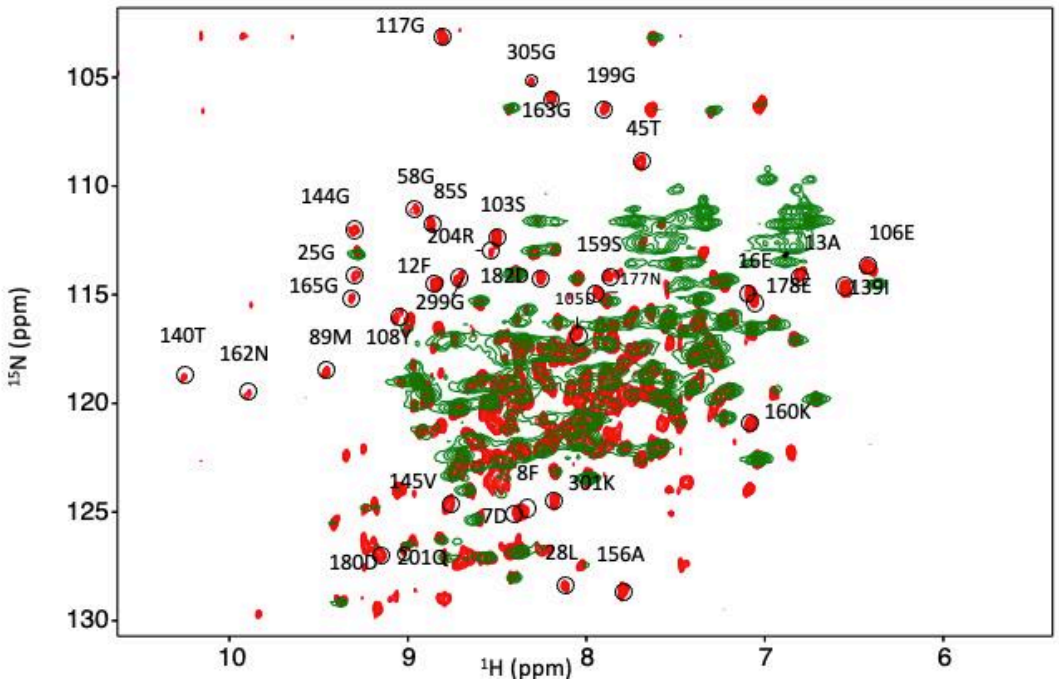

Figure 3.10: Overlay of spectra with apo-Dbh and Dbh with Mn^{2+}. Mn binds proteins like Mg^{2+}, however, it has paramagnetic properties that increase relaxation time which lead to disappearing of peaks for residues near the binding site. We observed 37 peaks disappeared in the presence of Mn. Most of them localized at near a predicted Mg^{2+} binding sit. It is important to note that all residues that shifted in the Mg^{2+} spectra also disappeared in the Mn^{2+} spectra except for residue 282Met (**Appendix R**). Note to be able to see through the green spectra we changed the contour level from level multiplier from 1.1 to 1.4 for the green spectra on CCPNMR Analysis 2.5.

Due to the low electron number of Mg^{2+}, it is difficult to visualize using crystallography if it has lower than 30 % occupancy (43)

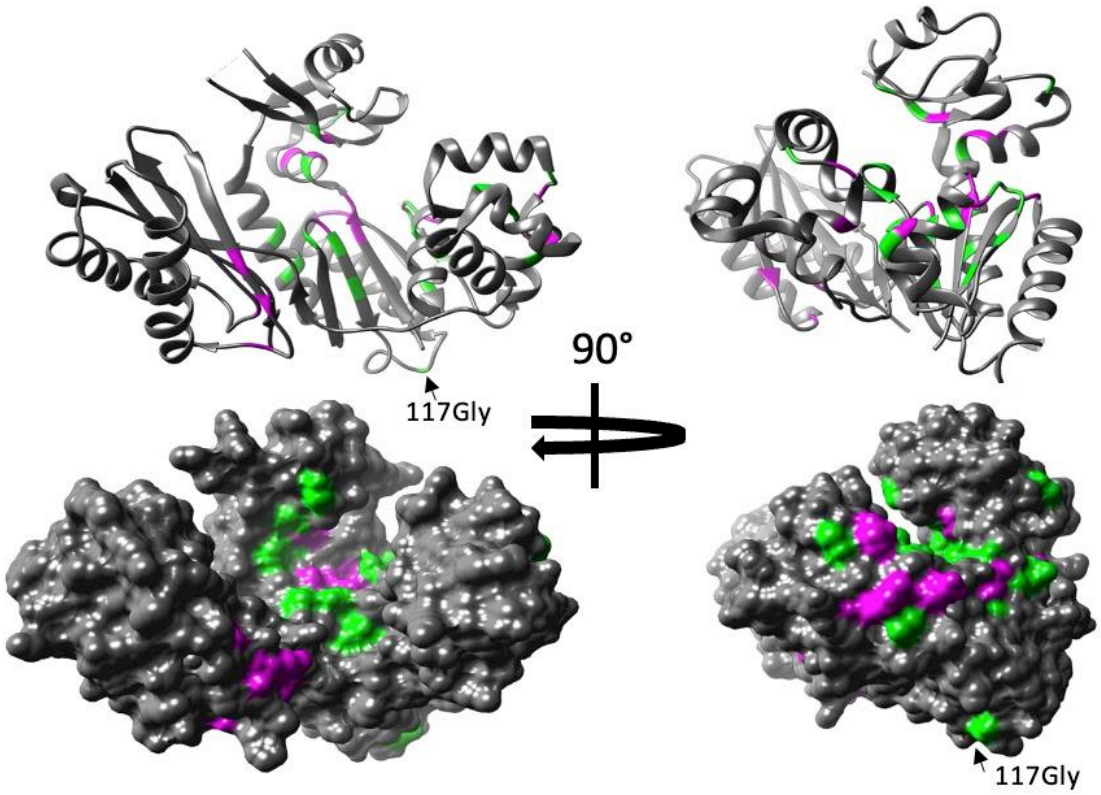

Figure 3.11: Residues affected by Mn^{2+} mapped on to Dbh structure. We mapped all the residues that disappeared from the Dbh + Mn HSQC spectra. We find that 36 of 37 residues localized in one of our three predicted Mg^{2+} binding cites. Mn^{2+} paramagnetic properties are far more reaching that Mg^{2+} effect which is why we greater coverage for Mn^{2+} spectra. The only residue that did not localized near the binding site was Gly117. Gly117 is found 23.0 Å to the nearest predicted binding site (Palm/finger domain). Residues that shifted in the presence of Mg^{2+} (Magenta), and Mn (green). Note the residues that shifted in Mg^{2+} spectra also disappeared in the Mn^{2+} spectra. These residues were colored in magenta to show the localization.

We confirmed ion binding sites by comparing ^{15}N-^{1}H HQC spectra with and without Mn^{2+}. Mn^{2+} binds proteins similar to Mg^{2+}, however, Mn^{2+} is paramagnetic, so instead of causing shifting of peaks, it increases relaxation time which leads to the disappearance of

peaks for residues near the binding site (16-25 Å) [42]. By overlaying the Mn^{2+} and non-metal spectra we should see the absence of peaks of residues near the metal binding sites **(Figure 3.10**). The paramagnetic effect of Mn^{2+} is more far-reaching than chemical shift perturbations from Mg^{2+}; consequently, the number of affected residues is increased in the Mn^{2+} samples compared to Mg^{2+} (**Appendix R)**. We observed the disappearance of 37 residues that correlate well with our predicted Mg^{+2} binding sites except for one;(Gly117), which did not localize to any of our predicted binding sites (**Figure 3.11**). 23 residues that disappeared in the presence of Mn^{2+} are near the palm/finger binding site, 3 are found near the LF binding site, and 10 were in the thumb binding site. It is important to note that all residues that shifted in the Mg^{2+} spectra also disappeared in the Mn^{2+} spectra (**Appendix R)** except for residue Met282. It is possible that Met282 chemical shift changes with Mg^{2+} are a result of long-range conformational change and this residue may not be involved directly in ion binding. Thus, the Mn^{2+} data serves as a secondary verification of our proposed ion-binding sites.

The Mg^{2+} and Mn^{2+} data show that there are three ion binding sites on Dbh. There is currently an active debate on whether the DNA synthesis mechanism requires two or three ions for synthesis. The third ion has been suggested to be involved in the active site interacting with the incoming nucleotide. Our experiment did not involve DNA or free-floating nucleotide. However, a third binding site is apparent even without DNA bound.

We have shown how a wide range(2-65°C) of temperature affect the tertiary struture and the dynamics of Dbh. In addition, we- characterized metal binding in solution.

Through NMR and CD spectra we showed that Dbh tertiary structure cold denatures beginning at 25 °C and increasing in denaturation as the temperature is lowered to 5 °C with little change observed by CD. We used hydrogen exchange protection factors, and temperature coefficient to reveal that both the thumb and finger domains are very dynamic relative to the palm and LF domains. These trends remain true at high temperatures with dynamics increasing as temperatures increase from 35 °C to 50 °C. Chemical shift perturbation analysis in the presence and absence of magnesium and manganese reveals three ion binding sites, even in the absence of DNA. In contrast, these bound metals are not apparent in any Dbh crystal structures of the protein without DNA. Two ion binding sites are confirmed to be near the active site, as reported in other Y-family polymerases, and we report a novel ion binding site in the LF domain.

Material and methods:

Protein expression: The Dbh gene was incorporated into the vector pKKT7-H (a derivative of pKK233, Promega) containing an N-terminal His6 tag (MHHHHHHLVPRGM). Quick-change mutagenesis (Stratagene) was used to change Cys31 to Ser to eliminate the potential formation of disulfide bonds. Transfected E. coli BL21 cells were grown in 1L Neidhart's minimal media [44] at 37 °C containing 1g 15N ammonium chloride (15N-labeled samples), expression was induced by the addition of 1mM IPTG. Protein was expressed for 5 hours; subsequently, the cells were harvested by centrifugation and frozen at -80 °C. Dbh was purified from cell lysate by Ni-NTA affinity chromatography under native conditions, and then dialyzed into buffer (20mM HEPES, 100mM NaCl, 50μM EDTA, 50μM NaN_3, pH 7.5) at 4°C, then one change of buffer without EDTA (20mM HEPES, 100mM

NaCl, 50μM NaN_3, pH 7.5). To prepare the NMR samples, Dbh protein was concentrated to at least 0.5mM and transferred into a 5-mm Shigemi tube. D_2O was added to the sample for a final concentration of 10% v/v.

NMR experiments:

Hydrogen exchange: Samples of 100% ^{15}N-labeled Dbh (0.5 mM or higher concentration) were transferred into deuterated NMR buffer (20mM HEPES, 100mM NaCl, 50μM NaN_3, pD 7.5), using a P10 desalting column equilibrated with the deuterated buffer. The sample was transferred to a Shigemi NMR tube and immediately placed in an 800MHz Varian Inova NMR spectrometer, containing an xyz triple resonance probe, equilibrated at 35 or 50 °C. After shimming and tuning the magnet, the acquisition of the first 15N-1H TROSY-HSQC (Pervushin et al., 1997) spectrum was started approximately 15 minutes after insertion of the protein sample into the magnet. Additional ^{15}N-^{1}H HSQC spectra were measured sequentially every 147 minutes and 13 seconds (2.454 hours), except for the last five spectra at 50°C, for which additional scans were taken (2x for the 17th through 20th spectra, 4x for the 21st spectrum) to improve the signal-to-noise ratio. A total of 20 spectra were collected at 35 °C and 50 °C. Due to the additional length of acquisition in the last five spectra at 50°C, the acquisition of the 18^{th}, 19^{th}, 20^{th}, and 21st spectra was started 4.907 hours after the start of the previous spectra. Representative spectra for various time points at both temperatures are shown in (**Figure 5**). The data were processed using NMRPipe [45], and analyzed using CCPNMR Analysis [46] (RRID:SCR_016984). The peak intensity was plotted as a function of time and fit a single-order exponential-decay function ($I(t) = I_0 \times e^{-kt}$) to extract the exchange rate. Representative rate fits to the experimental data are

displayed in (**Figure 5**). To obtain the protection factors the hypothetical exchange rate for the amide proton in a random coil conformation was calculated, corrected for the effect of side chain identity to the left and right of the amide proton according to [47] [35].

Temperature Coefficient (TC): Conventional 2D-^{15}N-^{1}H HSQC spectra were taken at 35°C, 45°C, 50°C, 55°C, and 65 °C, on samples containing at least 0.5 mM ^{15}N-labeled Dbh in 20 mM HEPES, 50 mM NaCl, 50 µM EDTA, pH 7.5, with 10 % (v/v) D_2O. The data were processed with NMRpipe[45], and visualized using CCPNMR Analysis 2.5 (RRID:SCR_016984, [46]. H chemical shift (ppm) for all peaks in **Figure 3.2** were plotted as a function of temperature (K) and fit to a straight line. The slope*1000 for each fit was used as TC for each residue. The standard error of the slope was used as TC uncertainty. Only fits with $R^2 > 0.75$ were used. Non-linear fits were not used, a total of 10 non-linear TC values were discarded. The TC average for each domain only includes amides located in secondary structure regions, and excluded amides in loop regions and amides that are exposed to solvent based on the 1K1S crystal structure.

Ion chemical shift: All samples were made with 20 mM HEPES, 100 mM NaCl, 50 µM NaN_3, at pH 7.5. The Mg^{2+} sample contained 5 mM NaCl. The Mn^{2+} contained X mM of Mn??. Data was analyzed with CCPNMR Analysis [46] (RRID:SCR_016984).

Circular Dichroism:

200 µL of 0.28mg/mL Dbh protein in buffered solution (50 mM sodium phosphate, 100 mM NaCl, 50 µM EDTA, pH 7.5) were transferred into a CD cuvette with a 1 mm path length. The cuvette was placed in the sample cell Jasco J-810 spectropolarimeter equipped with a Peltier temperature controller, and the cell was calibrated at 35 °C. A spectrum was

collected at 35 °C from 260 nm to 185 nm, with a scan rate of 50 nm/min, data points were collected every 0.5 nm and 10 total scans. The cell was then cooled at a rate of 0.5 °C/min to 7 °C, with the ellipticity value measured at 208 nm every 2 °C, then after a full spectrum was taken at 7 °C with the same parameters as above. The sample was then removed from the CD cuvette, the cuvette was cleaned, and a second 200 µL 0.28 mg/mL Dbh protein sample was transferred into the cuvette. The cuvette was placed into the cell equilibrated at 35°C, another full CD spectrum was taken at this temperature, and the sample was heated to 65 °C at a rate of 0.5 °C/min, with the ellipticity value at 208 nm taken every 2 °C. One full spectrum was then taken at 65 °C. After adjustments to the chiller unit, a third 0.28 mg/mL Dbh sample was used to collect full CD spectra again at 7 °C and then at 2 °C.

Protein visualization: We used UCSF chimera to visualize Dbh [48]. Structure 1K1S was used for all analyses [12]. Amides, hydrogen bonds, and solvent accessibility were obtained using chimera default settings.

Refefrences

1. Grogan, D.W., *Phenotypic characterization of the archaebacterial genus Sulfolobus: comparison of five wild-type strains.* J Bacteriol, 1989. **171**(12): p. 6710-9.
2. Rastädter, K., et al., *Physiological Characterization of Sulfolobus acidocaldarius in a Controlled Bioreactor Environment.* International Journal of Environmental Research and Public Health, 2021. **18**(11).
3. Baker-Austin, C. and M. Dopson, *Life in acid: pH homeostasis in acidophiles.* Trends in Microbiology, 2007. **15**(4): p. 165-171.
4. Potapova, O., N.D. Grindley, and C.M. Joyce, *The mutational specificity of the Dbh lesion bypass polymerase and its implications.* J Biol Chem, 2002. **277**(31): p. 28157-66.
5. Sakofsky, C.J., P.L. Foster, and D.W. Grogan, *Roles of the Y-family DNA polymerase Dbh in accurate replication of the Sulfolobus genome at high temperature.* DNA Repair (Amst), 2012. **11**(4): p. 391-400.
6. Pata, J.D., *Structural diversity of the Y-family DNA polymerases.* Biochim Biophys Acta, 2010. **1804**(5): p. 1124-35.
7. Johnson, R.E., et al., *Fidelity of human DNA polymerase eta.* Journal of Biological Chemistry, 2000. **275**(11): p. 7447-7450.
8. Johnson, R.E., S. Prakash, and L. Prakash, *The human DINB1 gene encodes the DNA polymerase Pol theta.* Proceedings of the National Academy of Sciences of the United States of America, 2000. **97**(8): p. 3838-3843.
9. Ohashi, E., et al., *Fidelity and processivity of DNA synthesis by DNA polymerase kappa, the product of the human DINB1 gene.* Journal of Biological Chemistry, 2000. **275**(50): p. 39678-39684.
10. Tang, M.J., et al., *Roles of E-coli DNA polymerases IV and V in lesion-targeted and untargeted SOS mutagenesis.* Nature, 2000. **404**(6781): p. 1014-1018.
11. Zhou, B.L., J.D. Pata, and T.A. Steitz, *Crystal structure of a DinB lesion bypass DNA polymerase catalytic fragment reveals a classic polymerase catalytic domain.* Mol Cell, 2001. **8**(2): p. 427-37.
12. Silvian, L.F., et al., *Crystal structure of a DinB family error-prone DNA polymerase from Sulfolobus solfataricus.* Nature Structural Biology, 2001. **8**(11): p. 984-989.
13. Wilson, R.C. and J.D. Pata, *Structural Insights into the Generation of Single-Base Deletions by the Y Family DNA Polymerase Dbh.* Molecular Cell, 2008. **29**(6): p. 767-779.
14. Boudsocq, F., et al., *Investigating the Role of the Little Finger Domain of Y-family DNA Polymerases in Low Fidelity Synthesis and Translesion Replication.* Journal of Biological Chemistry, 2004. **279**(31): p. 32932-32940.
15. Wang, W., et al., *Translesion synthesis of apurinic/apyrimidic site<?A3B2 ACK?>analogues by Y-family DNA polymerase Dbh from<?A3B2 ACK?><italic>Sulfolobus acidocaldarius</italic&gt.* Acta Biochimica et Biophysica Sinica, 2022. **54**(5): p. 637-646.
16. Sakai, H.D. and N. Kurosawa, *Saccharolobus caldissimus gen. nov., sp nov., a facultatively anaerobic iron-reducing hyperthermophilic archaeon isolated from an acidic terrestrial hot spring, and reclassification of Sulfolobus solfataricus as Saccharolobus solfataricus comb. nov and Sulfolobus shibatae as Saccharolobus shibatae comb. nov.*

International Journal of Systematic and Evolutionary Microbiology, 2018. **68**(4): p. 1271-1278.
17. Ohmori, H., et al., *The Y-family of DNA polymerases.* Mol Cell, 2001. **8**(1): p. 7-8.
18. Kulaeva, O.I., et al., *Identification of a DinB/UmuC homolog in the archeon Sulfolobus solfataricus.* Mutat Res, 1996. **357**(1-2): p. 245-53.
19. UniProt, C., *UniProt: the Universal Protein Knowledgebase in 2023.* Nucleic Acids Res, 2023. **51**(D1): p. D523-D531.
20. Ling, H., et al., *Crystal structure of a Y-family DNA polymerase in action: a mechanism for error-prone and lesion-bypass replication.* Cell, 2001. **107**(1): p. 91-102.
21. Trincao, J., et al., *Structure of the catalytic core of S. cerevisiae DNA polymerase eta: implications for translesion DNA synthesis.* Mol Cell, 2001. **8**(2): p. 417-26.
22. Irimia, A., et al., *Metal-ion dependence of the active-site conformation of the translesion DNA polymerase Dpo4 from Sulfolobus solfataricus.* Acta Crystallogr Sect F Struct Biol Cryst Commun, 2010. **66**(Pt 9): p. 1013-8.
23. Chu, X.K., et al., *Dynamic Conformational Change Regulates the Protein-DNA Recognition: An Investigation on Binding of a Y-Family Polymerase to Its Target DNA.* Plos Computational Biology, 2014. **10**(9).
24. Liyanage, P.S., et al., *Bulky Lesion Bypass Requires Dpo4 Binding in Distinct Conformations.* Sci Rep, 2017. **7**(1): p. 17383.
25. Chu, X., Z. Suo, and J. Wang, *Investigating the Conformational Dynamics of a Y-Family DNA Polymerase during Its Folding and Binding to DNA and a Nucleotide.* JACS Au, 2021. **2**(2): p. 341-356.
26. Wang, L.H., et al., *Accommodation of a 1S-(-)-Benzo[c]phenanthrenyl-N-6-dA adduct in the Y-family dpo4 DNA polymerase active site: Structural insights through molecular dynamics Simulations.* Chemical Research in Toxicology, 2005. **18**(3): p. 441-456.
27. Cramer, J. and T. Restle, *Pre-steady-state kinetic characterization of the DinB homologue DNA polymerase of Sulfolobus solfataricus.* J Biol Chem, 2005. **280**(49): p. 40552-8.
28. Fiala, K.A. and Z. Suo, *Mechanism of DNA polymerization catalyzed by Sulfolobus solfataricus P2 DNA polymerase IV.* Biochemistry, 2004. **43**(7): p. 2116-25.
29. Turvey, M.W., et al., *Single-molecule Taq DNA polymerase dynamics.* Sci Adv, 2022. **8**(10): p. eabl3522.
30. Ohnishi, M. and D.W. Urry, *Temperature dependence of amide proton chemical shifts: the secondary structures of gramicidin S and valinomycin.* Biochem Biophys Res Commun, 1969. **36**(2): p. 194-202.
31. Privalov, P.L., *Cold denaturation of proteins.* Crit Rev Biochem Mol Biol, 1990. **25**(4): p. 281-305.
32. Sherrer, S.M., et al., *Identification of an Unfolding Intermediate for a DNA Lesion Bypass Polymerase.* Chemical Research in Toxicology, 2012. **25**(7): p. 1531-1540.
33. Micsonai, A., et al., *BeStSel: a web server for accurate protein secondary structure prediction and fold recognition from the circular dichroism spectra.* Nucleic Acids Res, 2018. **46**(W1): p. W315-W322.
34. Wilson, R.C., M.A. Jackson, and J.D. Pata, *Y-family polymerase conformation is a major determinant of fidelity and translesion specificity.* Structure, 2013. **21**(1): p. 20-31.

35. Bai, Y., et al., *Protein stability parameters measured by hydrogen exchange.* Proteins, 1994. **20**(1): p. 4-14.
36. Baxter, N.J. and M.P. Williamson, *Temperature dependence of 1H chemical shifts in proteins.* J Biomol NMR, 1997. **9**(4): p. 359-69.
37. Andersen, N.H., et al., *Extracting information from the temperature gradients of polypeptide NH chemical shifts .1. The importance of conformational averaging.* Journal of the American Chemical Society, 1997. **119**(36): p. 8547-8561.
38. Cierpicki, T. and J. Otlewski, *Amide proton temperature coefficients as hydrogen bond indicators in proteins.* Journal of Biomolecular Nmr, 2001. **21**(3): p. 249-261.
39. Cierpicki, T., et al., *Hydrogen bonds in human ubiquitin reflected in temperature coefficients of amide protons.* Journal of Magnetic Resonance, 2002. **157**(2): p. 178-180.
40. Doyle, C.M., et al., *Concurrent Increases and Decreases in Local Stability and Conformational Heterogeneity in Cu, Zn Superoxide Dismutase Variants Revealed by Temperature-Dependence of Amide Chemical Shifts.* Biochemistry, 2016. **55**(9): p. 1346-1361.
41. Wu, J., et al., *DNA binding strength increases the processivity and activity of a Y-Family DNA polymerase.* Scientific Reports, 2017. **7**.
42. Pintacuda, G., et al., *Site-specific labelling with a metal chelator for protein-structure refinement.* J Biomol NMR, 2004. **29**(3): p. 351-61.
43. Yang, W., P.J. Weng, and Y. Gao, *A new paradigm of DNA synthesis: three-metal-ion catalysis.* Cell Biosci, 2016. **6**(1): p. 51.
44. Neidhardt, F.C., P.L. Bloch, and D.F. Smith, *Culture medium for enterobacteria.* J Bacteriol, 1974. **119**(3): p. 736-47.
45. Delaglio, F., et al., *NMRPipe: a multidimensional spectral processing system based on UNIX pipes.* J Biomol NMR, 1995. **6**(3): p. 277-93.
46. Vranken, W.F., et al., *The CCPN data model for NMR spectroscopy: development of a software pipeline.* Proteins, 2005. **59**(4): p. 687-96.
47. Molday, R.S., S.W. Englander, and R.G. Kallen, *Primary structure effects on peptide group hydrogen exchange.* Biochemistry, 1972. **11**(2): p. 150-8.
48. Pettersen, E.F., et al., *UCSF Chimera--a visualization system for exploratory research and analysis.* J Comput Chem, 2004. **25**(13): p. 1605-12.

Summary and Conclusion

Protein dynamics play a different role between the two proteins studied here. In p53 dynamics highlight regions of instability because p53 exists in a balance where a single missense mutation can destabilize (observed in cancer mutations) or stabilize it (in the case or rescue mutations). On the other hand, dynamics in Dbh highlight regions of functionality. Previous studies show that polymerases need to be dynamic to perform their function. More specifically we know that Dbh functions more efficiently at high temperatures, and in my work, we see that high temperatures increase dynamics for Dbh.

Here we have used solution-state NMR to understand the dynamics of two different proteins. By using hydrogen exchange, we reveal that rescue mutants N235K and N239Y have far-reaching effects on the dynamics of the DBD. Interestingly each rescue mutant is distinct: N235K strongly stabilizes the smaller sheet of the β-sandwich while N239Y results in extensive stabilization of both sheets. With the same HX technique, we revealed that the most dynamic domain in Dbh is the thumb domain, followed by the finger domain, and finally the LF domain. With the palm domain being the most rigid domain in the entire protein. We confirmed the dynamics of each domain through temperature coefficient analysis.

Chemical shift analysis was used to gain different insights into each protein. In the p53 study chemical shift analysis showed that each rescue mutant did not change the structure of the protein in solution. In the Dbh project, we used chemical shift analysis to pinpoint three different binding sites for divalent ions on the Dbh. Two ion binding sites

are confirmed to be near the active site, as reported in other Y-family polymerases, and we report a novel ion binding site in the LF.

Through NMR relaxation we were able to show regions with fast motion in the three different p53 DBDs. We see that while fast dynamics are conserved across all p53 variants in loop6, we also observed fast dynamics unique to rescue mutants near and far from the DNA binding region (S2'-S3 and S9-S10 regions).

To supplement our NMR analysis, we performed additional studies in each project. For p53 we performed protein sequence analysis that reveal that mutation N235K exists in rats and mice. Since 235K is known to be more resistant to cancer mutations, animal studies of cancer using mice or rats should include the humanized p53 sequence. In the Dbh project, we supplemented our NMR with CD. This supplemental study exposed that while tertiary structures in Dbh cold denature the secondary structures remain unchanged by lowered temperatures.

Appendix A: R1, R2, and NOE values for CytR DNA binding domain in the presence of *udp half-site* DNA at 800 MHz field strength.

Residue #	NOE + error	R1 + error	R2+ error
9	0.39 ± 0.03	1.34 ± 0.06	10.66 ± 0.09
10	0.57 ± 0.03	0.95 ± 0.03	15.75 ± 0.25
11	0.82 ± 0.03	0.96 ± 0.07	19.6 ± 0.18
12	0.75 ± 0.11	1.1 ± 0.36	13.99 ± 1.57
13			
14	0.86 ± 0.02	0.92 ± 0.05	23.89 ± 0.42
15	0.77 ± 0.04	0.85 ± 0.03	23.14 ± 0.25
16	0.92 ± 0.03	0.87 ± 0.04	21.67 ± 0.32
17	0.89 ± 0.02	0.87 ± 0.03	24.21 ± 0.24
18	0.87 ± 0.02	0.82 ± 0.01	21.02 ± 0.28
19	0.88 ± 0.02	0.9 ± 0.04	23.14 ± 1.01
20	0.85 ± 0.03	0.82 ± 0.04	26.18 ± 0.29
21	0.9 ± 0.02	0.85 ± 0.05	27.91 ± 0.63
22	0.87 ± 0.05	1 ± 0.08	26.46 ± 1.13
23	0.87 ± 0.03	1.15 ± 0.08	22.12 ± 0.9
24	0.94 ± 0.03	1.26 ± 0.1	28.9 ± 1.24
25	0.89 ± 0.03	1.16 ± 0.08	22.46 ± 0.58
26	0.93 ± 0.03	0.93 ± 0.05	23.56 ± 0.66
27	0.92 ± 0.03	1.07 ± 0.06	21.12 ± 0.44
28	0.94 ± 0.03	1.17 ± 0.08	24.53 ± 0.35
29	0.9 ± 0.03	1.01 ± 0.07	22.73 ± 0.24
30			
31	0.94 ± 0.03	0.99 ± 0.05	21.89 ± 0.58
32	0.8 ± 0.03	0.97 ± 0.03	19.7 ± 0.5
33			
34	0.81 ± 0.02	0.86 ± 0.03	23.21 ± 0.49
35	0.78 ± 0.03	0.98 ± 0.06	23.56 ± 0.62
36	0.86 ± 0.03	1.1 ± 0.05	27.65 ± 0.49
37	0.93 ± 0.04	1.16 ± 0.12	24.44 ± 0.68
38	0.87 ± 0.03	0.91 ± 0.06	26.68 ± 0.46
39	0.89 ± 0.02	0.92 ± 0.05	27.19 ± 0.28
40	0.93 ± 0.03	0.98 ± 0.06	25.32 ± 0.22
41	0.94 ± 0.03	0.87 ± 0.05	27.32 ± 0.3
42	0.84 ± 0.03	0.85 ± 0.04	25.73 ± 0.37
43	0.89 ± 0.03	0.86 ± 0.05	26.93 ± 0.53
44	1.02 ± 0.04	1.02 ± 0.05	19.85 ± 0.41
45	0.86 ± 0.03	0.76 ± 0.03	25.99 ± 0.72

46	0.97 ± 0.02	0.77 ± 0.03	27.16 ± 0.42
47	0.83 ± 0.03	0.81 ± 0.03	27.6 ± 0.42
48	0.9 ± 0.03	0.78 ± 0.03	26.53 ± 0.24
49	0.89 ± 0.02	0.82 ± 0.04	27.94 ± 0.63
50	0.83 ± 0.03	0.84 ± 0.02	16.72 ± 0.89
51	0.89 ± 0.03	0.85 ± 0.04	28.6 ± 0.29
52	0.92 ± 0.03	0.86 ± 0.03	24.75 ± 0.74
53	-0.17 ± -0.03	1.98 ± 0.15	4 ± 0.05
54	0.69 ± 0.04	0.91 ± 0.01	21.66 ± 0.35

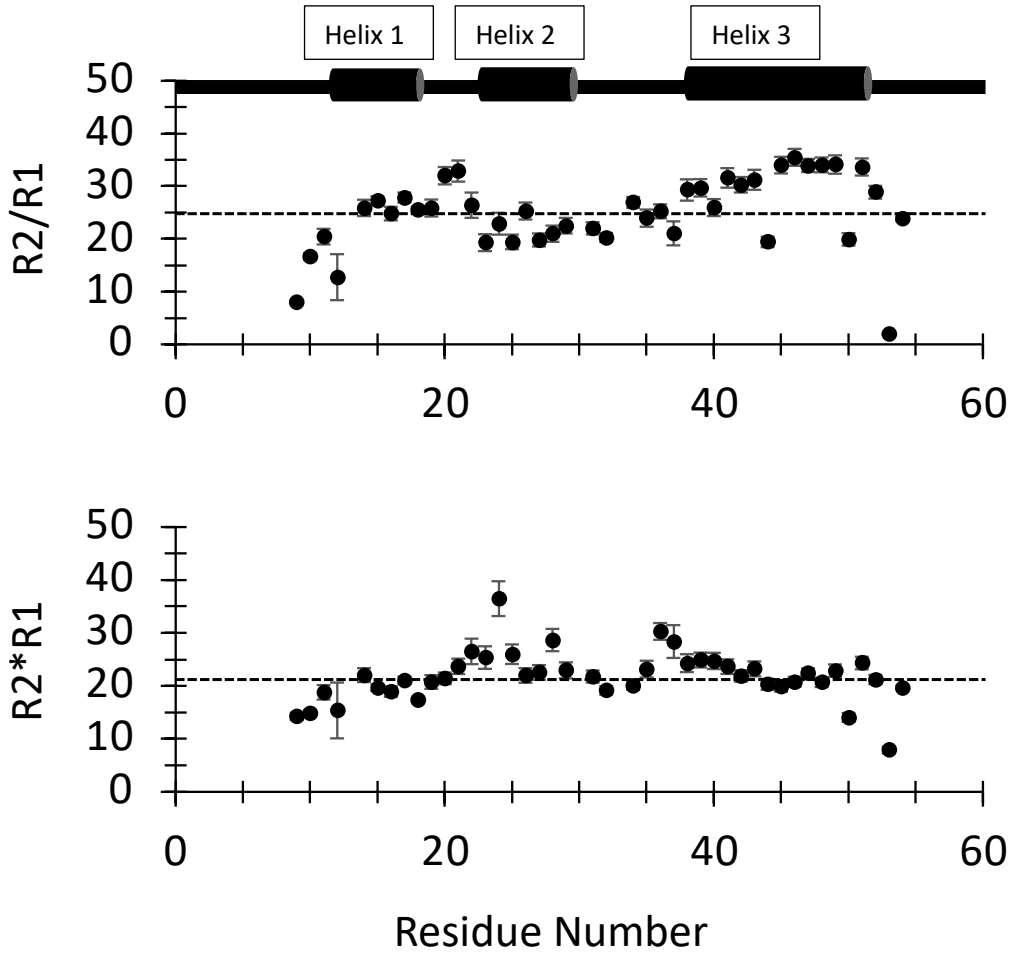

Quantitative analysis of relaxation parameters of CytR DNA binding domain in the presence of *udp half-site* DNA (R2/R1 and R2*). The diagram above the graphs illustrates CytR secondary structures. Dotted line is the rolling average of all value in each respective graph. R2/R1 analysis (above graph) distinguish between fast (ps-ns) and slow (ms-us) motions. Helix 3 appears exhibit slow motions. R2*R2 analysis distinguishes residues affected by chemical exchanged. Residues 24, 36-37 are the most affected by Chemical exchange. Further analyses was not possible do to the effect of DNA on overall protein tumbling and the lack CytR+DNA solved structure.

Appendix B. Peak assignment for rescue mutants

A)N235K and **B)**N239Y. N235K spectra at 27 minutes after initiation of exchange with D_2O and N239Y spectra 17 minutes after initiation of exchange with D_2O.

A.

.

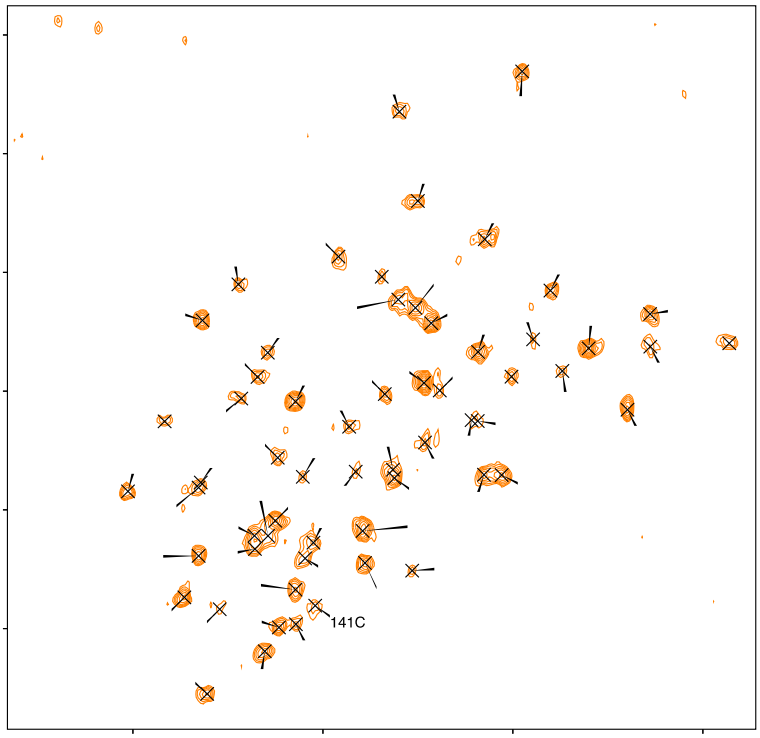

B.

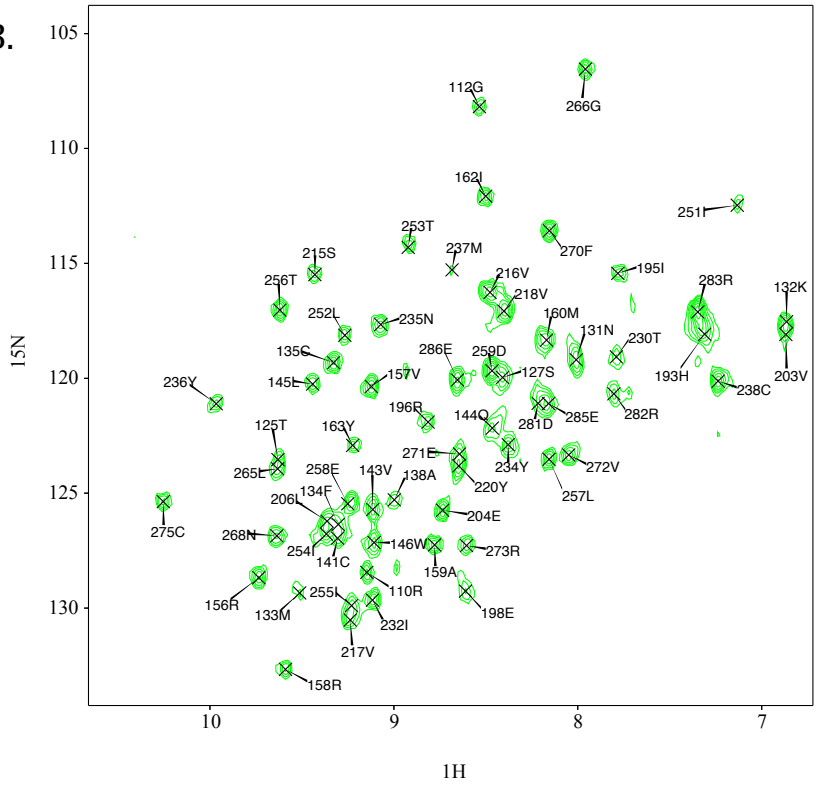

Appendix C: List of residues with significant perturbation in rescue mutants. Chemical Shifts of residues that showed significant change in peak positions compared to WT (from spectra in **figures 2.3, appendix B**).

	WT		N235K		N239Y	
Residue #	**H position (ppm)**	**^{15}N position (ppm)**	**H position (ppm)**	**^{15}N position (ppm)**	**H position (ppm)**	**^{15}N position (ppm)**
117	8.67	111.24	8.65	111.76	-	-
124	7.48	120.32	7.51	119.99	-	-
125	9.63	123.66	9.59	123.05	-	-
126	8.72	128.94	8.77	129.24	-	-
137	8.61	125.53	8.50	125.60	-	-
138	9.03	123.57	-	-	9.05	123.03
139	7.50	117.77	7.59	118.21	7.35	117.14
141	9.30	126.79	9.09	129.57	-	-
143	9.11	125.70	9.02	126.38	-	-
175	8.00	116.30	8.00	116.63	-	-
180	8.83	120.35	8.85	120.07	-	-
186	8.18	124.78	8.23	124.48	-	-
187	8.54	109.33	8.52	109.62	-	-
196	8.84	121.94	8.85	121.55	-	-
199	8.78	110.83	8.77	111.56	-	-
200	8.22	117.32	8.22	117.60	-	-
203	6.87	118.33	6.90	118.89	-	-
217	9.24	130.54	9.28	130.86	-	-
234	8.38	122.94	8.74	123.45	-	-
235	9.06	117.56	8.56	115.98	-	-
236	10.07	121.65	9.85	121.37	9.97	121.13
237	8.60	116.83	8.58	115.16	8.60	115.72
238	7.33	120.27	7.37	120.77	-	-
239	8.45	118.33	8.41	118.04	8.45	117.88
240	9.60	120.16	-	-	9.63	119.64
241	8.13	109.49	-	-	7.96	108.95
242	7.80	122.18	-	-	7.91	122.29
273	8.55	127.70	-	-	8.60	127.36
275	9.99	124.27	-	-	10.25	125.45
277	8.74	115.75	-	-	8.83	115.88
279	8.89	104.80	-	-	8.92	105.25

Appendix D: Measured exchange rate(k_{ex}), the calculated exchange rate of amide in random coil(k_{rc}), and protection factors(PF) for WT p53 amides.

k_{ex} = observed exchanged rate; k_{ex} was obtained from the rate of decay. R^2 errors correspond to deviation away from the regression line.

k_{rc} = calculated exchange rate of that residue in a random coil, according to {Molday, 1972 #1}.

PF = Protection factors were calculated by dividing the exchange rate of the residue in a random coil by the observed hydrogen exchange rate (k_{rc}/ k_{ex}).

Residue	k_{ex} (10^{-4}) /min	Error	k_{rc} (10^{-4})/min	PF (10^6)
110Arg	1.24	0.11	2.24E+06	1.81
112Gly	4.38	0.30	1.86E+06	0.43
127Ser	5.16	0.49	4.27E+06	0.83
132Lys	5.81	0.30	3.09E+06	0.53
133Met	2.98	1.43	2.09E+06	0.70
134Phe	3.39	0.54	1.20E+06	0.36
135Cys	4.48	0.19	7.76E+06	1.73
138Ala	26.20	5.27	1.00E+06	0.04
139Lys	6.32	0.15	1.48E+06	0.23
141Cys	4.37	0.31	1.07E+07	2.45
143Val	1.07	0.10	1.86E+05	0.17
144Gln	1.50	0.15	1.35E+06	0.90
145Leu	0.99	0.09	6.76E+05	0.68
146Trp	0.65	0.09	3.89E+05	0.60
156Arg	0.71	0.08	3.09E+06	4.34
157Val	0.53	0.06	5.37E+05	1.02
158Arg	0.70	0.09	1.41E+06	2.02
159Ala	0.41	0.06	2.69E+06	6.64
160Met	0.67	0.08	1.59E+06	2.38
162Ile	0.90	0.09	3.02E+05	0.34
163Tyr	37.70	3.64	5.13E+05	0.01
195Ile	1.14	0.13	1.86E+05	0.16
196Arg	1.27	0.16	1.15E+06	0.91

204Glu	4.58	0.18	3.63E+05	0.08
206Leu	30.50	4.95	4.79E+05	0.02
215Ser	6.60	0.51	5.25E+06	0.79
216Val	0.83	0.07	6.46E+05	0.78
217Val	1.12	0.09	2.34E+05	0.21
218Val	0.53	0.05	2.34E+05	0.45
220Tyr	1.65	0.10	5.01E+05	0.30
232Ile	0.93	0.09	4.79E+05	0.51
234Tyr	0.89	0.07	1.20E+06	1.35
235Asn	1.34	0.11	5.62E+06	4.18
236Tyr	1.24	0.11	1.82E+06	1.47
237Met	1.17	0.20	1.78E+06	1.52
238Cys	15.00	0.93	8.71E+06	0.58
252Leu	0.70	0.11	2.51E+05	0.36
253Thr	0.56	0.08	8.51E+05	1.53
254Ile	0.93	0.10	4.79E+05	0.52
255Ile	0.54	0.08	1.78E+05	0.33
256Thr	0.41	0.06	8.13E+05	2.00
257Leu	0.61	0.08	6.76E+05	1.11
258Glu	0.41	0.06	3.09E+05	0.75
259Asp	1.47	0.08	1.95E+07	13.30
265Leu	0.36	0.12	2.63E+05	0.72
266Gly	11.00	0.56	1.86E+06	0.17
268Asn	0.49	0.06	8.32E+06	17.03
270Phe	0.90	0.07	1.86E+06	2.07
271Glu	28.60	5.38	5.76E+05	0.02
272Val	1.51	0.13	2.29E+05	0.15
273Arg	3.36	0.19	1.41E+06	0.42
275Cys	4.26	0.19	4.90E+06	1.15
283Arg	1.88	0.27	3.24E+06	1.72
286Glu	42.40	4.12	3.55E+05	0.01

Appendix E: Measured exchange rate(k_{ex}), the calculated exchange rate of amide in random coil(k_{rc}), and protection factors(PF) for N235K p53 amides.

k_{ex} = observed exchanged rate; k_{ex} was obtained from the rate of decay. R^2 errors correspond to deviation away from the regression line.

k_{rc} = calculated exchange rate of that residue in a random coil, according to {Molday, 1972 #1}.

PF = Protection factors were calculated by dividing the exchange rate of the residue in a random coil by the observed hydrogen exchange rate (k_{rc}/ k_{ex}).

Residue	k_{ex} (10^{-4})/min	Error	k_{rc} (10^{-4})/min	PF (10^6)
110Arg	1.10	0.09	2.24E+06	2.04
112Gly	5.37	1.09	1.86E+06	0.35
132Lys	5.29	1.24	3.09E+06	0.58
134Phe	1.62	0.47	1.20E+06	0.74
135Cys	5.20	1.25	7.76E+06	1.49
139Lys	8.58	0.65	1.48E+06	0.17
141Cys	0.67	0.58	1.07E+07	16.03
143Val	0.21	0.05	1.86E+05	0.91
144Gln	3.69	1.38	1.35E+06	0.37
145Leu	1.65	0.28	6.76E+05	0.41
146Trp	1.18	0.25	3.89E+05	0.33
156Arg	0.33	0.04	3.09E+06	9.48
157Val	0.17	0.03	5.37E+05	3.09
158Arg	0.53	0.08	1.41E+06	2.68
159Ala	0.20	0.03	2.69E+06	13.14
160Met	0.26	0.05	1.59E+06	6.14
162Ile	0.45	0.14	3.02E+05	0.67
163Tyr	14.60	4.51	5.13E+05	0.04
195Ile	0.69	0.09	1.86E+05	0.27
196Arg	0.96	0.28	1.15E+06	1.20
204Glu	1.54	0.10	3.63E+05	0.24
206Leu	14.50	4.37	4.79E+05	0.03
215Ser	4.58	0.53	5.25E+06	1.15
216Val	0.21	0.03	6.46E+05	3.10

217Val	0.29	0.05	2.34E+05	0.81
218Val	0.14	0.02	2.34E+05	1.66
220Tyr	1.43	0.10	5.01E+05	0.35
232Ile	1.63	0.21	4.79E+05	0.29
234Tyr	1.63	0.21	1.20E+06	0.74
235Lys	1.53	0.16	2.19E+06	1.43
236Tyr	1.17	0.21	1.15E+06	0.98
237Met	0.04	0.10	1.78E+06	45.94
238Cys	6.00	0.42	8.71E+06	1.45
252Leu	0.52	0.08	2.51E+05	0.48
253Thr	0.66	0.16	8.51E+05	1.29
254Ile	0.68	0.10	4.79E+05	0.70
255Ile	0.19	0.04	1.78E+05	0.94
256Thr	0.09	0.03	8.13E+05	9.17
257Leu	0.67	0.07	6.76E+05	1.01
258Glu	0.23	0.03	3.09E+05	1.35
259Asp	0.98	0.05	1.95E+07	19.94
265Leu	0.35	0.09	2.63E+05	0.76
266Gly	10.10	1.28	1.86E+06	0.18
268Asn	0.25	0.03	8.32E+06	33.16
270Phe	0.69	0.19	1.86E+06	2.70
272Val	2.08	0.14	2.29E+05	0.11
273Arg	1.09	0.22	1.41E+06	1.29
275Cys	6.60	0.74	4.90E+06	0.74
283Arg	1.85	0.18	3.24E+06	1.75

Appendix F: Measured exchange rate (k_{ex}), the calculated exchange rate of amide in random coil(k_{rc}), and protection factors(PF) for N239Y p53 amides.

k_{ex} = observed exchanged rate; k_{ex} was obtained from the rate of decay. R^2 errors correspond to deviations away from the regression line.

k_{rc} = calculated exchange rate of that residue in a random coil, according to {Molday, 1972 #1}.

PF = Protection factors were calculated by dividing the exchange rate of the residue in a random coil by the observed hydrogen exchange rate (k_{rc}/ k_{ex}).

Residue	k_{ex} (10^{-4})/min	Error	k_{rc} (10^{-4})/min	PF (10^6)
110Arg	0.96	0.07	2.24E+06	2.33
112Gly	4.41	0.34	1.86E+06	0.42
127Ser	2.43	0.24	4.27E+06	1.76
132Lys	1.93	0.09	3.09E+06	1.60
133Met	1.67	0.27	2.09E+06	1.25
134Phe	1.92	0.34	1.20E+06	0.63
135Cys	1.36	0.06	7.76E+06	5.72
138Ala	10.90	1.29	1.00E+06	0.09
141Cys	2.94	0.29	1.07E+07	3.65
143Val	0.53	0.06	1.86E+05	0.35
144Gln	1.06	0.11	1.35E+06	1.27
145Leu	0.66	0.08	6.76E+05	1.02
146Trp	0.45	0.07	3.89E+05	0.87
156Arg	0.65	0.08	3.09E+06	4.79
157Val	0.35	0.05	5.37E+05	1.54
158Arg	0.33	0.06	1.41E+06	4.25
159Ala	0.26	0.04	2.69E+06	10.45
160Met	0.41	0.05	1.59E+06	3.89
162Ile	0.35	0.05	3.02E+05	0.85
163Tyr	13.70	1.11	5.13E+05	0.04
193His	2.46	0.33	2.57E+06	1.04
195Ile	0.60	0.06	1.86E+05	0.31
196Arg	1.02	0.12	1.15E+06	1.13
204Glu	3.12	0.14	3.63E+05	0.12
206Leu	0.80	0.14	4.79E+05	0.60
215Ser	5.29	0.49	5.25E+06	0.99

216Val	0.47	0.04	6.46E+05	1.38
217Val	0.47	0.06	2.34E+05	0.49
218Val	0.31	0.05	2.34E+05	0.76
220Tyr	1.75	0.11	5.01E+05	0.29
230Thr	46.57	6.14	4.90E+06	0.11
232Ile	0.44	0.05	4.79E+05	1.08
234Tyr	0.35	0.05	1.20E+06	3.46
235Asn	0.81	0.07	5.62E+06	6.96
236Tyr	0.47	0.06	1.82E+06	3.91
238Cys	3.15	0.21	8.71E+06	2.77
252Leu	0.44	0.06	2.51E+05	0.57
253Thr	0.27	0.04	8.51E+05	3.19
254Ile	0.69	0.11	4.79E+05	0.70
255Ile	0.40	0.04	1.78E+05	0.45
256Thr	0.30	0.04	8.13E+05	2.69
257Leu	0.30	0.04	6.76E+05	2.24
258Glu	0.35	0.05	3.09E+05	0.89
259Asp	1.74	0.07	1.95E+07	11.18
265Leu	0.60	0.13	2.63E+05	0.44
266Gly	12.80	0.90	1.86E+06	0.15
268Asn	0.35	0.06	8.32E+06	23.60
270Phe	0.43	0.05	1.86E+06	4.32
272Val	0.80	0.06	2.29E+05	0.29
273Arg	0.98	0.11	1.41E+06	1.44
275Cys	1.38	0.09	4.90E+06	3.54
283Arg	3.26	0.08	3.24E+06	0.99
286Glu	38.20	1.69	3.55E+05	0.01

Appendix G: Positions resistant to immediate hydrogen exchange

Positions resistant to immediate hydrogen exchange mapped onto the WT p53 structure; protected residues highlighted in blue. Mutated location highlighted in sky blue and labled.

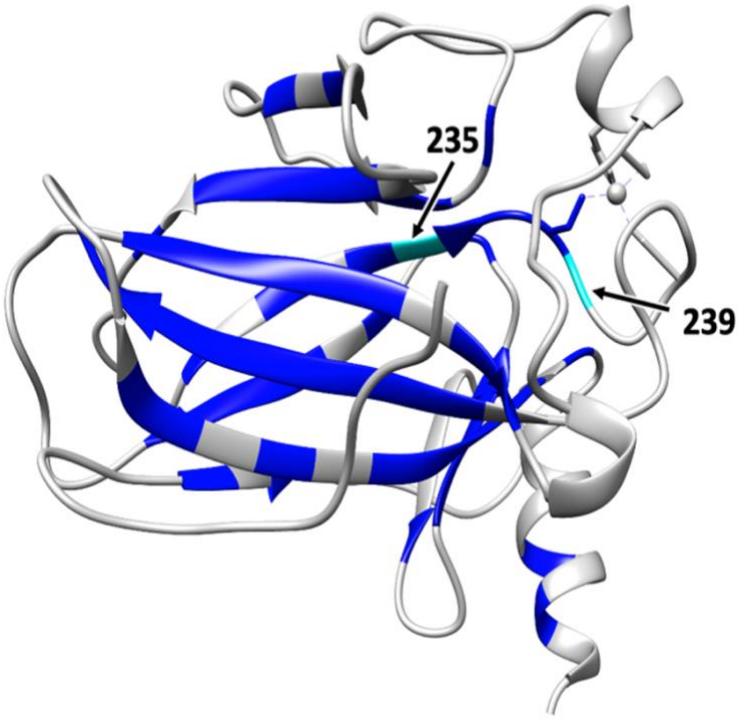

Appendix H: Bar graph of protection factors for WT and rescue mutants.

35 amide hydrogens had an increase in protection factors in the rescue mutant N235K (orange) compared to WT p53 (blue). A total of 45 amide hydrogens show an increase in protection factors in the rescued mutant N239Y (green) compared to WT. Residues 193 and 230 are protected in N239Y but exchange too fast to be detected in WT or N235K.

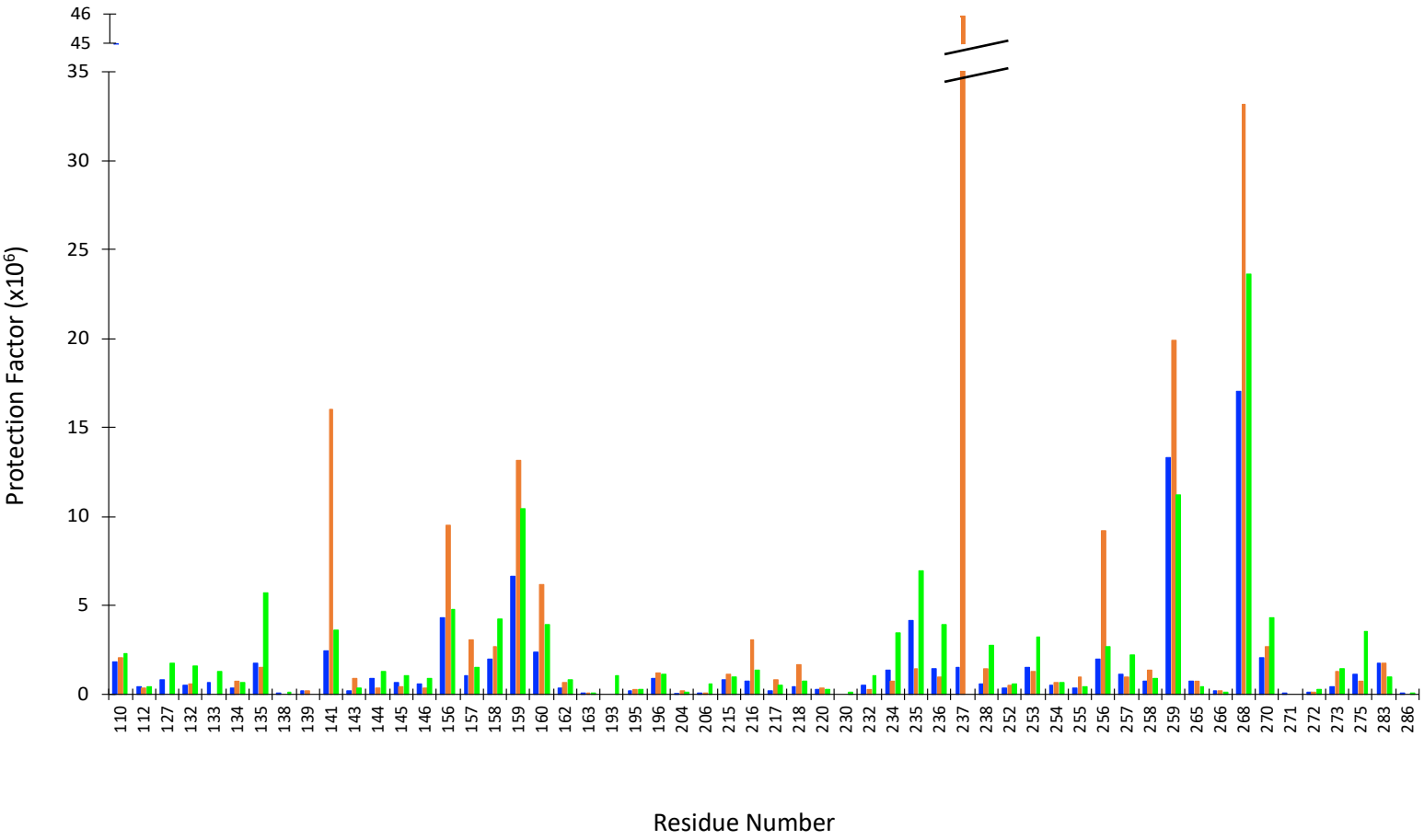

Appendix I: R1, R2, NOE, and S^2 values for Wildtype p53 DBD at 800 MHz field strength.

* Signal present up to .030 seconds

** Signal present up to .050 seconds

† *Modelfree* calculation did not assign a model to residue.

Blank spaces correspond to residues with relaxation values that could not be obtained.

Residue #	R1 ± error (s^{-1})	R2 ± error (s^{-1})	NOE ± error	S2 ± error
99	1.485 ± 0.361	30.43 ± 0.654	0.795 ± 0.010	†
100	1.318 ± 0.284	28.36 ± 2.246	0.765 ± 0.012	0.791 ± 0.066
101	1.260 ± 0.275	31.81 ± 1.290	0.907 ± 0.006	†
102	1.209 ± 0.254	33.77 ± 4.850	0.657 ± 0.010	0.788 ± 0.089
103	1.087 ± 0.162	28.69 ± 0.811	0.711 ± 0.010	0.857 ± 0.027
104				
105	1.383 ± 0.287	35.68 ± 1.806	0.717 ± 0.009	0.645 ± 0.141
106				
107	1.255 ± 0.233	33.81 ± 2.730	0.820 ± 0.009	†
108	1.048 ± 0.213	42.69 ± 3.544	0.977 ± 0.010	†
109				
110	1.056 ± 0.206	31.40 ± 4.243	0.830 ± 0.013	1.000 ± 0.080
111	0.806 ± 0.119	33.32 ± 1.186	0.745 ± 0.010	0.905 ± 0.047
112	0.773 ± 0.184	**	1.000 ± 0.018	
113		28.78 ± 2.079		
114	0.979 ± 0.197	28.25 ± 1.185	0.775 ± 0.011	0.848 ± 0.036
115	1.718 ± 0.671	24.75 ± 3.405	0.379 ± 0.016	0.854 ± 0.091
116				
117	1.561 ± 0.461	30.35 ± 4.726	0.779 ± 0.018	†
118	1.990 ± 0.508		0.923 ± 0.016	
119				
120				
121	2.192 ± 0.573	29.47 ± 3.104	0.732 ± 0.014	†
122				
123	1.407 ± 0.434	34.21 ± 3.314	1.000 ± 0.027	
124	1.172 ± 0.201	29.86 ± 0.850	0.876 ± 0.009	1.000 ± 0.024
125	0.923 ± 0.148	28.53 ± 0.271	0.854 ± 0.009	1.000 ± 0.008
126	1.355 ± 0.274	26.99 ± 2.243	0.913 ± 0.012	1.000 ± 0.063
127	0.884 ± 0.240	26.60 ± 3.197	0.866 ± 0.015	1.000 ± 0.080
128				
129				

130	0.933 ± 0.192	76.46 ± 22.161	0.930 ± 0.011	†
131				
132	0.923 ± 0.160	34.34 ± 1.178	0.730 ± 0.009	0.858 ± 0.062
133	0.820 ± 0.205		0.775 ± 0.021	
134	0.892 ± 0.114	30.62 ± 3.896	0.817 ± 0.013	1.000 ± 0.060
135	1.061 ± 0.205	32.10 ± 2.578	0.784 ± 0.009	0.872 ± 0.071
136	0.953 ± 0.174	29.92 ± 5.053	0.764 ± 0.011	0.940 ± 0.078
137	0.860 ± 0.150	27.96 ± 1.204	0.743 ± 0.013	0.872 ± 0.038
138	0.690 ± 0.164	28.16 ± 3.482	0.885 ± 0.016	0.906 ± 0.089
139	1.054 ± 0.204	27.36 ± 1.265	0.820 ± 0.010	0.898 ± 0.033
140	0.996 ± 0.163	30.71 ± 1.633	0.785 ± 0.008	0.879 ± 0.042
141	0.925 ± 0.190	36.04 ± 2.876	0.907 ± 0.013	1.000 ± 0.054
142				
143	0.827 ± 0.069	29.74 ± 3.598	0.642 ± 0.010	0.848 ± 0.031
144	1.371 ± 0.230		0.541 ± 0.009	0.289 ± 0.279
145	0.692 ± 0.093	39.78 ± 3.833	0.855 ± 0.013	1.000 ± 0.060
146	0.878 ± 0.158	29.38 ± 1.939		
147	0.950 ± 0.098	30.32 ± 1.871	0.711 ± 0.008	1.000 ± 0.038
148	0.893 ± 0.153	28.80 ± 2.982	1.000 ± 0.014	†
149	0.865 ± 0.145	27.82 ± 1.366	0.918 ± 0.007	†
150	0.979 ± 0.167	28.69 ± 0.651	0.832 ± 0.006	0.932 ± 0.018
151				
152				
153				
154				
155	0.870 ± 0.124	32.19 ± 2.627	0.689 ± 0.007	0.934 ± 0.055
156	0.823 ± 0.106	31.88 ± 0.328	0.830 ± 0.010	0.937 ± 0.011
157	0.774 ± 0.078	30.59 ± 1.577	0.858 ± 0.011	0.979 ± 0.037
158	1.037 ± 0.201	36.18 ± 5.200	0.896 ± 0.011	1.000 ± 0.083
159	1.009 ± 0.270	33.48 ± 3.200	0.833 ± 0.013	1.000 ± 0.053
160	1.040 ± 0.178	33.32 ± 1.551	0.983 ± 0.014	†
161	0.759 ± 0.168	**	0.609 ± 0.016	
162	0.887 ± 0.173	**	0.864 ± 0.011	
163	1.114 ± 0.299	*	0.978 ± 0.023	
164				
165				
166				
167				
168		32.56 ± 0.841		
169	1.164 ± 0.257	38.47 ± 2.541	0.849 ± 0.010	1.000 ± 0.046

170	1.885 ± 0.445		0.645 ± 0.010	
171	1.265 ± 0.262	35.89 ± 2.385	0.836 ± 0.007	1.000 ± 0.054
172	1.123 ± 0.206	31.12 ± 2.398	0.835 ± 0.010	1.000 ± 0.051
173	1.220 ± 0.170	*	0.871 ± 0.019	
174	1.208 ± 0.277	37.97 ± 4.934	1.000 ± 0.011	†
175	1.256 ± 0.365	**	0.638 ± 0.016	
176				
177				
178		30.25 ± 0.508	1.000 ± 0.006	
179	0.845 ± 0.094	34.63 ± 4.812	0.871 ± 0.011	1.000 ± 0.061
180	1.100 ± 0.195	37.32 ± 0.588	0.855 ± 0.010	1.000 ± 0.014
181	0.984 ± 0.166	38.27 ± 1.342	0.888 ± 0.010	1.000 ± 0.022
182	1.325 ± 0.231	33.77 ± 0.584	0.826 ± 0.008	†
183				
184	1.862 ± 0.468		0.855 ± 0.011	
185	0.959 ± 0.191	30.68 ± 1.257	0.824 ± 0.008	0.938 ± 0.029
186	1.831 ± 0.361	25.83 ± 0.958	0.876 ± 0.009	0.776 ± 0.027
187	1.544 ± 0.275	27.05 ± 1.468	0.669 ± 0.008	0.540 ± 0.131
188	1.250 ± 0.223	25.80 ± 1.758	0.544 ± 0.007	0.641 ± 0.118
189	1.000 ± 0.172	25.45 ± 2.785	0.944 ± 0.017	†
190				
191				
192	1.266 ± 0.273	21.52 ± 2.605	0.776 ± 0.011	0.675 ± 0.071
193	1.133 ± 0.278	36.58 ± 1.683	0.837 ± 0.011	1.000 ± 0.028
194				
195	1.669 ± 0.747		0.815 ± 0.022	
196	0.821 ± 0.150		0.719 ± 0.013	
197				
198	0.830 ± 0.116	28.91 ± 1.925	0.725 ± 0.010	0.904 ± 0.042
199	1.069 ± 0.193	26.88 ± 0.249	0.782 ± 0.010	0.889 ± 0.010
200	1.137 ± 0.195	26.18 ± 0.654	0.779 ± 0.007	0.798 ± 0.069
201	1.060 ± 0.314	29.00 ± 1.992	0.807 ± 0.019	0.851 ± 0.053
202	0.799 ± 0.098	31.51 ± 1.085	0.836 ± 0.008	1.000 ± 0.021
203	0.844 ± 0.088	28.17 ± 1.721	0.653 ± 0.007	0.837 ± 0.033
204	0.839 ± 0.057	31.78 ± 1.478	0.795 ± 0.010	0.906 ± 0.024
205	0.755 ± 0.105	33.81 ± 1.180	0.890 ± 0.010	1.000 ± 0.021
206	0.968 ± 0.169	33.20 ± 3.624	0.656 ± 0.012	0.815 ± 0.072
207				
208	1.005 ± 0.186	20.76 ± 1.623	0.636 ± 0.008	0.761 ± 0.058
209	0.955 ± 0.213	30.69 ± 2.027		

210	1.116 ± 0.156	28.50 ± 1.283	0.692 ± 0.007	0.824 ± 0.072
211	0.870 ± 0.173	27.78 ± 1.765	0.756 ± 0.015	0.911 ± 0.044
212	0.986 ± 0.130	33.73 ± 4.092	0.807 ± 0.012	0.862 ± 0.042
213	1.062 ± 0.255	32.79 ± 0.978		
214	1.530 ± 0.371	27.03 ± 7.639	0.830 ± 0.017	1.000 ± 0.127
215	1.065 ± 0.218	*	0.802 ± 0.014	
216	1.323 ± 0.276	30.35 ± 1.261	0.761 ± 0.006	0.659 ± 0.088
217	0.824 ± 0.166	29.17 ± 5.349	1.000 ± 0.012	†
218	0.869 ± 0.111	35.61 ± 4.136	0.844 ± 0.011	1.000 ± 0.064
219				
220	0.778 ± 0.090	25.48 ± 2.771	0.919 ± 0.010	†
221	0.694 ± 0.066	34.36 ± 2.672	0.766 ± 0.008	0.948 ± 0.025
222				
223				
224	0.982 ± 0.124	24.56 ± 0.762	0.482 ± 0.006	0.790 ± 0.026
225				
226	1.173 ± 0.222	25.92 ± 0.488	0.303 ± 0.009	0.755 ± 0.017
227				
228	1.476 ± 0.368	24.11 ± 2.166	0.528 ± 0.009	0.664 ± 0.065
229	1.143 ± 0.219	30.11 ± 1.104	0.805 ± 0.006	0.867 ± 0.025
230	1.375 ± 0.193	16.88 ± 0.410	0.727 ± 0.007	0.452 ± 0.017
231	0.909 ± 0.143	26.67 ± 0.665	0.891 ± 0.009	0.962 ± 0.022
232	0.773 ± 0.092	31.50 ± 1.835		
233	1.212 ± 0.167	13.47 ± 0.814	0.570 ± 0.007	0.360 ± 0.026
234	0.870 ± 0.164	26.40 ± 3.284	0.813 ± 0.013	0.909 ± 0.052
235	0.804 ± 0.132	32.41 ± 2.290	0.769 ± 0.010	0.933 ± 0.041
236	0.889 ± 0.224	27.46 ± 2.910	0.667 ± 0.015	0.889 ± 0.066
237	0.993 ± 0.222	**	0.789 ± 0.019	
238	0.922 ± 0.149	38.71 ± 2.767	0.828 ± 0.008	0.966 ± 0.037
239	0.910 ± 0.196	*	0.821 ± 0.020	
240	0.817 ± 0.265	30.28 ± 4.720	1.000 ± 0.020	†
241	1.390 ± 0.390	37.53 ± 1.806	0.818 ± 0.014	1.000 ± 0.053
242	1.290 ± 0.237	35.10 ± 1.120	0.857 ± 0.008	1.000 ± 0.028
243		**	0.641 ± 0.009	
244	0.691 ± 0.349		0.441 ± 0.024	
245	1.356 ± 0.316	29.32 ± 4.274	0.752 ± 0.011	0.750 ± 0.098
246				
247				
248				
249				

250				
251	1.238 ± 0.228	**	0.891 ± 0.017	
252	0.877 ± 0.152	32.91 ± 3.637	1.000 ± 0.016	†
253	0.777 ± 0.093	30.40 ± 3.035	0.794 ± 0.011	0.952 ± 0.041
254	0.905 ± 0.152	27.89 ± 6.521	0.749 ± 0.010	0.927 ± 0.060
255	0.735 ± 0.142	35.66 ± 3.189	0.804 ± 0.011	0.953 ± 0.045
256	1.019 ± 0.164	**	0.880 ± 0.011	
257	0.821 ± 0.151	32.81 ± 0.732	0.978 ± 0.014	†
258	0.797 ± 0.097	30.05 ± 4.498	0.744 ± 0.008	0.921 ± 0.038
259				
260	1.313 ± 0.234	28.84 ± 1.114	0.708 ± 0.009	0.720 ± 0.116
261	1.147 ± 0.195	30.43 ± 0.760	0.679 ± 0.006	0.805 ± 0.096
262	1.112 ± 0.200	28.30 ± 1.457	0.684 ± 0.007	0.766 ± 0.091
263	0.873 ± 0.088	29.22 ± 1.271	0.763 ± 0.006	0.884 ± 0.031
264	0.935 ± 0.140	25.10 ± 1.018	0.836 ± 0.008	0.939 ± 0.024
265	0.870 ± 0.112	24.07 ± 2.226	0.679 ± 0.011	0.843 ± 0.041
266	0.767 ± 0.099	35.92 ± 4.275	0.798 ± 0.012	0.979 ± 0.050
267	1.042 ± 0.181	34.64 ± 3.027	0.706 ± 0.013	0.777 ± 0.079
268	0.755 ± 0.134	36.05 ± 0.948	0.777 ± 0.009	0.913 ± 0.051
269	0.949 ± 0.176	28.42 ± 1.107	0.839 ± 0.008	0.941 ± 0.024
270	0.887 ± 0.130	32.60 ± 2.098	0.834 ± 0.010	1.000 ± 0.036
271	0.876 ± 0.163	23.84 ± 2.207	0.990 ± 0.011	†
272				
273	0.907 ± 0.154	33.35 ± 4.561	0.739 ± 0.012	0.948 ± 0.071
274	1.052 ± 0.308	**	0.748 ± 0.012	
275	0.917 ± 0.159	32.24 ± 3.800	0.831 ± 0.011	1.000 ± 0.068
276				
277	1.334 ± 0.288	30.05 ± 1.155	0.700 ± 0.007	0.872 ± 0.038
278				
279	1.037 ± 0.172	37.30 ± 4.563	0.704 ± 0.010	0.775 ± 0.079
280	0.969 ± 0.190	31.54 ± 2.781	0.885 ± 0.011	1.000 ± 0.054
281	1.014 ± 0.149	31.55 ± 1.412	0.893 ± 0.009	0.995 ± 0.028
282	0.907 ± 0.142	35.02 ± 4.009	1.000 ± 0.012	†
283	0.810 ± 0.133	32.90 ± 0.830	0.730 ± 0.007	0.892 ± 0.053
284	1.009 ± 0.151	30.11 ± 0.433	0.635 ± 0.005	0.899 ± 0.013
285	0.930 ± 0.124	29.24 ± 1.380	0.749 ± 0.007	0.879 ± 0.039
286	0.838 ± 0.105	32.58 ± 2.887	0.821 ± 0.009	0.909 ± 0.027
287	0.845 ± 0.107	28.96 ± 1.542	0.694 ± 0.007	0.904 ± 0.037
288	0.886 ± 0.101	32.04 ± 0.495	0.764 ± 0.006	0.853 ± 0.044
289	0.844 ± 0.066	27.71 ± 0.712	0.759 ± 0.006	0.868 ± 0.018

290			
291			
292	1.935 ± 0.323	18.56 ± 0.266	0.518 ± 0.004
293	2.608 ± 0.507	16.17 ± 0.553	0.382 ± 0.005
294	2.297 ± 0.365	12.48 ± 0.251	0.489 ± 0.002
295			
296			
297			
298	3.202 ± 0.661	9.95 ± 0.387	0.380 ± 0.003
299	2.166 ± 0.255	6.84 ± 0.121	0.322 ± 0.002
300			
301			
302			
303	3.522 ± 0.807	9.57 ± 0.600	0.374 ± 0.009
304			
305	3.965 ± 0.757	10.16 ± 0.646	0.281 ± 0.005
306	4.271 ± 0.877	8.21 ± 0.434	0.286 ± 0.005
307	3.801 ± 0.700	8.44 ± 0.224	0.256 ± 0.004
308	2.345 ± 0.363	5.96 ± 0.151	0.012 ± 0.002
309			
310	3.730 ± 0.835	7.93 ± 0.599	
311		10.82 ± 0.652	0.291 ± 0.005

Appendix J: R1, R2, NOE, and S^2 values for N235K p53 DBD at 800 MHz field strength.

* Signal present up to .030 seconds

** Signal present up to .050 seconds

*** Signal present up to 0.100 seconds

† *Modelfree* calculation did not assign a model to residue.

Residue #	R1 ± error	R2 ± error	NOE ± error	S2 ± error
99	1.248 ± 0.248	25.56 ± 1.136	0.813 ± 0.010	†
100	1.403 ± 0.338	27.94 ± 1.222	0.766 ± 0.014	0.661 ± 0.118
101	1.307 ± 0.247	29.19 ± 0.730	0.750 ± 0.008	0.740 ± 0.109
102	1.283 ± 0.285	**	0.800 ± 0.015	
103	1.117 ± 0.183	**	0.969 ± 0.017	
104				
105	1.391 ± 0.318	33.46 ± 1.780	0.691 ± 0.013	0.654 ± 0.150
106				
107	1.277 ± 0.243	33.71 ± 0.290	0.865 ± 0.012	1.000 ± 0.000
108	0.988 ± 0.146	23.85 ± 1.534	0.785 ± 0.010	0.898 ± 0.001
109	1.012 ± 0.165	27.40 ± 1.343		
110	0.836 ± 0.100	**	0.929 ± 0.017	
111	0.991 ± 0.078	35.40 ± 6.337	0.973 ± 0.024	†
112	1.092 ± 0.147	*	0.978 ± 0.028	
113	1.003 ± 0.139	30.73 ± 2.536	0.675 ± 0.014	0.856 ± 0.061
114				
115	**	*	0.759 ± 0.038	
116				
117	**	*		
118	1.417 ± 0.357	30.65 ± 2.806	0.752 ± 0.013	0.695 ± 0.138
119				
120				
121	4.456 ± 1.074	32.69 ± 15.977		
122	2.299 ± 0.430	26.42 ± 3.995	0.733 ± 0.024	†
123				
124	1.482 ± 0.274	26.93 ± 4.251	0.647 ± 0.023	0.605 ± 0.139
125	1.279 ± 0.212	26.48 ± 3.209	0.751 ± 0.020	0.758 ± 0.089
126	2.124 ± 0.527	**	0.632 ± 0.037	
127	1.289 ± 0.253	**	0.882 ± 0.019	

128				
129	1.024 ± 0.141	28.15 ± 1.751		
130	1.005 ± 0.205	*	0.989 ± 0.017	
131	1.235 ± 0.154	24.37 ± 0.501		
132	1.169 ± 0.178	**	0.851 ± 0.019	
133	**		0.746 ± 0.032	
134	0.822 ± 0.207	**	0.669 ± 0.019	
135	1.119 ± 0.159	36.35 ± 5.429	0.900 ± 0.016	1.000 ± 0.000
136	1.028 ± 0.179	**	0.828 ± 0.019	
137	0.847 ± 0.116	25.64 ± 1.906	0.733 ± 0.019	0.955 ± 0.072
138	1.073 ± 0.176	21.51 ± 3.824	0.562 ± 0.018	0.736 ± 0.058
139	1.074 ± 0.169	25.79 ± 2.137	0.671 ± 0.011	0.805 ± 0.075
140		*		
141	1.874 ± 0.635	*	0.856 ± 0.027	
142				
143	0.803 ± 0.130	27.54 ± 2.947	0.934 ± 0.024	1.000 ± 0.001
144	1.030 ± 0.200	23.60 ± 1.232	0.848 ± 0.021	1.000 ± 0.000
145	1.006 ± 0.142	28.21 ± 5.630	0.872 ± 0.019	1.000 ± 0.000
146	0.936 ± 0.176	30.04 ± 1.645	0.872 ± 0.013	1.000 ± 0.000
147	0.876 ± 0.122	30.19 ± 0.278	0.792 ± 0.012	0.932 ± 0.046
148	0.861 ± 0.152	27.34 ± 1.711	0.676 ± 0.013	0.921 ± 0.073
149	0.989 ± 0.174	28.92 ± 2.476	0.918 ± 0.011	†
150	1.093 ± 0.184	26.98 ± 0.520	0.801 ± 0.006	0.871 ± 0.058
151				
152				
153				
154				
155	0.929 ± 0.135	28.64 ± 1.003	0.793 ± 0.009	0.945 ± 0.050
156	0.815 ± 0.080	**	0.909 ± 0.014	
157	0.828 ± 0.107	32.85 ± 1.872	0.987 ± 0.015	†
158	1.121 ± 0.122	**	1.000 ± 0.021	
159	0.984 ± 0.165	27.05 ± 3.110	0.893 ± 0.018	1.000 ± 0.000
160	1.035 ± 0.208	27.50 ± 2.771	0.695 ± 0.012	0.847 ± 0.082
161	2.129 ± 0.192	**	0.951 ± 0.032	
162	1.023 ± 0.177	26.68 ± 2.544	0.786 ± 0.016	0.898 ± 0.067
163	1.506 ± 0.408	**	1.000 ± 0.033	
164				
165				
166				
167				

168	1.224 ± 0.204	30.78 ± 0.968		
169	1.056 ± 0.231	**	0.999 ± 0.016	
170		25.59 ± 3.538		
171	1.099 ± 0.187	**	0.724 ± 0.010	
172	0.952 ± 0.200	26.89 ± 1.524	0.750 ± 0.014	0.920 ± 0.078
173	3.687 ± 0.983	*	0.852 ± 0.025	
174	1.513 ± 0.359	**	0.924 ± 0.017	
175	2.855 ± 0.134	*	0.628 ± 0.027	
176				
177				
178	0.915 ± 0.131	29.77 ± 1.705	0.838 ± 0.011	1.000 ± 0.000
179	1.022 ± 0.213	**	0.676 ± 0.014	
180	1.405 ± 0.304	**	0.806 ± 0.016	
181	0.804 ± 0.110	33.95 ± 5.478	0.867 ± 0.022	0.941 ± 0.094
182	1.226 ± 0.228	33.17 ± 0.392	0.839 ± 0.015	1.000 ± 0.000
183				
184				
185	1.042 ± 0.180	32.06 ± 1.980	0.860 ± 0.011	1.000 ± 0.000
186	1.953 ± 0.377	25.64 ± 2.076	0.721 ± 0.016	0.379 ± 0.163
187	1.802 ± 0.428	27.36 ± 0.744	0.621 ± 0.013	0.428 ± 0.223
188	1.249 ± 0.181	23.82 ± 0.953	0.725 ± 0.010	0.762 ± 0.082
189				
190				
191				
192	3.232 ± 0.837	17.22 ± 2.267	0.925 ± 0.033	0.753 ± 0.001
193	1.420 ± 0.345	33.36 ± 2.593	0.958 ± 0.017	†
194				
195	2.277 ± 0.506	*	0.882 ± 0.026	
196	1.192 ± 0.173	**	0.973 ± 0.024	
197				
198	***	*		
199	1.581 ± 0.416	24.11 ± 0.772	0.633 ± 0.013	0.539 ± 0.199
200	1.227 ± 0.215	27.43 ± 1.074		
201	1.443 ± 0.517	**	0.557 ± 0.023	
202			0.527 ± 0.008	
203	0.814 ± 0.083	26.90 ± 0.661	0.775 ± 0.013	0.962 ± 0.001
204	0.940 ± 0.123	**	0.818 ± 0.012	
205	0.787 ± 0.139	27.57 ± 0.493	0.796 ± 0.014	0.954 ± 0.058
206	0.969 ± 0.136	**	0.918 ± 0.016	
207	0.848 ± 0.085	26.33 ± 0.698	0.699 ± 0.007	0.951 ± 0.048

208	1.113 ± 0.193	21.01 ± 1.071	0.678 ± 0.012	0.923 ± 0.001
209	1.170 ± 0.208	31.43 ± 1.939	0.712 ± 0.011	0.797 ± 0.088
210	1.110 ± 0.163	26.70 ± 1.624	0.825 ± 0.011	1.000 ± 0.000
211	0.948 ± 0.183	25.48 ± 1.787	0.758 ± 0.018	0.913 ± 0.069
212	1.087 ± 0.140	30.62 ± 2.749	0.850 ± 0.015	1.000 ± 0.000
213	1.210 ± 0.209	30.45 ± 1.003		
214	1.300 ± 0.338	**	0.859 ± 0.018	
215	1.816 ± 0.540	**	0.774 ± 0.018	
216	1.228 ± 0.204	**	0.850 ± 0.009	
217	0.757 ± 0.076	**	0.758 ± 0.015	
218	0.907 ± 0.128	29.35 ± 1.154	0.734 ± 0.011	0.897 ± 0.053
219				
220	0.973 ± 0.113	35.53 ± 1.626	1.000 ± 0.014	†
221	0.714 ± 0.088	31.10 ± 0.856	0.961 ± 0.015	†
222				
223				
224	0.879 ± 0.090	21.73 ± 1.020	0.522 ± 0.010	0.871 ± 0.000
225	0.842 ± 0.077	20.49 ± 0.609	0.634 ± 0.008	0.847 ± 0.001
226	1.145 ± 0.159	25.93 ± 1.199	0.276 ± 0.012	0.625 ± 0.100
227				
228	1.480 ± 0.301	21.97 ± 1.624	0.598 ± 0.011	0.565 ± 0.148
229	1.201 ± 0.216	27.33 ± 1.829	0.786 ± 0.009	†
230	1.382 ± 0.202	12.18 ± 0.734	0.755 ± 0.013	0.388 ± 0.014
231	0.938 ± 0.175	29.45 ± 0.894	0.763 ± 0.014	0.908 ± 0.064
232	0.876 ± 0.139	**	0.839 ± 0.020	
233	2.246 ± 0.285	7.80 ± 0.609		
234	***	**		
235	0.986 ± 0.175	**	0.762 ± 0.015	
236	1.701 ± 0.382	**	1.000 ± 0.036	
237	2.718 ± 0.815	**	0.504 ± 0.028	
238	1.084 ± 0.183	**	0.776 ± 0.013	
239	2.865 ± 0.522	16.74 ± 0.800	0.303 ± 0.016	†
240	1.941 ± 0.373	**	0.737 ± 0.020	
241	2.102 ± 0.474	**	0.671 ± 0.016	
242	1.105 ± 0.224	31.09 ± 0.705	0.850 ± 0.011	1.000 ± 0.000
243				
244	***		0.514 ± 0.028	
245	1.215 ± 0.163	34.39 ± 4.164	0.850 ± 0.017	1.000 ± 0.000
246				
247				

248				
249				
250				
251	1.056 ± 0.240	**	0.693 ± 0.033	
252	0.927 ± 0.187	**	0.641 ± 0.019	
253	0.899 ± 0.157	**	0.816 ± 0.020	
254	1.505 ± 0.220	**	0.998 ± 0.020	
255	0.810 ± 0.123	**	0.805 ± 0.014	
256	0.986 ± 0.189	28.83 ± 1.723	0.755 ± 0.014	0.866 ± 0.078
257	0.843 ± 0.160	26.95 ± 3.706	0.863 ± 0.015	1.000 ± 0.000
258	0.867 ± 0.100	31.89 ± 1.429	0.738 ± 0.013	0.889 ± 0.043
259	2.227 ± 0.430	10.14 ± 0.580	0.263 ± 0.004	0.315 ± 0.000
260	1.305 ± 0.239	28.97 ± 2.414	0.757 ± 0.013	0.745 ± 0.100
261	1.110 ± 0.197	28.59 ± 0.850	0.700 ± 0.009	0.808 ± 0.090
262	1.046 ± 0.139	28.35 ± 1.099	0.888 ± 0.013	1.000 ± 0.000
263	1.032 ± 0.159	33.79 ± 0.328	0.950 ± 0.011	†
264	0.873 ± 0.109	27.05 ± 0.368	0.867 ± 0.009	1.000 ± 0.000
265	1.205 ± 0.234	**	1.000 ± 0.028	
266	0.822 ± 0.101	**	0.646 ± 0.012	
267	1.389 ± 0.467	*	0.788 ± 0.025	
268	0.811 ± 0.179	**	0.888 ± 0.016	
269	0.967 ± 0.161	**	0.810 ± 0.015	
270	0.935 ± 0.105	31.28 ± 1.234	0.790 ± 0.016	0.931 ± 0.038
271	1.011 ± 0.172	21.81 ± 2.589	0.774 ± 0.013	0.924 ± 0.001
272	1.041 ± 0.168	25.73 ± 1.695	0.843 ± 0.012	1.000 ± 0.000
273	1.332 ± 0.205	**	0.989 ± 0.021	
274	***	**	0.870 ± 0.023	
275	1.042 ± 0.143	28.96 ± 1.269	0.723 ± 0.018	0.862 ± 0.058
276				
277	2.122 ± 0.484	29.11 ± 0.595	0.615 ± 0.017	0.249 ± 0.225
278				
279	***	*	1.000 ± 0.048	
280	1.668 ± 0.420	*	0.667 ± 0.029	
281	1.185 ± 0.232	28.63 ± 0.999	0.915 ± 0.014	1.000 ± 0.000
282	1.536 ± 0.367	**	0.896 ± 0.024	
283	1.022 ± 0.156	**	0.763 ± 0.017	
284	1.098 ± 0.181	27.76 ± 1.189	0.685 ± 0.008	0.791 ± 0.087
285	0.993 ± 0.171	30.76 ± 1.553	0.885 ± 0.011	1.000 ± 0.000
286	0.924 ± 0.118	29.16 ± 1.380	0.799 ± 0.013	0.886 ± 0.047
287	0.949 ± 0.109	29.43 ± 1.518	0.756 ± 0.010	0.886 ± 0.046

288	0.905 ± 0.101	32.66 ± 1.741	0.788 ± 0.009	0.937 ± 0.040
289	0.925 ± 0.080	27.66 ± 1.047	0.742 ± 0.008	0.874 ± 0.037
290	1.222 ± 0.125	4.02 ± 0.232		
291	1.214 ± 0.141	23.51 ± 0.468		
292	1.686 ± 0.241	18.50 ± 0.466	0.510 ± 0.006	
293	2.318 ± 0.412	14.95 ± 0.169	0.454 ± 0.006	
294	1.988 ± 0.296	12.81 ± 0.441	0.499 ± 0.003	
295				
296				
297				
298	3.253 ± 0.617	9.94 ± 0.468	0.432 ± 0.004	
299	2.123 ± 0.217	6.55 ± 0.085	0.310 ± 0.003	
300				
301				
302				
303	3.866 ± 0.748	8.43 ± 0.321	0.321 ± 0.008	
304				
305	3.708 ± 0.718	9.12 ± 0.519	0.317 ± 0.005	
306	3.528 ± 0.582	6.63 ± 0.538	0.269 ± 0.005	
307	3.424 ± 0.571	7.65 ± 0.225	0.203 ± 0.004	
308	2.197 ± 0.266	5.09 ± 0.233	-0.009 ± 0.002	
309				
310	2.561 ± 0.502	8.35 ± 0.592		
311	1.880 ± 0.385	10.60 ± 1.273		

Appendix K: R1, R2, NOE, and S^2 values for N239Y p53 DBD at 800 MHz field strength.

* Signal present up to .030 seconds

** Signal present up to .050 seconds

*** Signal present up to 0.100 seconds

† *Modelfree* calculation did not assign a model to residue

Residue #	R1 ± error	R2 ± error	NOE ± error	S2 ± error
99	1.357 ± 0.320	25.88 ± 0.202	0.646 ± 0.011	0.725 ± 0.143
100	1.702 ± 0.598	**	0.661 ± 0.013	
101	1.153 ± 0.244	28.61 ± 2.150	0.933 ± 0.008	†
102	1.591 ± 0.716	**	0.849 ± 0.010	
103	1.038 ± 0.191	*	0.885 ± 0.018	
104				
105	1.139 ± 0.256	**	0.964 ± 0.014	
106				
107	1.256 ± 0.185	31.03 ± 3.450	0.816 ± 0.008	0.875 ± 0.050
108	0.906 ± 0.352	26.78 ± 1.790	0.748 ± 0.011	0.969 ± 0.045
109	1.158 ± 0.181	27.51 ± 1.730	0.846 ± 0.007	1.000 ± 0.038
110	0.708 ± 0.147	*	0.988 ± 0.017	
111	0.632 ± 0.122	**	0.891 ± 0.014	
112	0.495 ± 0.156	**	0.575 ± 0.016	
113		31.05 ± 5.830	0.900 ± 0.013	
114	1.305 ± 0.408	28.51 ± 3.516	0.549 ± 0.015	1.000 ± 0.072
115	***	*	0.540 ± 0.029	
116				
117	**	*	0.518 ± 0.029	
118	***	27.12 ± 3.483	0.651 ± 0.011	
119				
120				
121	2.504 ± 1.149	**	0.311 ± 0.018	
122		*		
123				
124		**		
125	0.836 ± 0.144	**	0.650 ± 0.011	
126	1.187 ± 0.376	*	0.760 ± 0.026	
127	0.932 ± 0.300	19.55 ± 3.556	0.887 ± 0.017	0.814 ± 0.125
128				

129		28.17 ± 1.521	0.666 ± 0.010	
130	0.808 ± 0.234	58.78 ± 21.182	0.823 ± 0.015	1.000 ± 0.023
131	1.382 ± 0.177	29.22 ± 2.027	0.680 ± 0.005	0.654 ± 0.089
132	0.878 ± 0.242	26.83 ± 3.965	0.736 ± 0.012	0.962 ± 0.078
133	0.781 ± 0.330		0.815 ± 0.026	
134	0.886 ± 0.207	**	1.000 ± 0.015	
135	0.923 ± 0.216	29.73 ± 3.908	0.806 ± 0.011	0.923 ± 0.072
136				
137	***			
138	1.209 ± 0.420		0.528 ± 0.026	
139	0.866 ± 0.178	19.69 ± 0.572	0.860 ± 0.014	0.798 ± 0.022
140	0.814 ± 0.407	18.97 ± 2.464	0.792 ± 0.013	0.751 ± 0.073
141	0.738 ± 0.149	**	0.855 ± 0.016	
142				
143	0.560 ± 0.132	*	0.844 ± 0.016	
144	1.848 ± 0.381	12.58 ± 2.134	0.520 ± 0.013	0.518 ± 0.113
145	0.565 ± 0.118	*	0.891 ± 0.023	
146	0.652 ± 0.125	**	0.895 ± 0.013	
147	0.760 ± 0.162	**	0.849 ± 0.012	
148	0.845 ± 0.158	**	0.697 ± 0.012	
149	0.786 ± 0.191	34.22 ± 5.465	0.974 ± 0.011	†
150	0.864 ± 0.164	26.18 ± 0.925	0.756 ± 0.007	0.937 ± 0.031
151				
152				
153				
154				
155	0.666 ± 0.153	27.84 ± 0.863	0.768 ± 0.010	0.963 ± 0.021
156	0.789 ± 0.124	**	0.735 ± 0.013	
157	0.492 ± 0.131	**	0.824 ± 0.014	
158	0.785 ± 0.183	*	0.906 ± 0.018	
159	0.736 ± 0.174	**	1.000 ± 0.015	
160	1.051 ± 0.195	**	0.887 ± 0.013	
161	0.916 ± 0.155	*	0.743 ± 0.020	
162	0.596 ± 0.135	**	0.805 ± 0.014	
163	1.682 ± 0.491	*	0.300 ± 0.018	
164				
165				
166				
167				
168			0.785 ± 0.008	

169	1.045 ± 0.345	**	0.955 ± 0.011	
170				
171	0.992 ± 0.227	29.80 ± 3.132	0.815 ± 0.011	1.000 ± 0.075
172	0.778 ± 0.143	**	0.905 ± 0.016	
173	0.861 ± 0.267	*	0.962 ± 0.014	
174	0.790 ± 0.156	*	0.810 ± 0.013	
175	1.390 ± 0.487	*	0.708 ± 0.017	
176				
177				
178	1.180 ± 0.110	32.17 ± 0.737	0.807 ± 0.008	†
179	0.838 ± 0.194	**	1.000 ± 0.019	
180	0.802 ± 0.141	*	0.949 ± 0.014	
181	0.563 ± 0.168	*	0.720 ± 0.011	
182	1.217 ± 0.302	**	0.841 ± 0.012	
183				
184	***	*		
185	0.912 ± 0.187	28.69 ± 0.351	0.858 ± 0.009	0.982 ± 0.011
186	1.293 ± 0.278	24.08 ± 3.119	0.576 ± 0.012	0.893 ± 0.091
187	1.249 ± 0.241	26.01 ± 3.113	0.501 ± 0.011	1.000 ± 0.073
188	1.152 ± 0.169	28.56 ± 4.640	0.719 ± 0.011	0.852 ± 0.070
189	0.869 ± 0.294	*	0.706 ± 0.018	
190				
191				
192	0.833 ± 0.240	22.06 ± 4.489	0.731 ± 0.016	0.995 ± 0.085
193	1.106 ± 0.301	**	0.651 ± 0.010	
194				
195	1.071 ± 0.266	*	1.000 ± 0.035	
196	0.799 ± 0.169	*	0.751 ± 0.019	
197				
198	0.631 ± 0.138	**	0.751 ± 0.013	
199	1.141 ± 0.255	25.87 ± 1.338	0.623 ± 0.010	0.897 ± 0.045
200	1.219 ± 0.220	22.93 ± 0.997	0.798 ± 0.008	0.816 ± 0.037
201	***	*		
202	0.657 ± 0.176	24.15 ± 4.957	0.685 ± 0.009	0.873 ± 0.096
203	0.589 ± 0.104	26.55 ± 0.924	0.834 ± 0.010	0.971 ± 0.028
204	0.554 ± 0.095	**	0.851 ± 0.014	
205	0.565 ± 0.132	**	0.735 ± 0.012	
206	0.802 ± 0.169	**	0.962 ± 0.014	
207			0.540 ± 0.005	
208	0.893 ± 0.397	18.26 ± 2.532	0.844 ± 0.012	0.952 ± 0.083

209	1.428 ± 0.297	*	0.808 ± 0.014	
210	0.881 ± 0.208	26.04 ± 1.704	0.737 ± 0.009	0.910 ± 0.049
211	0.836 ± 0.206	27.76 ± 2.159	0.705 ± 0.016	0.957 ± 0.047
212	0.916 ± 0.241	**	0.840 ± 0.015	
213			0.840 ± 0.008	
214	0.934 ± 0.261	*	0.718 ± 0.016	
215	0.863 ± 0.258	*	0.824 ± 0.019	
216	1.110 ± 0.210	32.84 ± 0.508	0.882 ± 0.007	1.000 ± 0.012
217	0.658 ± 0.134	**	0.963 ± 0.016	
218	0.651 ± 0.173	32.72 ± 2.026	0.694 ± 0.010	0.840 ± 0.110
219				
220	0.524 ± 0.229	18.07 ± 3.171	0.815 ± 0.013	0.738 ± 0.118
221	0.557 ± 0.117	28.14 ± 1.830	0.543 ± 0.011	0.529 ± 0.092
222				
223				
224	1.005 ± 0.272	19.09 ± 1.297	0.480 ± 0.009	0.849 ± 0.049
225				
226	1.299 ± 0.289	28.39 ± 3.462	0.411 ± 0.013	0.571 ± 0.155
227				
228	1.274 ± 0.219	26.23 ± 3.677	0.742 ± 0.015	1.000 ± 0.076
229	1.095 ± 0.391	24.03 ± 1.485	0.765 ± 0.009	0.833 ± 0.050
230	1.125 ± 0.210	13.92 ± 0.737	0.675 ± 0.008	0.436 ± 0.030
231	0.884 ± 0.180	23.15 ± 0.924	0.855 ± 0.012	0.861 ± 0.038
232	0.630 ± 0.220	*	0.961 ± 0.012	
233	1.312 ± 0.186		0.778 ± 0.011	
234	0.790 ± 0.213			
235	0.642 ± 0.109	25.94 ± 2.308	0.962 ± 0.017	†
236	0.743 ± 0.199	*	0.694 ± 0.024	
237	***	*	1.000 ± 0.035	
238	0.871 ± 0.166	**	0.944 ± 0.013	
239	1.271 ± 0.431	22.75 ± 5.606	0.691 ± 0.016	0.716 ± 0.150
240	1.000 ± 0.502	**	1.000 ± 0.031	
241	1.186 ± 0.295	*	0.541 ± 0.015	
242	0.858 ± 0.121	33.14 ± 0.944	0.906 ± 0.010	1.000 ± 0.022
243	1.358 ± 0.423	*	0.960 ± 0.011	
244	***		0.469 ± 0.023	
245	1.173 ± 0.225	*	0.799 ± 0.012	
246				
247				
248				

249				
250				
251	0.803 ± 0.226	*	0.886 ± 0.023	
252	0.620 ± 0.106	*	0.730 ± 0.015	
253	0.566 ± 0.136	**	0.722 ± 0.016	
254	0.596 ± 0.121	24.21 ± 0.895	0.674 ± 0.010	0.878 ± 0.030
255	0.631 ± 0.184	*	0.834 ± 0.014	
256	0.803 ± 0.201	*	0.764 ± 0.013	
257	0.640 ± 0.163	**	0.860 ± 0.015	
258	0.568 ± 0.137	26.50 ± 1.068	0.813 ± 0.012	0.905 ± 0.036
259	1.179 ± 0.278	11.77 ± 0.938	0.467 ± 0.006	0.353 ± 0.035
260	0.960 ± 0.220	28.86 ± 5.055	0.617 ± 0.011	0.877 ± 0.091
261	1.028 ± 0.180	26.60 ± 0.643	0.822 ± 0.007	0.897 ± 0.021
262	0.810 ± 0.211	31.19 ± 1.075	0.764 ± 0.011	0.926 ± 0.071
263	0.688 ± 0.139	32.63 ± 0.558	0.741 ± 0.008	0.737 ± 0.094
264	0.599 ± 0.175	25.85 ± 1.377	0.913 ± 0.008	†
265	0.745 ± 0.226	**	0.796 ± 0.013	
266	0.664 ± 0.154	**	0.813 ± 0.015	
267	0.715 ± 0.156	*	0.804 ± 0.019	
268	0.602 ± 0.113	**	0.707 ± 0.012	
269	0.996 ± 0.138	28.06 ± 0.399	0.889 ± 0.013	1.000 ± 0.009
270	0.773 ± 0.140	**	0.853 ± 0.012	
271	0.717 ± 0.245	26.19 ± 4.550	0.490 ± 0.013	1.000 ± 0.085
272	1.007 ± 0.205	29.58 ± 1.930	0.766 ± 0.009	1.000 ± 0.035
273	0.748 ± 0.153	*	0.980 ± 0.018	
274				
275	0.810 ± 0.218	**	0.750 ± 0.015	
276				
277	1.279 ± 0.290		0.754 ± 0.016	
278				
279	0.836 ± 0.164		0.852 ± 0.023	
280	0.799 ± 0.261	**	0.613 ± 0.010	
281	0.555 ± 0.280			
282	0.787 ± 0.152	**	0.743 ± 0.014	
283	0.839 ± 0.166	31.75 ± 2.480	0.974 ± 0.010	1.000 ± 0.048
284	0.954 ± 0.174	27.66 ± 1.374	0.659 ± 0.006	0.856 ± 0.074
285	0.956 ± 0.158	31.53 ± 3.338	0.933 ± 0.010	†
286	0.599 ± 0.090	**	0.963 ± 0.015	
287	0.680 ± 0.106	28.56 ± 2.047	0.783 ± 0.008	0.978 ± 0.035
288	0.790 ± 0.129	30.77 ± 2.294	0.800 ± 0.009	0.878 ± 0.063

289	1.125 ± 0.258	26.32 ± 0.778	0.818 ± 0.006	0.893 ± 0.027
290				
291	1.347 ± 0.193	27.14 ± 1.805	0.616 ± 0.005	
292	1.762 ± 0.498	16.97 ± 0.616	0.445 ± 0.005	
293	4.463 ± 3.428	14.83 ± 0.804	0.426 ± 0.007	
294	1.723 ± 0.214	11.56 ± 0.388	0.565 ± 0.003	
295				
296				
297				
298	2.069 ± 0.391	8.81 ± 0.609	0.440 ± 0.004	
299	2.053 ± 0.256	6.09 ± 0.381	0.372 ± 0.003	
300			-0.080 ± 0.011	
301				
302				
303	***	7.36 ± 0.417		
304				
305	7.190 ± 2.443	7.65 ± 0.640	0.377 ± 0.006	
306	6.658 ± 2.951	7.77 ± 1.349	0.253 ± 0.005	
307	2.135 ± 0.337	6.57 ± 0.329	0.282 ± 0.005	
308	2.215 ± 0.352	4.37 ± 0.186	0.010 ± 0.002	
309				
310	14.001 ± 5.062	6.93 ± 0.518		
311	5.643 ± 2.730	10.07 ± 0.395	0.335 ± 0.006	

Appendix L: R2*R1 analysis for rescue mutants.

A) N235K and B) N39Y. R2*R1 is plotted as a function of amino acid residue. The diagram above the graphs illustrates p53 secondary structures. In N235K we see chemical exchange in L1 (122), L2 (192, 193, 199), and L3 (239). N239Y only shows chemical exchange for residue 130 and 131. Dotted lined indicates 10 % trimmed value after excluding residue with NOE< 0.7.

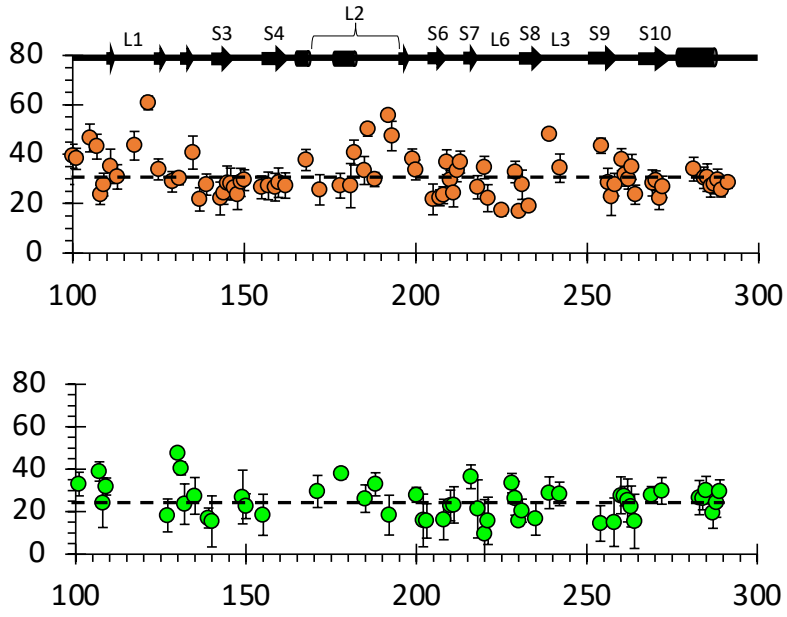

Appendix M: Comparison of NMR S2 Calculated from Mutant Crystal or WT NMR Structures.

Use of mutant p53 crystal or WT NMR coordinate files do not change *Modelfree* S^2 calculation results. **(A)** Difference between S^2 values calculated from N235K relaxation data when using N235K crystal (PDB: **4LO9**) or WT NMR as the structure file (PDB: **2FEJ**) **(B)** Difference in S^2 values calculated from N239Y data when using N239Y crystal (PDB: **4LOE**) or WT NMR as the structure file (PDB: **2FEJ**).

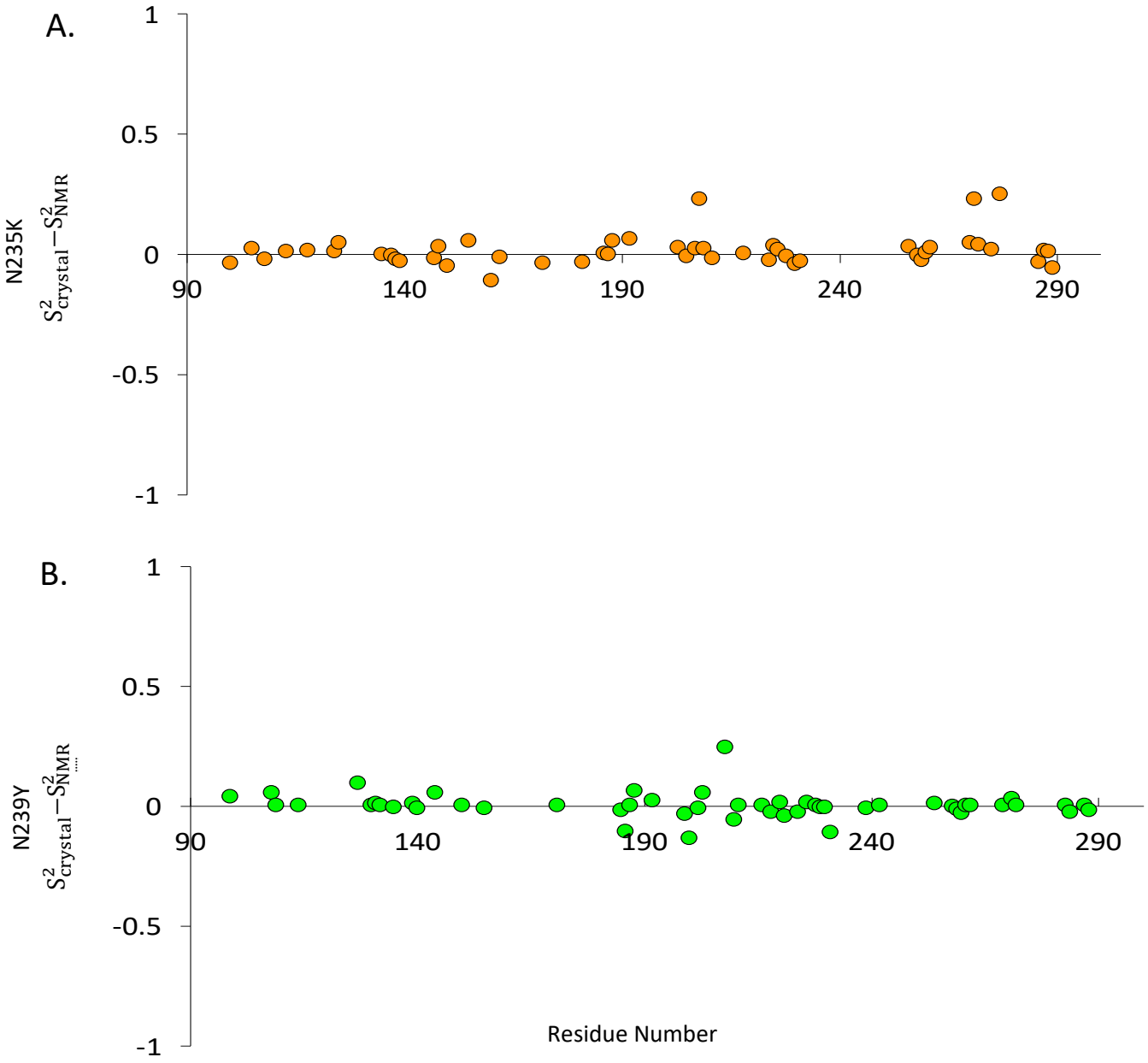

Appendix N: Differences in order parameters between rescue mutants and WT:

A) Difference between N235K and WT. **B)** Difference between N239Y and WT.

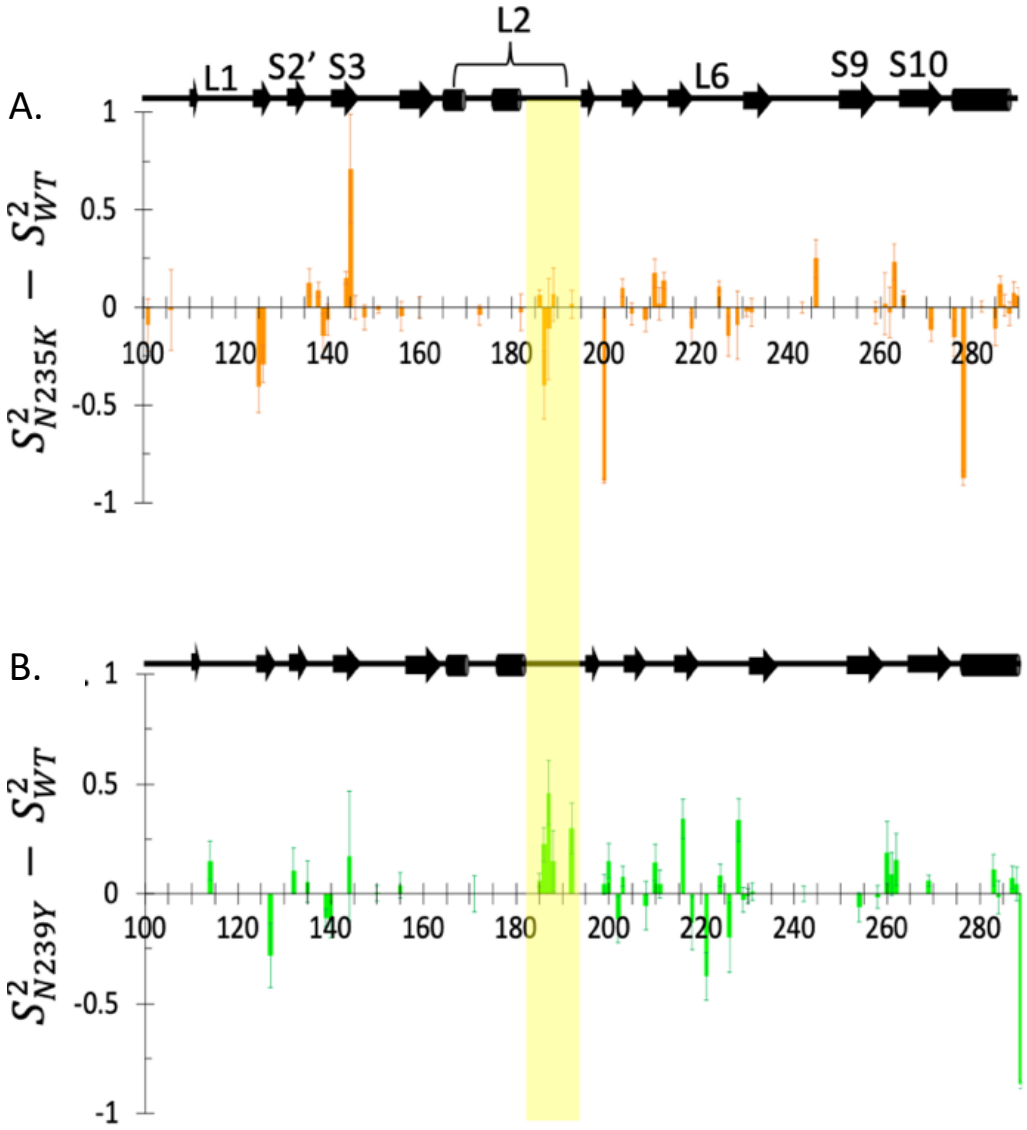

Appendix O: Hydrogen exchange rate for DBH at 30 and d50 C.

(A) ^{15}N-HSQC spectra of Dbh at 35 °C (blue, top) and 50 °C (teal, bottom) at different time points after being transferred into D_2O. Peaks were integrated at each time point over a period of two weeks and plotted as a function of time. Hydrogen exchange rates (k_{ex}) were calculated from a fit to a single exponential. Representative data: **(B)** 271Asn and 304His hydrogen signal intensities in Dbh at 35 °C. **(C)** 130Lys and 106Glu hydrogen signal intensities in Dbh at 50 °C.

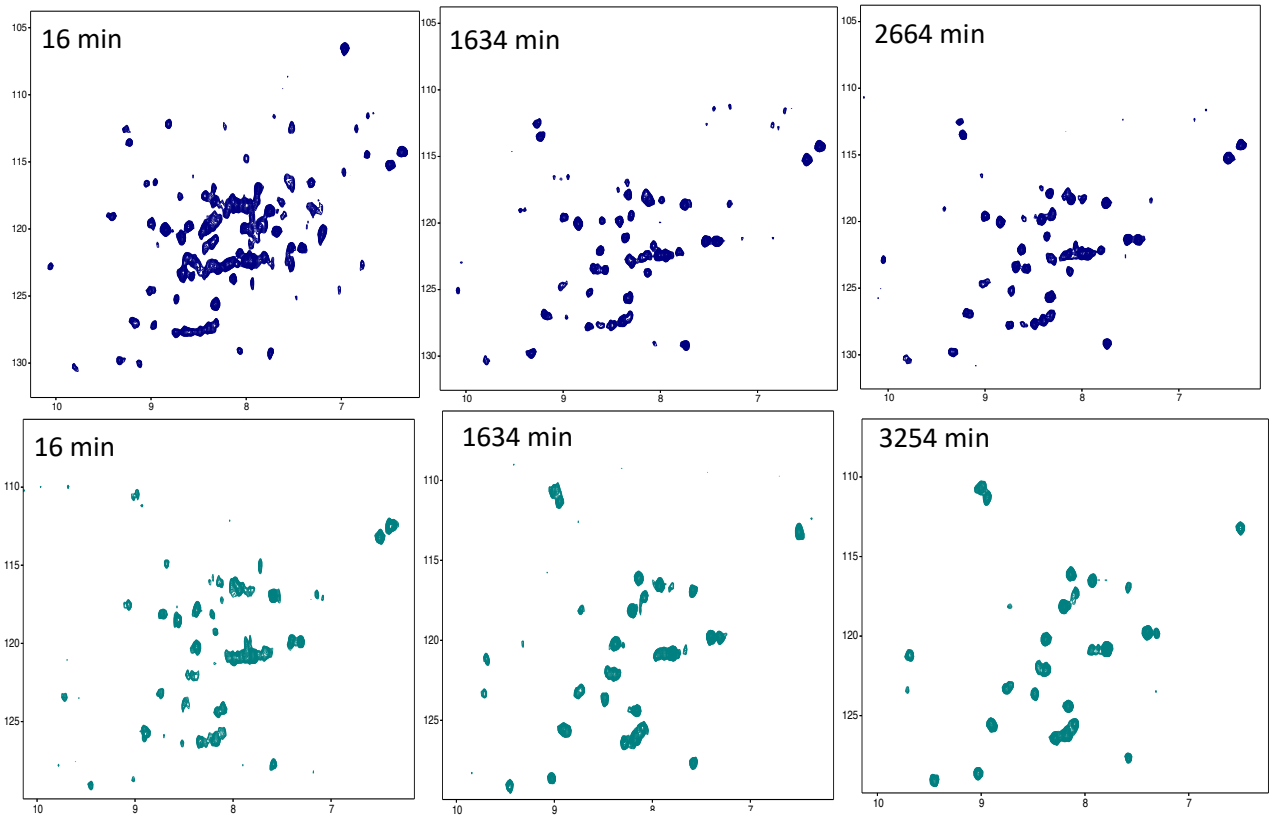

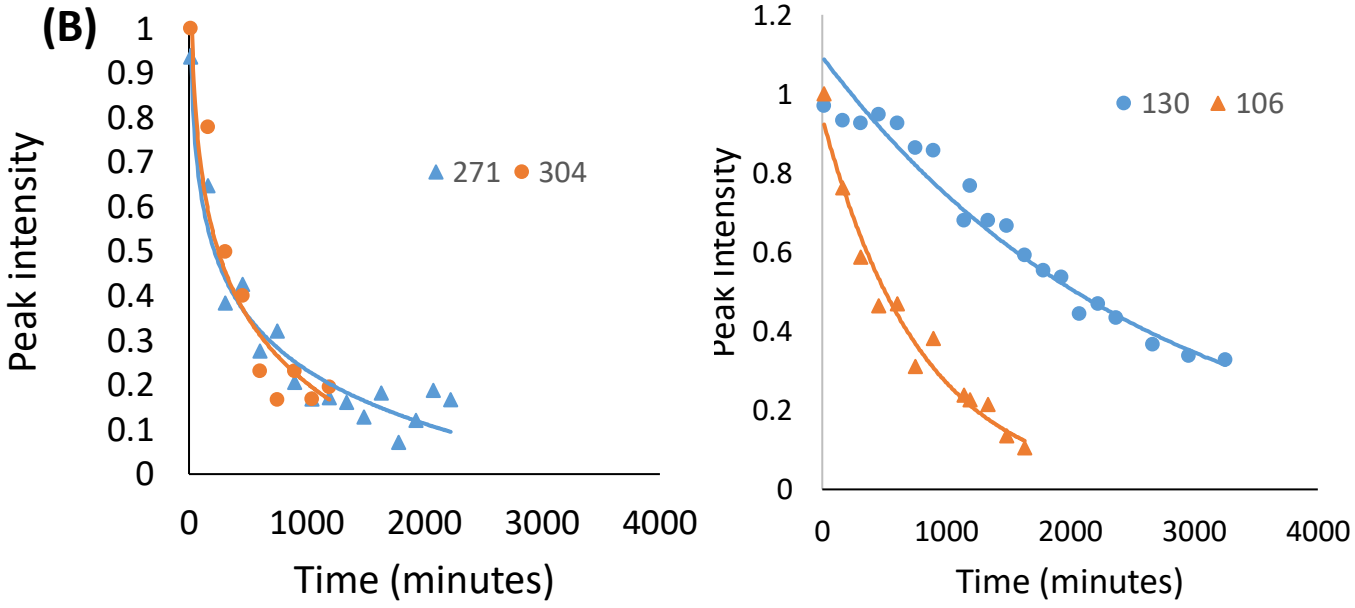

Appendix P: Measured exchange rate and calculated protection factors for DBH at 35 C and 50 °C. TC value for all amides.

Include measures exchange rates (k_{ex}) and Protection Factors (PF) at 35 °C and 50°C for all measured amides. Also includes Temperature Coefficient (TC). Cells with 'stable' showed no signs of decay overall the course of the experiment. Cells denoted with these symbols (*, †, ‡) exchange too fast to fit. They completely exchanged after 10 min (*), 16 min (†), or 310 min (‡).

Residue #	k_{ex} ± error at 35 °C	PF at 35 °C	k_{ex} ± error at 50 °C	PF at 50 °C	TC ± S.E of the slope
2	6.4E-04 ± 9.7E-05	6.65E+06			-5.60 ± 1.50
3			stable	stable	-2.85 ± 0.51
4					-2.64 ± 0.21
5	stable	stable	stable	stable	-2.61 ± 0.13
6	stable	stable	stable	stable	-2.96 ± 0.09
7	5.1E-05 ± 1.4E-05	6.76E+07	stable	stable	-1.11 ± 0.08
8	8.4E-05 ± 1.6E-05	6.19E+07	1.65E-03 ± 2.90E-04	1.37E+07	-3.29 ± 0.01
9					Non-linear
10					-7.33 ± 0.62
12					-10.08 ± 0.52
13					1.70 ± 0.16
14					-4.15 ± 0.33
15	2.2E-04 ± 2.6E-05	3.20E+07			-3.09 ± 0.07
16					-0.93 ± 0.11

18	9.0E-04 ± 6.2E-05	6.09E+06			
19	2.3E-04 ± 7.9E-05	6.43E+06	1.38E-04 ± 5.03E-05	3.95E+07	
20	*	*			
22					-8.10 ± 1.04
23					-3.70 ± 0.10
24					
25					-6.35 ± 0.20
28	3.5E-04 ± 5.8E-05	6.95E+06			-2.44 ± 0.26
29					
30	3.7E-04 ± 3.9E-05	9.98E+06			-5.30 ± 0.10
31					-1.45 ± 0.09
32					-2.45 ± 0.10
33			1.5E-04 ± 3.7E-05	2.82E+07	
42					-1.86 ± 0.21
44					-5.51 ± 0.16
45					-1.15 ± 0.14
50	1.3E-03 ± 8.7E-05	2.17E+07			
51					-4.01 ± 0.08
53					Non-linear

54					-1.94 ± 0.17
55	7.2E-03 ± 2.3E-03	3.46E+05			-2.35 ± 0.36
56					Non-linear
58					-2.90 ± 0.25
59					-3.60 ± 0.32
61					-1.10 ± 0.05
62					-7.00 ± 0.59
63					Non-linear
64					-3.17 ± 0.05
65					-3.26 ± 0.09
66					-1.75 ± 0.12
68	*	*			
72					-1.50 ± 0.16
73					-7.27 ± 0.14
74	1.1E-04 ± 1.2E-05	5.09E+07			
76					-4.36 ± 0.20
77					-0.85 ± 0.11
78					-7.73 ± 0.44
80					Non-linear

81					-1.17 ± 0.06
82					-5.73 ± 0.32
83					-1.73 ± 0.17
84	2.7E-04 ± 8.9E-05	1.73E+07			-1.12 ± 0.06
85	2.4E-03 ± 5.6E-04	1.29E+07			-2.73 ± 0.07
86					-5.72 ± 0.11
87					-2.69 ± 0.07
88	4.5E-05 ± 2.4E-05	3.40E+07			
89	1.9E-04 ± 3.7E-05	4.11E+07	†	†	-5.38 ± 0.24
90					-2.34 ± 0.06
91	8.8E-04 ± 1.8E-04	8.20E+06			
92	2.1E-04 ± 3.1E-05	1.40E+07	2.64E-03 ± 4.36E-04	3.88E+06	-1.79 ± 0.21
93					-1.09 ± 0.03
94					-1.62 ± 0.17
95					-2.15 ± 0.18
96					-0.75 ± 0.05
98					-1.23 ± 0.06
99	*	*			
100					-3.63 ± 0.12

103					-2.55 ± 0.16
104					-2.51 ± 0.16
105					1.34 ± 0.18
106	1.4E-04 ± 1.2E-05	4.49E+07	1.29E-03 ± 8.75E-05	2.43E+07	Non-linear
107					-3.28 ± 0.57
108	stable	stable	1.20E-03 ± 4.52E-04	1.24E+07	-4.02 ± 0.25
109	stable	stable	stable	stable	-2.99 ± 0.15
114					-7.12 ± 0.44
115					-2.72 ± 0.14
116					-3.03 ± 0.14
117					-5.39 ± 0.04
120					-0.90 ± 0.18
121					-5.56 ± 0.36
122	*	*			-3.22 ± 0.10
123					-2.65 ± 0.05
124	1.9E-04 ± 3.7E-05	1.31E+07	1.59E-03 ± 6.89E-04	2.75E+06	
127	1.6E-03 ± 1.8E-04	1.82E+07	*	*	-1.63 ± 0.09
128	stable	stable	stable	stable	
129	stable	stable	stable	stable	-3.35 ± 0.10

130	stable	stable	3.55E-04 ± 2.08E-05	2.69E+08	-3.51 ± 0.02
132					-0.39 ± 0.09
133	9.7E-05 ± 1.9E-05	1.81E+07	stable	stable	
134	stable	stable	2.33E-04 ± 3.64E-05	1.40E+08	-1.36 ± 0.08
135	4.2E-04 ± 2.6E-05	1.94E+07	‡	‡	-2.81 ± 0.08
136	*	*			-3.95 ± 0.07
137	*	*			-1.86 ± 0.09
138	2.0E-04 ± 1.1E-04	1.64E+07			-0.68 ± 0.14
139	stable	stable	1.28E-04 ± 2.75E-05	9.29E+07	Non-linear
140					-7.92 ± 0.53
141					-1.05 ± 0.11
142	stable	stable	2.68E-04 ± 3.81E-05	1.69E+08	-3.27 ± 0.17
143	6.8E-05 ± 2.8E-05	3.03E+07			-1.74 ± 0.06
144	stable	stable	stable	stable	Non-linear
145	stable	stable	stable	stable	-2.85 ± 0.25
146	Stable	Stable	stable	stable	-3.11 ± 0.19
152	stable	stable	stable	stable	-2.55 ± 0.21
153					-4.13 ± 0.60
155	stable	stable	stable	stable	

156	stable	stable	stable	stable	-2.63 ± 0.02
157					-2.22 ± 0.31
159					-2.30 ± 0.08
160					-2.35 ± 0.19
161					0.00 ± 0.00
162					-2.59 ± 0.26
163					Non-linear
165					-3.69 ± 0.10
167	3.3E-04 ± 3.1E-05	1.18E+07	stable	stable	-4.44 ± 0.30
171					-3.26 ± 0.12
172					-0.76 ± 0.12
173					0.00 ± 0.00
174					-10.16 ± 0.47
175	‡	‡			
176					-6.48 ± 0.35
177					-3.96 ± 0.10
178	†	†			-0.28 ± 0.05
180					-7.61 ± 0.29
181					-2.64 ± 0.13

182					Non-linear
183					-1.33 ± 0.34
184	†	†			-2.01 ± 0.23
188					-6.21 ± 0.42
192					-6.12 ± 0.25
193					-2.24 ± 0.08
194	1.4E-03 ± 9.7E-05	5.53E+07			
198					-1.05 ± 0.11
199					-1.48 ± 0.07
200					-3.91 ± 0.22
201	4.6E-04 ± 3.7E-05	4.89E+07			
202					-2.06 ± 0.09
203					-1.63 ± 0.16
204					-6.98 ± 0.48
206	†	†			
207					-1.62 ± 0.12
212					-2.45 ± 0.15
213					-5.56 ± 0.27
214					-3.99 ± 0.37

216					-2.11 ± 0.43
218					-3.45 ± 0.10
223	*	*			Non-linear
229					-3.50 ± 0.52
231					-2.65 ± 0.59
252					-2.87 ± 0.15
254					-2.14 ± 0.48
258	stable	stable			
259					-8.99 ± 0.62
262	6.4E-04 ± 1.1E-04	3.15E+06			-2.99 ± 0.13
265	‡	‡			-1.80 ± 0.29
266	stable	stable	1.56E-04 ± 3.46E-05	8.90E+07	0.27 ± 0.11
267	‡	‡			
268					-0.74 ± 0.21
269					-3.08 ± 0.22
270	stable	stable	stable	stable	
271	1.4E-03 ± 1.7E-04	2.82E+07			
274					-5.31 ± 0.16
275					-1.83 ± 0.04

277					-1.14 ± 0.17
278					
279					-1.30 ± 0.12
280	1.6E-04 ± 2.8E-05	2.61E+07			
282					-1.19 ± 0.15
283	‡	‡			-1.86 ± 0.27
284	stable	stable			-1.40 ± 0.13
285			1.43E-04 ± 1.10E-04	4.75E+07	
286	stable	stable			-2.10 ± 0.14
287			stable	stable	-1.62 ± 0.15
288	stable	stable	stable	stable	-2.99 ± 0.07
289	stable	stable	stable	stable	
290	stable	stable	stable	stable	
291	3.6E-04 ± 3.3E-05	3.26E+07	*	*	
293					-1.77 ± 0.23
294					-3.11 ± 0.18
296	1.1E-03 ± 2.8E-04	1.50E+06			-3.59 ± 0.09
301					-4.37 ± 0.15
302					-5.10 ± 0.07

304	2.0E-03 ± 1.9E-04	1.44E+07	*	*	
307					-7.87 ± 0.32
310					-1.75 ± 0.15
311					-4.37 ± 0.10
312					-0.37 ± 0.11
313					-2.07 ± 0.08
314					-2.86 ± 0.19
315	1.2E-04 ± 1.3E-05	1.49E+08	1.90E-03 ± 5.31E-05	1.42E+08	
316					-2.23 ± 0.08
317	*	*			-3.53 ± 0.18
318	5.3E-05 ± 1.4E-05	3.26E+07	2.34E-04 ± 1.55E-04	1.17E+07	-1.21 ± 0.30
320	3.7E-04 ± 3.6E-05	5.49E+07	*	*	
321	*	*			
322	2.9E-04 ± 2.0E-05	2.55E+07	†	†	-4.94 ± 0.09
323	*	*			Non-linear
324					Non-linear
326					-5.69 ± 0.14
329					-2.14 ± 0.25
330					-2.79 ± 0.06

331	2.0E-03 ± 5.4E-04	2.08E+06			-3.54 ± 0.07
332					-3.96 ± 0.31
333	stable	stable			-2.89 ± 0.07
334					-3.67 ± 0.09
335	stable	stable	stable	stable	-2.26 ± 0.13
336					-6.36 ± 0.57
337			stable	stable	
339	*	*			-3.48 ± 0.10

Appendix Q: Table of TC average across secondary structures of Dbh

Average excludes amides in loop regions, amides not involved in hydrogen bonds, and amides exposed to solvent. Structural analysis based on the Dbh crystal structure 1K1S. Cells denoted with this symbol (**) did not have three or more TC values so an average could not be calculated. Averaging TC values secondary struture and domains can give a measure of local stability. Dynamic regions have a TC average that is more negative compared to rigid regions.

TC average by secondary structure	
Helix	
A (10-20)	-1.62
B (21-24	**
C (47-52)	**
D (60-66)	-2.84
E (77-94)	-2.61
F (121-138)	-2.58
G (148-158)	-2.88
H (171-178)	-2.95
I (180-188)	-3.96
J (189-198)	-3.14
K (202-209)	-3.07
L (210-219)	-3.51
M (220-230)	**
N (258-276)	-2.21
O (307-324)	-2.59
Strands	
1 (3-8)	-2.58
2 (28-33)	-2.91
3 (41-45)	-2.84
4 (72-74)	**
5 (98-103)	-2.58
6 (106-110)	-3.43
7 (141-147)	-2.4
8 (164-166)	**
9 (241, 242)	**
10 (246-256)	**
11 (283-290)	-1.99
12 (295-301)	**
13 (331-339)	-3.74
14 (341,342)	**

Appendix R: List of residues that shifted in the presence of Mg^{2+} and Mn^{2+}

List of peaks that disappeared in the presence of Mg^{2+}or Mn^{2+} (**Figures 3.7 and 3.9**). The domain, residue number, residue type, and binding site are given.

Domain	Residue #	Type of residue	Binding site	Mg^{2+}	Mn^{2+}
Palm	7	Asp	1	✓	✓
Palm	8	Phe	1	✓	✓
Palm	9	Asp	1	✓	✓
Palm	12	Phe	1		✓
Palm	13	Ala	1	✓	✓
Palm	16	Glu	1	✓	✓
Finger	25	Gly	1		✓
Finger	44	Ala	1		✓
Finger	45	Thr	1	✓	✓
Finger	58	Gly	1		✓
Palm	85	Ser	1		✓
Palm	89	Met	1		✓
Palm	103	Ser	1		✓
Palm	105	Asp	1	✓	✓
Palm	106	Glu	1		✓
Palm	108	Tyr	1		✓
Palm	117	Gly	1		✓
Palm	139	Ile	1	✓	✓
Palm	140	Thr	1	✓	✓
Palm	144	Gly	1		✓
Palm	145	Val	1		✓
Palm	156	Ala	1		✓
Palm	159	Ser	1	✓	
Palm	160	Lys	1		✓
Palm	162	Asn	1		✓
Palm	163	Gly	1		✓
Palm	165	Gly	1		✓
Thumb	177	Asn	2		✓
Thumb	178	Glu	2	✓	✓
Thumb	180	Asp	2		✓
Thumb	182	Asp	2		✓
Thumb	199	Gly	2		✓

Thumb	201	Gln	2	✓	✓
Thumb	204	Arg	2	✓	✓
LF	282	Met	3	✓	
LF	299	Gly	3	✓	✓
LF	301	Lys	3	✓	✓
LF	305	Gly	3	✓	✓